

学位論文

Studies on hygroscopicity and wet removal of
black carbon aerosol

(ブラックカーボンエアロゾルの吸湿特性と
湿性除去に関する研究)

平成 26 年 12 月博士 (理学) 申請

東京大学大学院理学系研究科

地球惑星科学専攻

大畑 祥

Abstract

Black carbon (BC) aerosols are emitted by incomplete combustion of carbonaceous matter such as fossil fuels and biomass. BC particles strongly absorb short-wave solar radiation and contribute to global warming. In addition, BC particles deposited in or on snow can reduce snow albedo and may accelerate snow melting. Despite continuous efforts to quantify the effect of BC aerosols on Earth's radiative balance, however, estimates of this effect remain uncertain. A major factor contributing to this uncertainty derives from an incomplete understanding of the wet removal of BC aerosols. The efficiency of wet removal depends on the hygroscopicity of the BC aerosols and strongly controls the temporal and spatial variations of BC concentrations in the atmosphere. In this study, a new method for measuring the hygroscopicity of ambient BC particles was developed, a method for measuring the mass concentration and size distribution of BC particles suspended in rain and snow samples was evaluated, and the methods were employed in an intensive field observation of the hygroscopicity and wet removal of BC-containing particles in the urban atmosphere of Tokyo.

To establish a new method for the simultaneous, independent measurement of the hygroscopic growth of BC-free and BC-containing particles, a humidified single-particle soot photometer (h-SP2) was developed by modifying a standard SP2. The h-SP2 measures the BC mass and the amount of coating material within individual aerosol particles under a controlled relative humidity (RH) by detecting both the laser-induced incandescence emitted and the laser light scattered from each BC-containing particle. The growth factor (GF) and hygroscopicity parameter κ for

both BC-free and BC-containing particles were measured by combining an aerosol particle mass analyzer with the h-SP2.

The h-SP2 was tested in the laboratory using both homogeneous ammonium sulfate (AS) and internally mixed particles of BC and AS. A core-shell structure was assumed for the BC-containing particles, and the reduction in the refractive index of the BC-free particles and BC-coating materials due to their hygroscopic growth was taken into account. The measured growth factors of the pure AS and thickly coated BC particles agreed with the growth factors predicted by κ -Köhler theory to within measurement uncertainty, demonstrating the applicability of the h-SP2 for ambient measurements.

A method for measuring the number and mass size distributions of BC particles suspended in rainwater was also evaluated. In this method, a nebulizer extracts BC particles from liquid water to air with efficiency ε , and the extracted particles are detected by the SP2. The dependence of ε on particle size was determined by using polystyrene latex (PSL) sphere suspensions; the PSL number concentrations in water were measured by the extinction of a laser beam. Repeated measurements of the size distribution of BC in a rainwater sample showed that the effect of coagulation of BC particles in water during storage was not significant.

These new methods were used to intensively observe the hygroscopicity and wet removal of BC-containing particles in the urban atmosphere of Tokyo during summer 2014. The h-SP2 measured the detailed temporal variation of BC-free and BC-containing particles in Tokyo air for the first time. Throughout the observation

period, thinly coated BC particles tended to be less hygroscopic than thickly coated BC particles, and the number fraction of the less hygroscopic ($GF < 1.2$ at 85% RH) BC-containing particles was more than 70% of the total BC-containing particles with a dry diameter of about 200 nm. The chemical compositions of BC-coating materials were generally similar to those of BC-free particles.

The number size distributions of BC in air and BC in rainwater measured during rain events indicated that BC-containing particles with larger BC cores were efficiently removed by cloud precipitation processes. This size-dependent wet removal was successfully explained by the estimated critical supersaturation (S_c) of BC-containing particles in air and the maximum supersaturation of 0.1% (0.05–0.2 %) that the particles would have experienced during the rain events. On average, the number fraction of cloud condensation nuclei (CCN)-activated BC-containing particles under a maximum supersaturation of 0.1% was estimated to be 0.27 for particles with $D_{BC-core} = 200$ nm and 0.45 for particles with $D_{BC-core} = 350$ nm, indicating that BC-containing particles in Tokyo air, especially particles with small BC cores (or with high S_c), were efficiently transported upward without being removed by precipitation. Thus the simultaneous observation of BC in air and BC in rainwater near BC emission sources provides useful data for directly assessing various model schemes related to wet removal of aerosols.

Contents

1. General Introduction	1
1.1. Black Carbon Aerosol.....	2
1.2. Aerosol Hygroscopicity.....	4
1.2.1. Hygroscopic Growth Factor.....	5
1.2.2. κ -Köhler Theory.....	6
2. Development of a Humidified Single-Particle Soot Photometer	9
2.1. Introduction.....	9
2.2. Single-Particle Soot Photometer	10
2.2.1. Instrumental Configuration.....	11
2.2.2. Calibration.....	13
2.2.3. Measurement of the Dry Shell/Core Ratio.....	15
2.3. Humidified-SP2.....	21
2.3.1. Flow System	21
2.3.2. Control of Relative Humidity	23
2.4. APM-hSP2 Method.....	26
2.4.1. Experimental Setup.....	26
2.4.2. Data-Processing Procedure	27
2.4.3. Laboratory Experiments.....	29
2.4.4. Measurement Uncertainty	34

2.5. Summary.....	39
3. Field Observation of the Hygroscopicity and Wet Removal of Particles Containing Black Carbon in Tokyo Air	41
3.1. Introduction.....	41
3.2. Observation Site and Experimental Setup	43
3.3. Results and Discussion.....	45
3.3.1. Microphysical Properties of BC-containing Particles.....	45
3.3.1.1. Hygroscopicity	45
3.3.1.2. Dry Shell/Core Ratio.....	52
3.3.1.3. Average Single BC-Core Mass.....	56
3.3.2. Wet Removal of BC-Containing Particles.....	58
3.3.2.1. Estimates of Critical Supersaturation.....	58
3.3.2.2. BC in Rainwater.....	64
3.4. Summary.....	68
4. Evaluation of a Method to Measure BC particles Suspended in Rain and Snow Samples	70
4.1. Introduction	70
4.2. Methods	72
4.2.1. Experimental Setup.....	72
4.2.2. PSL Number Concentration in Water	76
4.2.3. Laboratory BC Samples.....	77
4.3. Size-Dependent Nebulizer Efficiency	79

4.4. Reproducibility.....	86
4.4.1. Change of Size Distribution and Mass Concentration of BC in Water During Storage	86
4.4.2. Attachment of BC Particles to the Walls of Glass Container during Storage	87
4.4.3. Effect of Water-Soluble Species.....	88
4.4.4. Change in BC Size in the Nebulizer	91
4.5. BC Size Distributions in Rainwater and Snow Samples	93
4.6. Ultrasonic Nebulizer Compared to Collison-Type Nebulizer	96
4.7. Wet Deposition of BC at a Remote Site in the East China Sea.....	99
4.8. Summary.....	100
Appendix 4A: Recent Improvements in Measurements of BC Particles in Rainwater	101
5. General conclusions	103
References	107
Acknowledgements	118
Publication List	119

1. General Introduction

Atmospheric aerosols are suspensions of small solid particles, small liquid particles, or both in air. Particle sizes range from a few nanometers to 100 μm . Individual particles have various sizes, compositions, and shapes, which lead to their various optical and hygroscopic properties. Aerosols play an important role in Earth's climate system through direct and indirect effects [Intergovernmental Panel on Climate Change (IPCC), 2013].

Atmospheric aerosols mainly consist of sulfates, nitrates, organic material, black carbon (BC), sea salt, and dust. Of these species, BC, some organics, sea salt, and dust are released directly into the atmosphere from their emission sources and form primary aerosols. In contrast, sulfates, nitrates, and some organics form secondary aerosols via gas-particle chemical reactions in the atmosphere (gas-to-particle conversion).

Secondary inorganic aerosols generally scatter solar radiation and cool the atmosphere, whereas some primary aerosols, especially BC particles, strongly absorb short-wave solar radiation and contribute to global warming [Bond et al., 2013; IPCC, 2013]. In addition, BC particles deposited in or on snow can reduce snow albedo and may accelerate snow melting [Warren and Wiscombe, 1980; Clarke and Noone, 1985].

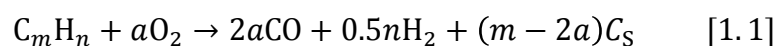
In spite of continuous efforts to quantify the effect of BC aerosols on Earth's radiative balance, estimates of this effect remain uncertain [Bond et al., 2013]. A major factor contributing to this uncertainty derives from an incomplete understanding of wet removal of BC aerosols during their vertical transport from the atmospheric boundary layer to the free troposphere. The efficiency of the wet removal depends on the

hygroscopicity of BC aerosols, and strongly controls the temporal and spatial variations of BC number and mass concentrations in the atmosphere. In this dissertation, laboratory studies and field observations focusing on the hygroscopicity and wet removal of BC aerosols were conducted. In particular, the objectives of this dissertation include development of a new method to measure the hygroscopicity of ambient BC particles, evaluation of a method to measure the mass concentration and size distribution of BC particles suspended in rain and snow samples, and application of the methods to field observations.

In this chapter, characteristics of BC aerosols and theoretical representations of aerosol hygroscopicity are described. In Chapter 2, a new method for measuring BC hygroscopicity is reported. Chapter 3 discusses application of the newly developed measurement system to an atmospheric field campaign in Tokyo. In Chapter 4, a method for measuring BC particles in water is evaluated using laboratory and field samples. The principal conclusion of this dissertation is presented in Chapter 5.

1.1. Black Carbon Aerosols

BC is formally defined as an ideally light-absorbing substance composed of carbon [Petzold et al., 2013]. BC aerosols are emitted by incomplete combustion of carbonaceous matter such as fossil fuels and biomass. The formation of BC depends critically on the carbon/oxygen ratio in the hydrocarbon fuel–air mixture. When the C_mH_n –air mixture has insufficient oxygen to form CO_2 and CO combustion products exclusively, the combustion stoichiometry is



where C_S is the BC formed and $m/2a$ is the ratio of carbon to oxygen [Seinfeld and Pandis, 2006]. Practically, BC is distinguishable from other forms of carbon and carbon compounds in atmospheric aerosols because it has a unique combination of the following physical properties: (1) It strongly absorbs visible light with a mass absorption cross section of at least $5 \text{ m}^2 \text{ g}^{-1}$ at a wavelength of 550 nm. (2) It is refractory; that is, it retains its basic form at very high temperatures, with a vaporization temperature near 4000 K. (3) It is insoluble in water, in organic solvents including methanol and acetone, and in other components of atmospheric aerosols. (4) It exists as an aggregate of carbon spherules with a diameter of a few tens of nanometers [Bond et al., 2013].

During transport in the atmosphere, BC particles acquire “coating materials” through the condensation of semivolatile gaseous components and coagulation with other aerosols. Freshly emitted BC particles are generally hydrophobic, so the hygroscopicity of BC-containing particles is largely controlled by the composition and amount of coating materials. Through this aging process during transport, BC-containing particles can be active as cloud condensation nuclei (CCN) and removed from the atmosphere via cloud-precipitation processes. Observation and modeling of the aging and removal processes of BC particles are the keys to improving estimates of direct radiative forcing from BC aerosols [e.g., Moteki et al., 2007; Matsui et al., 2013].

Note that throughout this dissertation, internally mixed aerosols that consist of BC and non-BC (inorganic, organic, or inorganic + organic) materials are termed BC-containing particles, as suggested by Petzold et al. [2013]. For clarity, BC and the non-BC fraction within a BC-containing particle are sometimes called the BC core and

the BC coating, respectively. Atmospheric aerosols not including the BC fraction are termed BC-free particles.

1.2. Aerosol Hygroscopicity

Interaction of aerosols with water vapor (i.e., aerosol hygroscopicity) is crucial for the optical properties and wet removal of atmospheric aerosols. For both subsaturated (<100% relative humidity (RH)) and supersaturated (>100% RH) conditions, Köhler theory predicts the relationship between equilibrium saturation ratio over the surface of the droplet (S) and diameter of the droplet (D):

$$S = \frac{\text{RH}}{100} = a_w \exp\left(\frac{4\sigma M_w}{RT\rho_w D}\right), \quad [1.2]$$

where a_w is the activity of water in solution, ρ_w is the density of water, M_w is the molecular weight of water, σ is the surface tension at the solution–air interface, R is the universal gas constant, and T is the absolute temperature [Köhler, 1936]. The activity of water depends on the solute properties in solution, and several representations for a_w have been developed in previous studies [e.g., Mikhailov et al., 2009, and references therein]. This solute effect tends to decrease the equilibrium saturation ratio. In contrast, the exponential term in Equation [1.2], which accounts for the effect of curvature of the droplet, tends to increase the equilibrium saturation ratio. Because of the competition between these two effects, a plot of S as a function of D (Köhler curve) has a maximum value, termed the critical supersaturation (S_c). S_c is an important parameter representing the CCN activity of a particle. If the environment has reached a level of saturation

greater than S_c , the particle starts growing rapidly, becoming a cloud droplet.

1.2.1. Hygroscopic Growth Factor

Particle water uptake depends on the ambient RH. As a simple experimental measure, the hygroscopic growth factor (GF) is defined in terms of the droplet diameter (D) and the dry aerosol diameter (D_d):

$$GF = \frac{D}{D_d}, \quad [1.3]$$

The change in GF with increasing or decreasing RH for pure ammonium sulfate (AS), which is a typical inorganic aerosol in the atmosphere, is well understood [e.g., Mikhailov et al., 2009]. As the RH increases, the AS particles remain solid until the RH reaches the deliquescence RH (DRH) of 79.9%. At the DRH, the solid particles spontaneously absorb water, producing a saturated aqueous solution. Further increase in RH leads to additional water condensation onto the particles. In contrast, as the RH over the AS particles decreases, water evaporates. However, the solution generally does not crystallize at the DRH owing to the persistence of a metastable aqueous solution that is supersaturated with respect to crystalline AS [Martin, 2000]. This hysteresis phenomenon is not common to some other aerosol species. Species like H_2SO_4 are highly hygroscopic, and therefore the change in GF is smooth as RH increases or decreases. Although the hygroscopic properties of organic compounds are more complicated and highly dependent on the organic species, they are, in general, less hygroscopic than those of inorganic compounds. Some organic species do not exhibit

clear deliquescence behavior owing to their amorphous nature [Huff Hartz et al., 2006; Koehler et al., 2006; Mikhailov et al., 2009].

1.2.2. κ -Köhler Theory

Petters and Kreidenweis [2007] have presented a method to describe particle hygroscopic growth and CCN activity using a single hygroscopicity parameter κ . The parameter κ is defined through its effect on the water activity of the solution:

$$\frac{1}{a_w} = 1 + \kappa \frac{V_s}{V_w}, \quad [1.4]$$

where V_s is the volume of the dry particle matter and V_w is the volume of the water. For a multiple-component system (multiple solutes i + water) at equilibrium, the Zdanovskii–Stokes–Robinson assumption, which assumes that the total volume of the water is the sum of the water contents due to the individual components, is applied:

$$V_w = \sum_i V_{wi} = \frac{a_w}{1 - a_w} \sum_i \kappa_i V_{si}. \quad [1.5]$$

Here, Equation [1.4] is rearranged, and $a_{wi} = a_w$ is assumed. The total volume of the system, V_T , is calculated assuming volume additivity of the solutes and water:

$$V_T = \sum_i V_{si} + \sum_i V_{wi} = V_s + V_w \quad [1.6]$$

Defining the individual dry-component volume fractions as $\varepsilon_i = V_{si}/V_s$, Equation [1.5]

becomes

$$V_w = V_T - V_s = \frac{a_w}{1 - a_w} V_s \sum_i \varepsilon_i \kappa_i. \quad [1.7]$$

Using volume equivalent diameters defined by $D_d^3 = 6V_s/\pi$ and $D^3 = 6V_T/\pi$, Equation [1.7] is solved for a_w :

$$a_w = \frac{D^3 - D_d^3}{D^3 - D_d^3(1 - \kappa)}, \quad [1.8]$$

where the overall value for κ is given by the simple mixing rule

$$\kappa = \sum_i \varepsilon_i \kappa_i. \quad [1.9]$$

By substituting Equation [1.8] into Equation [1.2], the relationship between the equilibrium saturation ratio and D for a particle with D_d and κ is obtained by the following equation:

$$S = \frac{RH}{100} = \frac{D^3 - D_d^3}{D^3 - D_d^3(1 - \kappa)} \exp\left(\frac{4\sigma M_w}{RT\rho_w D}\right). \quad [1.10]$$

The parameter κ depends only on the dry-particle composition and can be physically understood as expressing the volume of water that is associated with a unit volume of dry particle. Lower values of κ indicate less hygroscopic and less CCN-active behavior.

For $\kappa = 0$, water activity $a_w = 1$, representing wetting of the dry particle by a pure water film. The value $\kappa \sim 1.4$ is an upper limit for the most hygroscopic species typically observed in an atmospheric aerosol (e.g., sodium chloride). The applicability of the κ -Köhler theory is confirmed for single- and multiple-component particles containing varying amounts of inorganic, organic, and surface-active compounds [Petters and Kreidenweis, 2007]. Typical values of κ for NaCl, $(\text{NH}_4)_2\text{SO}_4$, secondary organic aerosols, and BC are 1.12, 0.53, 0.05–0.20, and 0.0, respectively [e.g., Petters and Kreidenweis, 2007; Huff Hartz et al., 2005; VanReken et al., 2005; King et al., 2009].

Combining Equations [1.3] and [1.10], the following equation is obtained:

$$\frac{\text{RH}}{100} = \frac{\text{GF}^3 - 1}{\text{GF}^3 - (1 - \kappa)} \exp\left(\frac{4\sigma M_w}{RT\rho_w D_d \text{GF}}\right). \quad [1.11]$$

The value of κ for an unknown particle is experimentally determined by measurements of D_d and GF at a specific RH and T , assuming that σ is equal to the surface tension of pure water.

2. Development of a Humidified Single-Particle Soot Photometer

2.1. Introduction

To date, several methods have been developed to quantify aerosol hygroscopicity. One of the most widely used instruments for quantifying aerosol hygroscopicity is the hygroscopic tandem differential mobility analyzer (HTDMA) [e.g., Duplissy et al., 2009]. In the HTDMA, dry (<20% relative humidity (RH)) particles with a specific mobility diameter are selected by the first DMA; the particles are then humidified (~90% RH), and their size distributions are measured by the second DMA with a condensation particle counter. The HTDMA has been utilized to examine the hygroscopicity of various laboratory-generated black carbon (BC)-containing particles [e.g., Zhang et al., 2008; Henning et al., 2010, 2012]. However, the HTDMA is not specific to BC-containing particles; that is, the HTDMA measures the total aerosol hygroscopicity without explicitly distinguishing BC-containing particles from other aerosols. Therefore, the HTDMA is not suitable for obtaining information about the relationship between the amount and characteristics of the BC coating and the hygroscopicity in the ambient air.

To measure the hygroscopic properties of BC-containing particles in the atmosphere, techniques for direct detection of BC particles must be coupled with hygroscopic measurements. The volatility tandem DMA has previously been used for this purpose. The volatility tandem DMA is employed to isolate the less volatile aerosols, which consist mainly of BC particles [e.g., Kuwata et al., 2007]. A

single-particle soot photometer (SP2), which utilizes a laser-induced incandescence technique, has an extremely high sensitivity to BC and can quantify BC mass within individual aerosol particles. McMeeking et al. [2011] coupled the HTDMA with the SP2 to quantify the mobility hygroscopic growth of BC-containing particles. Liu et al. [2013] applied the HTDMA–SP2 system to field observations of aerosols and highlighted the importance of the effect of BC mixing state on the hygroscopic properties of BC-containing particles. However, relatively few measurement data of the hygroscopic properties of ambient BC-containing particles currently exist.

In this chapter, a new method for the simultaneous, independent measurement of the hygroscopic growth of BC-free and BC-containing particles is presented. A humidified-SP2 (h-SP2), developed by modifying a standard SP2, was used to quantify the BC mass and the amount of coating material within individual aerosol particles under a controlled RH by detecting both the laser-induced incandescence emitted and the laser light scattered from each BC-containing particle. The growth factor (GF) and hygroscopicity parameter κ for both BC-containing and BC-free particles were measured by combining an aerosol particle mass analyzer (APM) with the newly developed h-SP2.

The characteristics of the standard SP2 are described in section 2.2. Section 2.3 describes the configuration of the h-SP2. In section 2.4, the data-processing procedure of the measurement system is explained. Tests with laboratory-generated BC-free and BC-containing particles and measurement uncertainty are also discussed in section 2.4. This chapter is summarized in section 2.5.

2.2. Single-Particle Soot Photometer

2.2.1. Instrument Configuration

The SP2 measures both the BC mass and the optical diameter of individual aerosol particles under dry conditions (<20% RH). A schematic diagram of the SP2 optics is shown in Figure 2.1. In the SP2, sample air containing aerosol particles is introduced into a Nd:YAG laser beam ($\lambda = 1064 \text{ nm}$). During transit in the laser beam, a BC-free particle (non-light-absorbing particle) elastically scatters laser light, whereas the BC

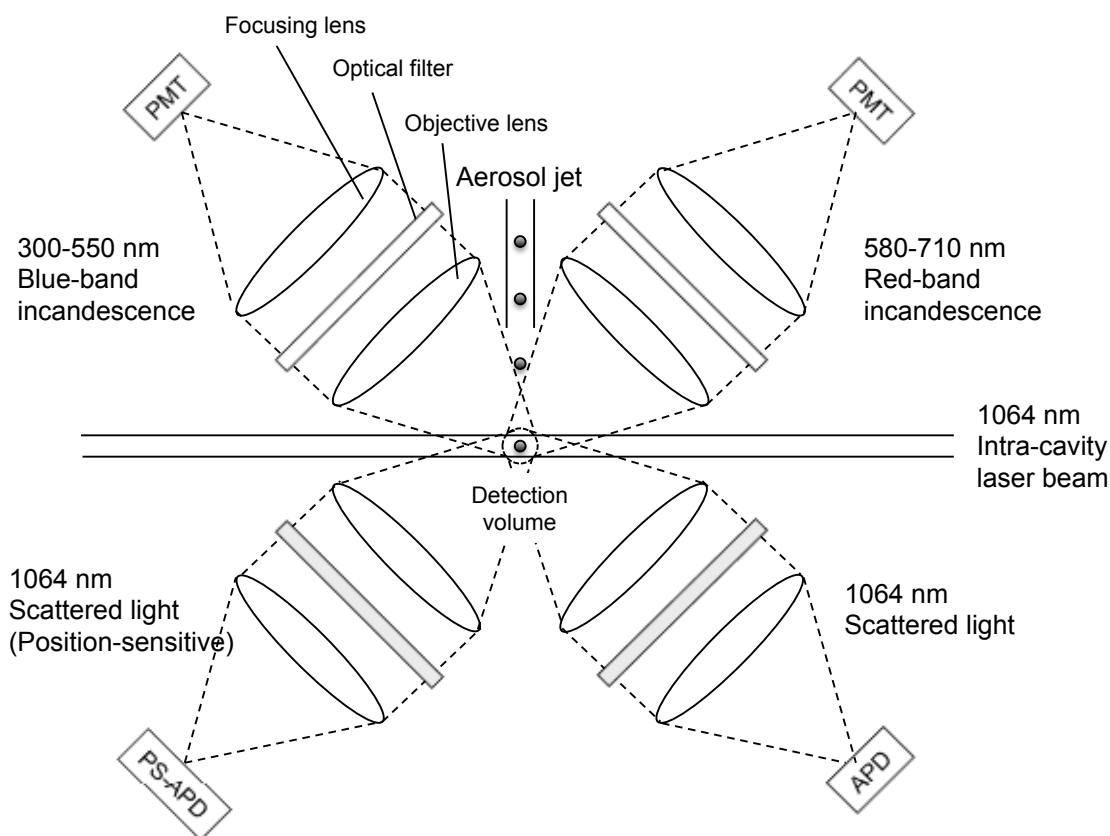


Figure 2.1. Schematic diagram of the SP2 optics. Although the axis of the aerosol jet is perpendicular to the plane containing the optical detectors and the laser beam, it is drawn in parallel for simplicity. PMT, photomultiplier tube; PS-APD, position-sensitive APD.

core within a BC-containing particle absorbs enough energy from the laser to vaporize at its boiling temperature (about 4200 K) and emit visible thermal light (incandescence). Figure 2.2 schematically shows how BC-free and BC-containing particles interact with the laser beam in the SP2. The intensity of the light scattered from each BC-free particle is detected by an avalanche photodiode detector (APD), and the optical diameters of the particles are determined from their refractive indices, assuming the particles are spherical. The intensity of the incandescence emitted from each BC core is detected by photomultiplier tubes and is, in general, linearly related to the mass of the BC core (see

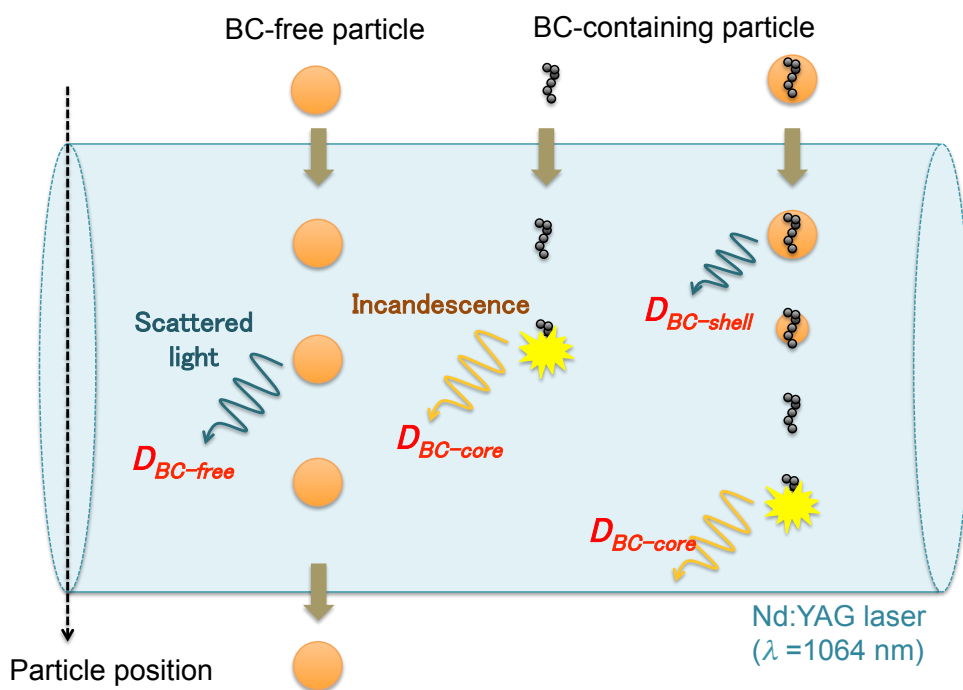


Figure 2.2. Schematic diagram of the transit of the aerosol particles introduced into the SP2 laser beam. Output measurement parameters are shown in red. $D_{BC-free}$ is the optical diameter of the BC-free particles, $D_{BC-core}$ is the mass-equivalent diameter of the BC cores, and $D_{BC-shell}$ is the optical diameter of the BC-containing particles before BC-coating materials evaporate due to heated BC cores.

section 2.2). The mass-equivalent diameter of the BC core ($D_{\text{BC-core}}$) is determined by assuming that the true density of the BC core is 1.8 g cm^{-3} , as discussed in Moteki and Kondo [2010].

In addition, the SP2 measures the amount of non-BC component within a BC-containing particle. Just after entering the laser beam, a BC-containing particle scatters the laser light without suffering from perturbation due to the heated BC core. In other words, evaporation of the non-BC component can be ignored at the edge of the laser beam. Therefore, assuming a core-shell structure for the BC-containing particle, detection of the scattered light at the edge of the Gaussian laser beam by the APD and a position-sensitive APD enables measurement of the optical diameter of the whole BC-containing particle [Gao et al., 2007]. This technique is evaluated in section 2.3. The size range of BC core detected by the SP2 is between 70 and 850 nm in mass-equivalent diameter. The detection range of optical diameters of BC-free particles is between around 170 and 850 nm. Note that throughout this dissertation the term “BC-free particles” is used for particles not emitting detectable incandescence in the SP2, and therefore it is possible that aerosol particles with a BC core of less than about 50 nm are counted as BC-free particles, if their whole particle sizes are optically large enough to be detected.

2.2.2. Calibration

The relationship between the BC mass and the intensity of the incandescence is crucial for accurate measurement with the SP2. The incandescence properties of three types of commercially available BC particles were tested: two fullerene soot (FS) samples (Stock No. 40971, Lots F12S011 and G25N20; Alpha Aeser, Inc., Wardhill, MA, USA),

which are dry powders; and Aqua-Black162 (Tokai Carbon Co. Ltd., Tokyo, Japan), a carbon black liquid ink. The experimental setup is shown in Figure 2.3. The laboratory BC samples were aerosolized from a water suspension by an atomizer and a diffusion dryer with silica gel. An aerosol particle mass analyzer (APM; [Ehara et al., 1996; Tajima et al., 2013] with a neutralizer was used to select BC mass prior to the SP2 measurements of incandescence. The width of the selected mass was theoretically estimated to be $\pm 16\%$ of the selected center mass, based on Tajima et al. [2013].

Relationships between the peak amplitude of the incandescence signal and the BC mass are shown in Figure 2.4, which also includes ambient BC data of Moteki and Kondo [2010]. The relationships, which are highly dependent on the laboratory BC sample, are similar for Lot F12S011 FS and ambient BC in Tokyo; therefore, this batch of FS is a suitable laboratory BC sample for calibrating the SP2, as discussed in previous studies [Moteki and Kondo, 2010; Baumgardner et al., 2012]. Laborde et al. [2012] also reported that the incandescence–BC mass relationship for SP2s would be different between batches of FS.

For laboratory BC particles of mass less than about 10 fg, the absorption (i.e., emission) cross section of the particles do not depend on particle shape because the particle size is small compared to the wavelength of the visible light. Therefore, the

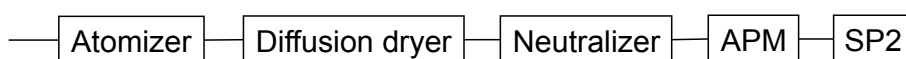


Figure 2.3. Schematic diagram of the experimental setup for measurement of the relationship between BC mass and the intensity of the incandescence.

intensity of the incandescence is proportional to the BC mass. In contrast, the incandescence properties of larger BC particles are more affected by their particle shape. For practical use of the SP2 data analysis, the experimental data of the relationship between the signal amplitude of the incandescence and the BC mass (greater than about 10 fg) are fitted by a power function of the form $y = ax^b$, where a and b are the calibration coefficients. The detailed theoretical interpretation of the measured incandescence of BC particles is described in Moteki and Kondo [2010].

In the SP2 data analysis, the scattering signals detected by the APD are converted to the scattering cross sections of the particles to quantify individual optical diameters. The relationship between the scattering peak amplitude and the scattering cross section is experimentally determined using polystyrene latex spheres with a known diameter and refractive index. Note that in the strict sense, the SP2 measures the differential scattering cross section integrated over the solid angle of SP2 detectors by detecting scattered light from the particles. For practical purposes, however, the term “scattering cross section” is used throughout this chapter.

2.2.3. Measurement of the Dry Shell/Core Ratio

The leading edges of the scattering signals from the BC-containing particles provide their scattering cross sections before coating materials evaporate due to the heated BC cores in the SP2 laser. To derive the whole dry-particle sizes (D_d or $D_{BC-shell}$) from the measured scattering cross sections, it is assumed that the BC-containing particles have a core-shell structure (Figure 2.5). Given the refractive indices of the BC core and BC coating at $\lambda = 1064$ nm, $D_{BC-shell}$ is determined by Mie theory from the measured $D_{BC-core}$ and scattering cross sections of the particles [Bohren and Huffman, 1983].

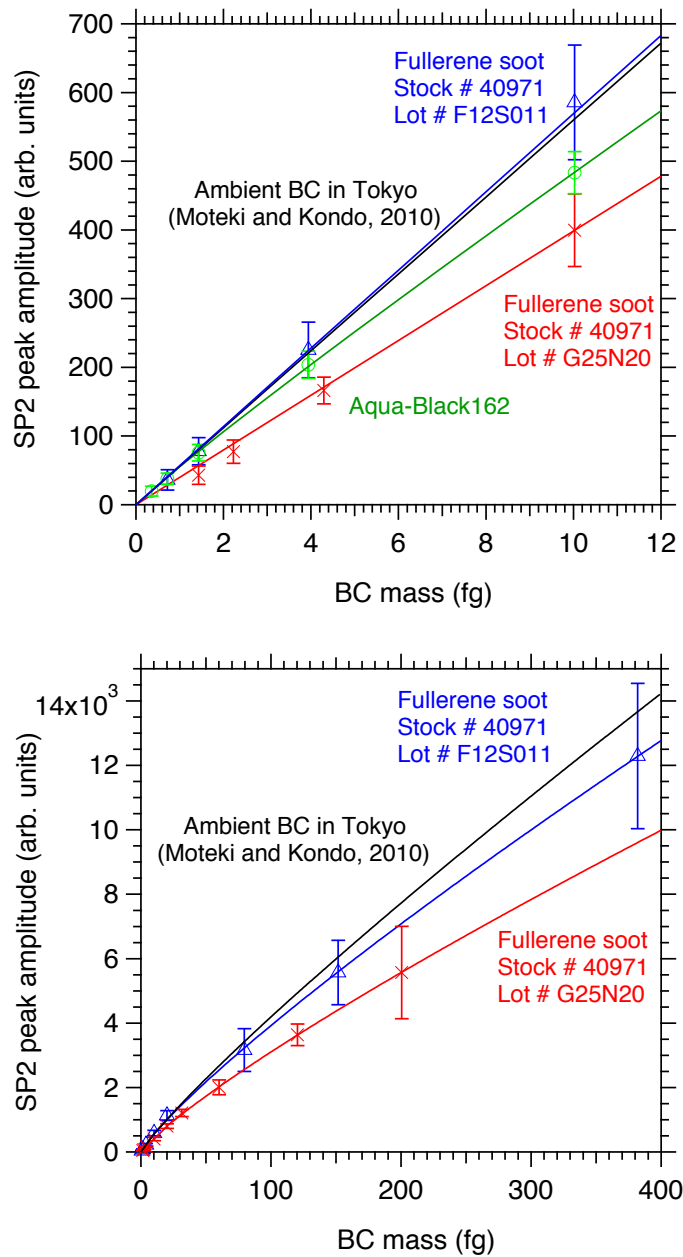


Figure 2.4. Relationship between peak amplitude of the incandescence signal and BC mass for particle masses less than 12 fg (upper panel) and up to 400 fg (lower panel). The fitted lines and curves are also shown. Bars indicate 1σ .

The dry shell/core ratio (SCr) and coating thickness (CT) of BC-containing

particles are defined as follows:

$$SCr = \frac{D_{BC-shell}}{D_{BC-core}}, \quad [2.1]$$

$$CT = \frac{1}{2}(D_{BC-shell} - D_{BC-core}). \quad [2.2]$$

To evaluate the validity of the core-shell assumption, the amount of dry coating on the laboratory BC particles was measured using the experimental setup shown in Figure 2.3. To generate internally mixed BC particles, ammonium sulfate (AS) was added to a water suspension of Lot F12S011 FS and then atomized. The total dry mass of the individual BC-containing particles (m_d) was selected to be 7.4 ± 1.2 fg by the APM. Masses of the BC cores ($m_{BC-core}$) are measured from each incandescence signal; therefore, the amount of coating materials (here AS) is determined from the difference between the m_d and the $m_{BC-core}$ for each particle.

In parts a and b of Figure 2.6, the APM-derived coating amount is compared with the coating amount measured via SP2 leading-edge scattering signals, where

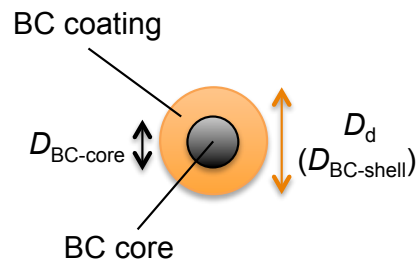


Figure 2.5. Schematic diagram of the core-shell structure of a BC-containing particle.

assumptions of core–shell structure, refractive indices of BC and AS, and real densities of BC and AS are made. The coating amounts agreed to within 23% for BC-containing particles with a coating amount greater than 4 fg (i.e., for the cases where the mass fraction of AS to total mass was greater than 56%). However, for thinly coated BC particles with a coating amount of 2.4 fg (i.e., for BC-containing particles with a mass fraction of AS to total mass of about 33%), the SP2-scattering coating amount was underestimated by 47% as compared to the APM-derived coating amount. This result implies that the core–shell assumption tends to produce larger relative uncertainties for thinly coated BC particles, because the scattering cross sections of thinly coated BC particles can be more affected by the complicated shape of the particles.

The dry shell/core ratio for laboratory BC particles measured using SP2-scattering signals was also evaluated by the APM-derived shell/core ratio (Figure 2.6c,d). The coating thicknesses for BC-containing particles with a relatively thick coating (shell/core ratio greater than about 1.3) agreed within 12%, whereas the SP2-scattering coating thicknesses for particles with a shell/core ratio of about 1.19 were underestimated by 44%. Although the relative uncertainties of the SP2-scattering coating thicknesses are generally smaller than those of the SP2-scattering coating volumes, the thinly coated BC particles still tend to contain relatively large measurement uncertainties.

For measurement of the dry shell/core ratio using the leading-edge scattering signals, both the scattering and the incandescence signals from a BC-containing particle must be within the detection range of the SP2. Although the detectable incandescence signals correspond to BC-core sizes between 70 and 850 nm, scattered light from BC-containing particles with a BC-core size less than 180 nm is usually not detectable.

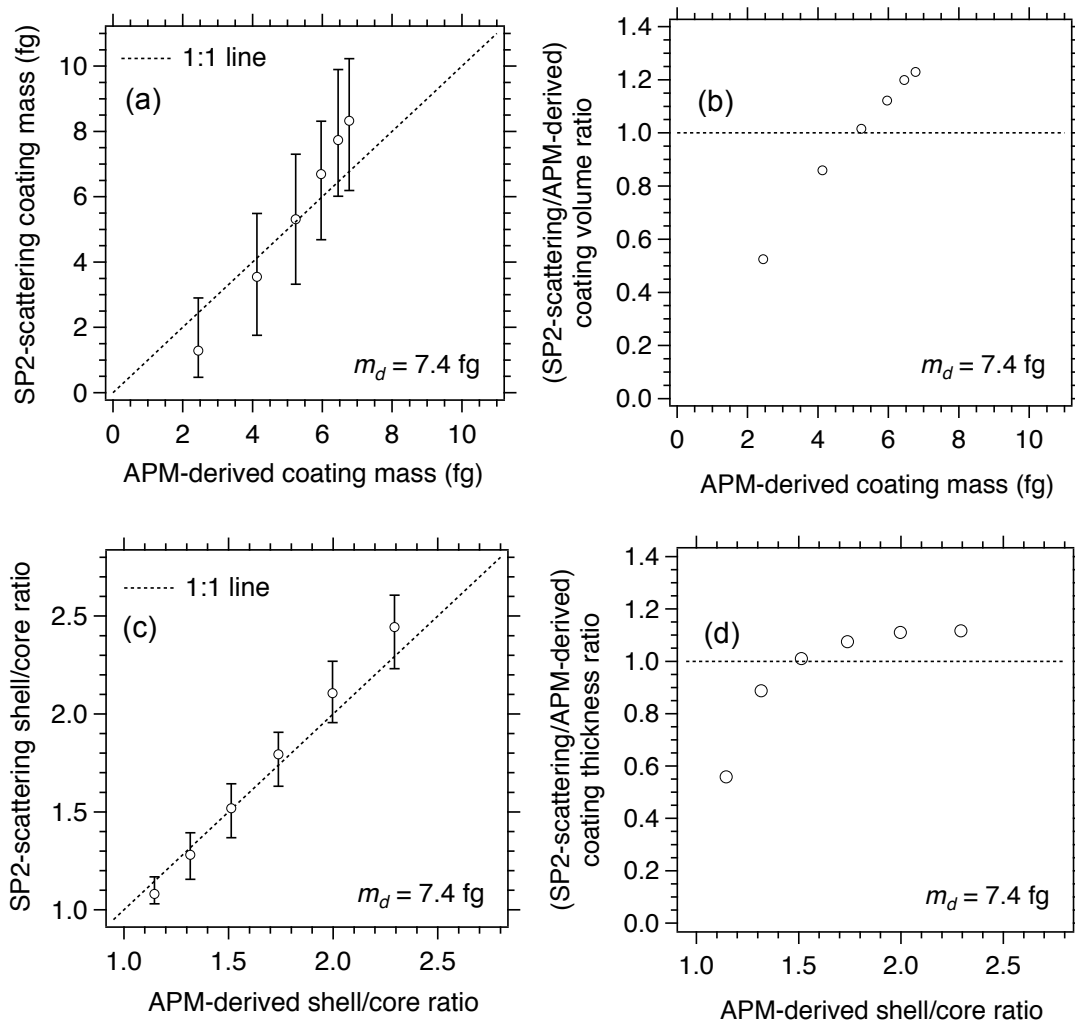


Figure 2.6. (a) Coating amounts of laboratory BC particles (FS) internally mixed with AS measured via the dry-particle mass selected by the APM (APM method) and measured via the leading edge of the SP2-scattering signals (SP2-scattering method). For both methods, masses of the BC cores are derived from the incandescence signals of the SP2. For data analysis of the SP2-scattering method, it is assumed that the BC-containing particles have a core-shell structure, that the refractive index of FS is $2.49 + 1.49i$ at $\lambda = 1064$ nm [Moteki et al., 2010], that the refractive index of AS is $1.52 + 0i$, that the real density of BC is 1.80 g cm^{-3} , and that the real density of AS is 1.77 g cm^{-3} . (b) Ratios of the coating mass (volume) measured by the SP2-scattering method to that measured by the APM method. (c) Dry shell/core ratios measured by the two methods. (d) Ratios of the coating thickness measured by the SP2-scattering method to that measured by the APM method.

Therefore, under the normal operating conditions of the SP2, measurement of the shell/core ratio is limited to BC-containing particles with a BC-core size larger than about 180 nm. Figure 2.7 shows the number fraction of BC-containing particles that had detectable scattering signals as a function of BC core diameter. These data were obtained by ambient measurements in Tokyo for 1 week in February 2014 and for 3 weeks in July–August 2014. The dry shell/core ratio for almost all of the BC-containing particles with BC cores larger than about 180 nm was measured, whereas for BC-containing particles with smaller BC cores, only particles that had relatively thick coating materials could be optically detected. The BC-containing particles tended to have thicker coatings, and the SP2 detectors had higher sensitivity, during the February 2014 observation period than during the July–August 2014 observation period.

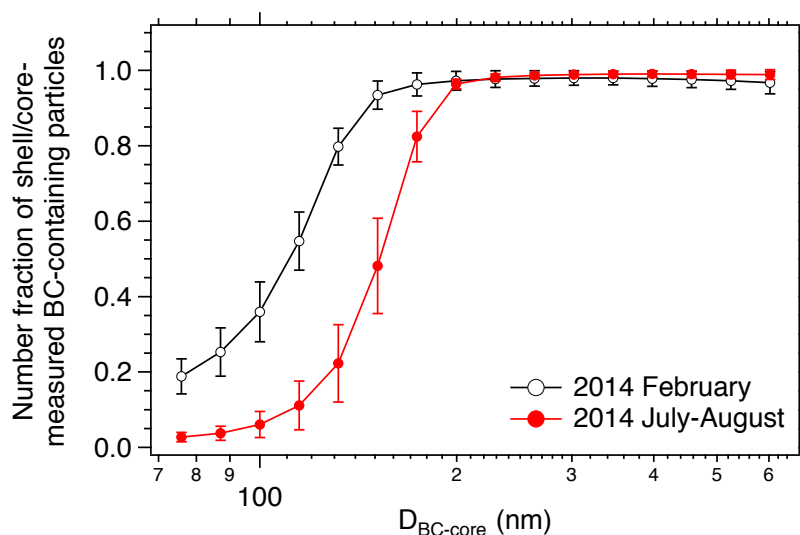


Figure 2.7. Average number fraction of BC-containing particles optically sized by the leading edge of the scattering signals. The data were obtained in Tokyo during February 2014 and July–August 2014. Bars indicate 1σ of 1-h data.

Therefore, the number fraction of shell/core-measured BC-containing particles was generally higher during the winter (Figure 2.7). Note that if the APM is coupled with the SP2, as shown in Figure 2.3, the total mass of dry BC-containing particles is fixed by the APM, and thus the shell/core ratio of BC-containing particles with smaller BC cores can be measured with higher number fraction.

2.3. Humidified-SP2

2.3.1. Flow System

In the SP2 chamber, the particle-free sheath air cylindrically surrounds the sample (aerosol-containing) air and generates an aerosol jet (see Figure 2.1) to prevent aerosol particles from circulating and/or depositing within the chamber and to introduce aerosol particles into the laser beam with high stability. The width of the aerosol jet is about one-tenth the width of the laser beam. The flow rate of the sheath air is set to be about 8–10 times as high as that of the sample air. To measure the optical size of the BC-containing particles under the specific RH condition, the RH of both the sample air and the sheath air must be controlled.

Figure 2.8 shows a schematic diagram of the flow system of the h-SP2. The sample air and sheath air are independently humidified by separate humidification units. A detailed description of the humidification unit is given in section 2.3.2. After humidification, the sample air passes through a $\frac{1}{4}$ " stainless steel tube with a length of about 180 cm in order to achieve equilibrium between aerosol particles and water vapor. The sample air is then split into the sample flow and the bypass flow. The sample flow is introduced into the SP2 chamber for particle measurement, whereas the bypass flow is introduced into an RH/temperature probe assembly (Vaisala HMP60; Helsinki,

Finland). By using the bypass flow for measurement of the RH of the sample air, the unknown particle loss in the assembly does not affect particle measurement. The sheath flow is particle-free, and the RH of the sheath air is monitored by another RH/temperature probe assembly just before the sheath air enters the SP2 chamber. The SP2 chamber, RH measurement units, and stainless tube for equilibrium are thermally insulated using a blanket to minimize fluctuations of the temperature and RH of the sample air and sheath air after passing through the humidification units.

The residence time of the sample air in the stainless steel tube depends on the sample and bypass flow rates. In this study, the sample, bypass, and sheath flow rates were set at 2.0, 4.7, and 16.7 cm³ s⁻¹, respectively. Under these operating conditions, the residence time is estimated to be 3.4 s. This residence time is generally sufficient for aerosol particles to achieve equilibrium before sizing in the SP2 chamber. Chuang

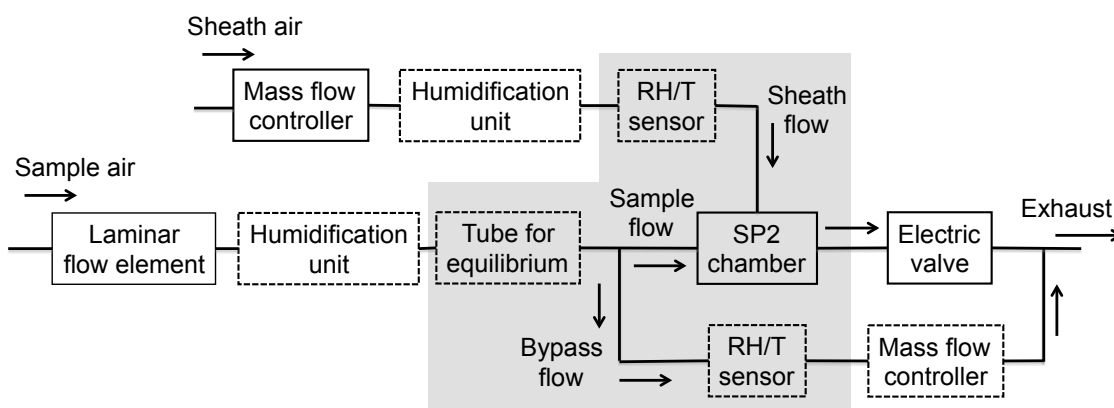


Figure 2.8. Flow system of the h-SP2. Components added to the original configuration of the standard SP2 are shown with dashed boxes. Thermally insulated components are shown with shaded boxes. Dry particle-free airflow to purge the optical detectors in the SP2 chamber (purge flow), which is employed in both the standard SP2 and the newly developed h-SP2, is not shown in the diagram for clarity.

[2003] conducted a field study of the hygroscopic growth of aerosol particles in Mexico City and reported that a limited number fraction (0–2.0%) of aerosol particles required a residence time of longer than 2–3 s to reach equilibrium hygroscopic growth at ~90% RH. Sjogren et al. [2007] confirmed that equilibration of pure AS is fast (<1 s) and showed that even for aerosol particles that required longer than 40 s to reach equilibrium at 85% RH, a 4-s residence time was sufficient to reach the equilibrium GF within 7%. Therefore, although the hygroscopic growth of some particles can be underestimated because of their slow water uptake, the measurement uncertainty due to this effect should not be statistically significant in the current h-SP2 system.

2.3.2. Control of Relative Humidity

The newly developed humidification unit consists of two Nafion (TT-110; Perma Pure LLC, Toms River, NJ, USA) water-permeable tubes, an aluminum water bath, and Peltier elements with fans. Figure 2.9 shows pictures of the unit. The Nafion tubes are immersed in the water bath. The surface of the Nafion behaves as a pure water surface, and therefore water vapor molecules diffuse from the inside wall of the Nafion tubes. The amount of diffusing water vapor depends on the water temperature, the humidity of the original airflow before entering the Nafion tubes, and the flow rate of the air. Two-step humidification using two Nafion tubes in the water bath was required for both the sample air and the sheath air to reach high (~90%) RH under the conditions of the flow rate settings and water temperature (between 15 and 35 °C). The RH of the sample air and sheath air after passing through the humidification units is monitored by RH/temperature probes (see Figure 2.8), allowing feedback control of the water temperature by the Peltier elements to achieve a target RH. The Peltier elements can be

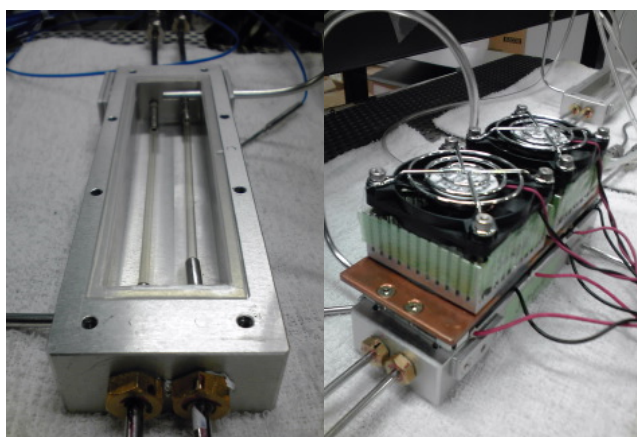


Figure 2.9. Pictures of the humidification unit. Two Nafion tubes were immersed in the water bath (left). Three Peltier elements and two fans were mounted on the water bath to control the water temperature (right).

used as either a heater or a cooler by switching the direction of the electric current, which is automatically controlled by a newly developed software program.

Figure 2.10 shows time series of the SP2 chamber temperature, the water temperature in the humidification units, and the sample air RH and sheath air RH. These data were obtained on 8 August 2014 during a field campaign in Tokyo (Chapter 3), where the hygroscopic growth of aerosol particles at 85% RH was measured. To achieve 85% RH, the water temperature for the sheath air was controlled to be about 1 °C higher than that for the sample air since the flow rate of the sheath air is greater than that of the sample air (section 2.3.1). When the chamber temperature increases from a stable state, the amount of water vapor in the sample air and sheath air needs to be increased to maintain a stable RH. Therefore, the time series of the chamber temperature and water temperature are synchronized with each other in Figure 2.10. Under the stable condition, the variance of the water temperature for the sample air and

sheath air was within 0.1 °C. As a result, the sample air RH and sheath air RH were controlled at $85.0 \pm 0.2\%$ and $85.0 \pm 0.3\%$, respectively. The RH/temperature probes were calibrated using a chilled mirror dew point hygrometer (DPH-203B, Tokyo

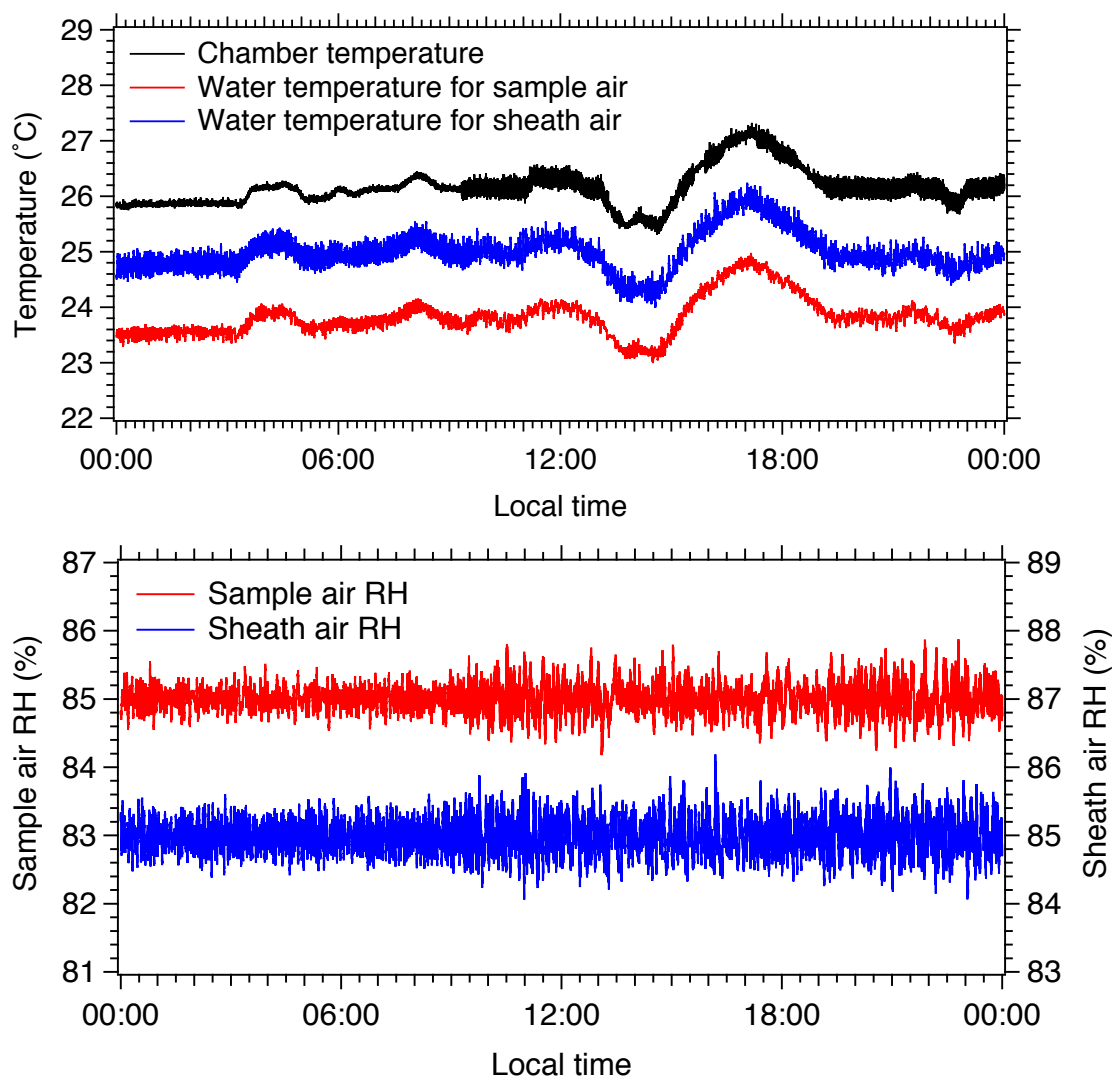


Figure 2.10. (Top panel) Example 1-s data of the water temperature in the humidification units, controlled to achieve 85% RH for the sample air and sheath air. A time series of the temperature of the SP2 chamber is also shown. (Bottom panel) Resulting RH of the sample air and sheath air.

Opto-Electronics Co., Ltd., Tokyo, Japan). The precision of the measured RH is $\pm 3\%$ according to the manufacturer.

The response time of the RH sensor depends on the flow rate of air over the sensor. Although a higher flow rate improves the response of the sensor, higher flow rates tend to suppress the humidification of the air because of a reduced residence time in the humidification unit. In addition, a higher flow rate of sample air reduces the residence time in the equilibration tube. Considering these points, the bypass flow rate for the system shown in Figure 2.8 was set at $4.7 \text{ cm}^3 \text{ s}^{-1}$ as described in the previous section. Under this flow rate condition, the time required for stable measurement of RH after a change in the amount of water vapor in the sample air can be longer than several minutes. However, the time variation of the SP2 chamber temperature and water temperature is generally slower than the response time required for the sensor. Therefore, a flow rate of $4.7 \text{ cm}^3 \text{ s}^{-1}$ should not result in significant errors in the measured RH of the sample air. Since the sheath air flow rate is greater than the sample air and bypass flow rates, the response of the RH sensor is faster for the sheath air than for the sample air.

2.4. APM–hSP2 Method

2.4.1. Experimental Setup

Combining an APM with the h-SP2 allows measurement of the hygroscopic growth of individual BC-containing and BC-free particles with known dry mass. A schematic diagram of the APM–hSP2 method is shown in Figure 2.11. The sample air containing the aerosol particles is dried ($<10\%$ RH) by diffusion dryers filled with silica gel and molecular sieve desiccant. The particles of a given dry mass (m_d) are selected by the

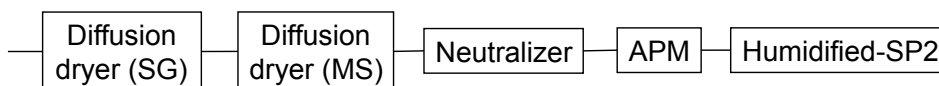


Figure 2.11. Schematic diagram of the experimental setup for measurement of the hygroscopic growth of individual BC-containing and BC-free particles of a given mass. SG, silica gel; MS, molecular sieves.

APM with a neutralizer prior to h-SP2 measurements. The width of the transfer function of the APM under the operating conditions was theoretically estimated to be less than about $\pm 16\%$ of the selected particle mass [Tajima et al., 2013]. The optical diameter (D) of the selected particles under the controlled RH condition is then measured by the h-SP2, using the data-processing algorithm described in the next section.

The volume-equivalent dry diameter (D_d) of the BC-free particles is determined from m_d and their real density ($\rho_{\text{BC-free}}$), assuming spherical particles. D_d and the dry shell/core ratio of the BC-containing particles are determined from m_d , the BC-core mass ($m_{\text{BC-core}}$) measured by SP2 incandescence signals, and the real densities of the BC core ($\rho_{\text{BC-core}}$) and BC coating ($\rho_{\text{BC-coat}}$), assuming core-shell particles. If particles of unknown composition are measured, the values of the densities $\rho_{\text{BC-free}}$, $\rho_{\text{BC-core}}$, and $\rho_{\text{BC-coat}}$ are assumed. The GF values of individual aerosol particles are determined from D_d and D for each particle. Measurement uncertainties in the values of the GF due to the assumed values of $\rho_{\text{BC-free}}$, $\rho_{\text{BC-core}}$, and $\rho_{\text{BC-coat}}$ are discussed in section 2.4.4.

2.4.2. Data-Processing Procedure

The h-SP2 measures the scattering cross sections of the individual particles by detecting their scattering signals, as discussed in sections 2.2.2 and 2.2.3 for the standard SP2. To

derive D of the particles from the measured scattering cross sections by Mie theory, the refractive indices of the particles are required. However, due to particle water uptake in the h-SP2 system, the refractive indices of the original dry BC-free particles and BC-coating materials approach the refractive index of water ($n_{\text{water}} = 1.33$), affecting quantification of D from the measured scattering cross sections. Figure 2.12 shows the change in refractive index of pure AS particles ($n_{\text{AS}} = 1.52$) with D_d of 200 nm as a function of GF. The volume-mixed refractive index of the particles decreases to 1.39 at GF = 1.5.

Considering the change in refractive index due to particle water uptake, a data-processing algorithm to determine GF values for BC-free and BC-containing particles was developed. Figure 2.13 summarizes the data-processing procedure. For a BC-free particle, the diameter of the humidified particle is initially guessed. The

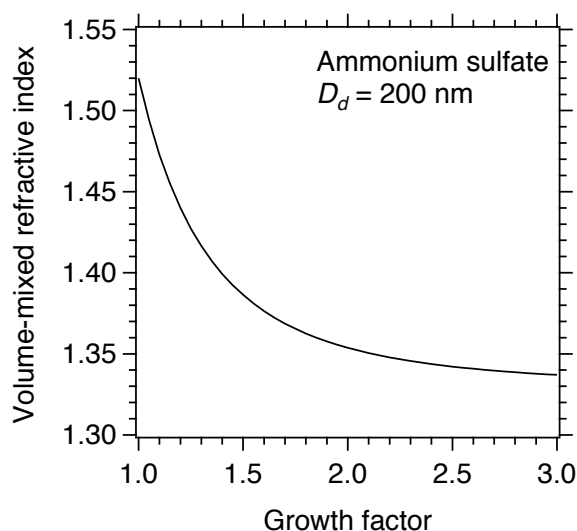


Figure 2.12. Change in refractive index due to water uptake by pure ammonium sulfate particles with D_d of 200 nm.

refractive index of the humidified particle is then calculated from the volume mixing of the dry particle and water. If unknown BC-free particles are measured, the refractive index of dry particles is assumed to be that of AS, as explained in section 2.4.4. After the refractive index of the humidified particle is calculated, the diameter of the humidified particle is calculated by Mie theory from the refractive index and scattering cross section of the particle. If the newly calculated diameter agrees with the initially guessed diameter, this value should be the best estimate for the diameter of the humidified particle, and thus the growth factor of the particle is determined. Iteration on the guessed D is carried out in 1-nm steps. This algorithm assumes that particulate matter is completely dissolved in the humidified particles. The measurement uncertainty due to the assumptions in this algorithm is discussed in section 2.4.4. The data-processing procedure for a BC-containing particle is similar to that for a BC-free particle, except that a core-shell particle is assumed. According to Moteki et al. [2010], the refractive indices of laboratory FS and ambient BC particles are assumed to be $2.49 + 1.49i$ and $2.26 + 1.26i$, respectively. For measurement of ambient BC-containing particles, the refractive index of the dry coating materials is assumed to be that of AS.

2.4.3. Laboratory Experiments

The APM-hSP2 measurement system was tested in the laboratory using both homogeneous AS and internally mixed particles of BC (FS) and AS. Homogeneous AS particles were produced by atomizing a pure AS solution, whereas internally mixed particles of FS and AS were generated by atomizing water suspensions of FS that contained dissolved AS. These particles were then dried by the diffusion dryers and selected by the APM at 7.4 ± 1.2 fg ($D_d \sim 200$ nm), and the growth factor of the

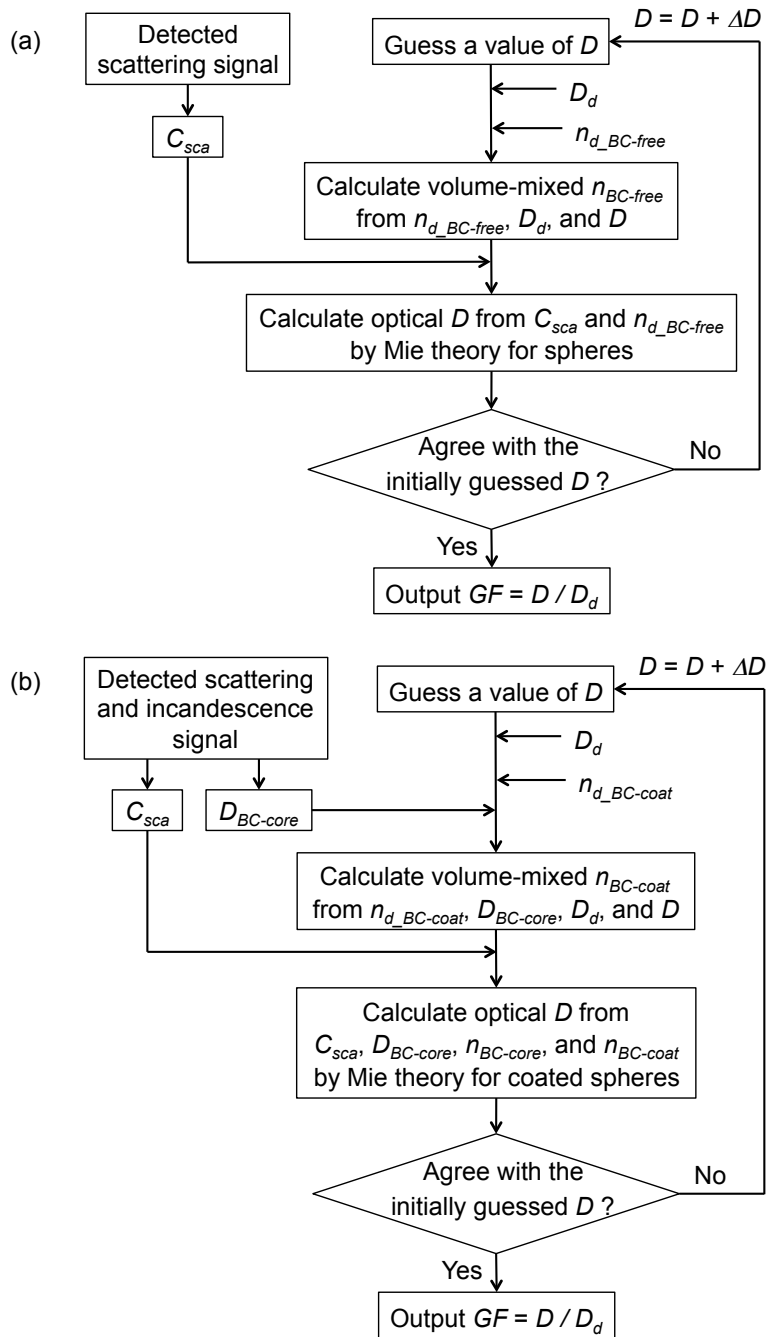


Figure 2.13. Data-processing procedure for the APM–hSP2 method for (a) BC-free and (b) BC-containing particles. D , D_d , and $D_{BC-core}$ are the diameters of the humidified particle, dry particle, and BC core, respectively. D_d is determined from the dry-particle mass selected by the APM and the assumed densities of the non-BC and BC materials. $D_{BC-core}$ is determined from the incandescence signals detected by the h-SP2. C_{sca} is the scattering cross section of the humidified particle measured by the h-SP2. $n_{d_BC-free}$ and $n_{BC-free}$ are the refractive indices of the BC-free particles under the dry and humidified

conditions, respectively. $n_{\text{BC-core}}$ is the refractive index of the BC core. $n_{\text{d_BC-coat}}$ and $n_{\text{BC-coat}}$ are the refractive indices of the BC-coating material under the dry and humidified conditions, respectively. GF is the growth factor calculated by D/D_d .

particles was measured from 60% RH to 90% RH. Figure 2.14 shows the measured hygroscopic growth of the pure AS particles. The histogram of the measured growth factor was bimodal. The fractions in the second mode (~10% to total) were multiply charged particles that passed through the APM and therefore were not included in the analysis. The measured growth factor agreed well with the growth factor predicted by κ -Köhler theory, confirming the overall accuracy of the measurement system and the data-processing algorithm. The slight difference between measured and predicted growth factors might be partly due to impurities in the AS solution. Even though the RH of the sample air in the SP2 chamber was controlled at less than the deliquescence RH of pure AS (79.9%), particles in the humidification unit could experience a higher RH than the deliquescence RH. In Figure 2.14, for RH of the air in the SP2 chamber greater than 65%, all AS particles appeared to have deliquesced. The growth factor measured under the assumption of a constant refractive index was much less than the predicted growth factor (Figure 2.14), indicating that the reduction in the refractive index of the particles due to their water uptake must be taken into account for the growth factor measurements.

Figure 2.15 shows the measured growth factors of the internally mixed particles of FS and AS. The thickly coated BC particles (dry $\text{SCr} = 1.86\text{--}2.14$; derived from m_d and $m_{\text{BC-core}}$) showed a higher hygroscopic growth than did the thinly coated BC particles (dry $\text{SCr} = 1.07\text{--}1.23$). The measured growth factors for the thickly coated BC

particles agreed well with the growth factors predicted by κ -Köhler theory. The larger dispersion of the data obtained for RH less than 70% indicates that some particles deliquesced and others did not during the humidification process. For RH greater than 75%, all BC-containing particles appeared to have deliquesced.

For the thinly coated BC particles, the measured growth factors were less than the predicted growth factors. This discrepancy is partly due to the assumption of a core-shell structure for the BC-containing particles. As discussed in section 2.2.3, the amount of coating on the thinly coated BC particles derived from the SP2-scattering and incandescence signals tended to be underestimated by about 50%, resulting in an

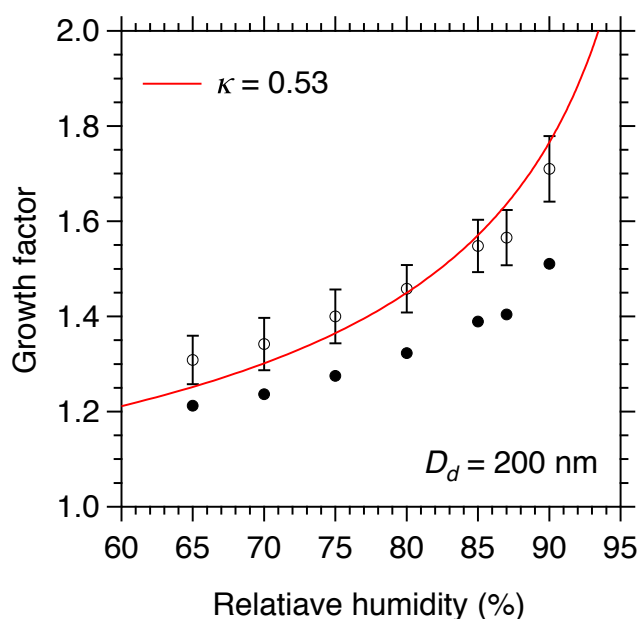


Figure 2.14. Measured and predicted growth factors of AS as a function of RH. Open circles show the measured growth factors using the data-processing algorithm described in section 2.4.2. Bars indicate 1σ . Closed circles show the measured growth factors, assuming a constant dry refractive index for AS.

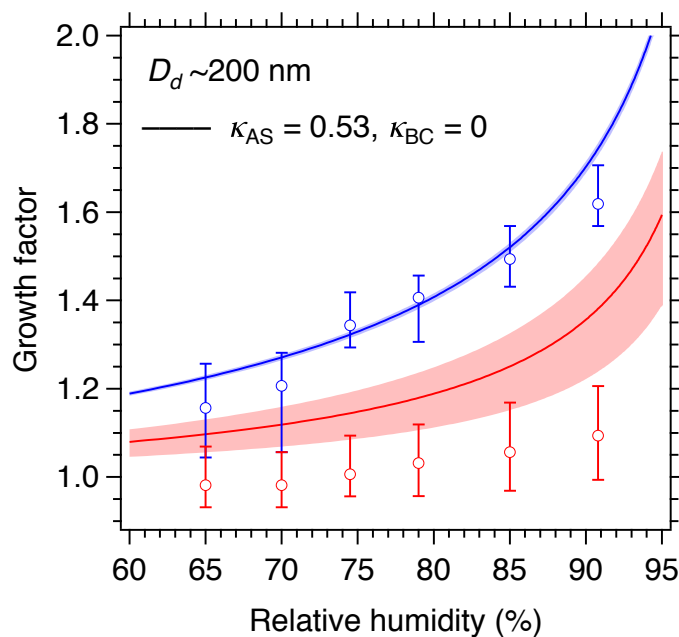


Figure 2.15. Measured and predicted growth factors of internally mixed particles of laboratory BC (FS) and AS as a function of RH. Data for BC-containing particles with dry shell/core ratios of 1.86–2.14 and 1.07–1.23 are shown in blue and red, respectively. Bars indicate the 25th–75th percentile.

underestimate of the hygroscopicity of these particles. To improve the measurement accuracy of the hygroscopic growth of thinly coated BC particles, scattering cross sections of BC-containing particles with a complicated structure (that is, an aggregate of primary carbon spherules and non-BC compounds) should be approximated by assuming a more realistic shape than a perfect coated sphere (core–shell model). In this dissertation, however, the assumption of a core–shell model has been used exclusively, and thus the measurement uncertainty for thinly coated BC particles is significantly larger than that for thickly coated BC particles. Measurement uncertainties of the APM–hSP2 method are summarized in the next section.

2.4.4. Measurement Uncertainty

In the APM–hSP2 method, several assumptions are made in determining the growth factors for ambient (unknown) BC-free and BC-containing particles. To derive D_d from the APM-selected m_d , the dry-particle densities $\rho_{d_BC-free}$, $\rho_{BC-core}$, and $\rho_{d_BC-coat}$ are assumed. In addition, the dry refractive indices $n_{d_BC-free}$, $n_{BC-core}$, and $n_{d_BC-coat}$ at $\lambda = 1064$ nm are assumed in the data-processing procedure outlined in Figure 2.13.

Determination of D for BC-free and BC-containing particles is based on Mie theory for spheres and coated spheres, respectively.

The measurement uncertainties due to these assumptions can be estimated by changing the assumed values of the densities and refractive indices within their possible ranges and reanalyzing the raw data obtained by the APM–hSP2 system. The particle densities of AS aerosol and ammonium nitrate aerosol, which are typical inorganic aerosols in the atmosphere, are 1.77 and 1.72 g cm⁻³, respectively. Although atmospheric organic aerosols include numerous kinds of species, literature values suggest that 1.2 g cm⁻³ is a reasonable estimate for the organic aerosol density [Turpin and Lim, 2001, and references therein]. McMurry et al. [2002] measured the densities of urban aerosol particles of size ~100 and ~300 nm to be 1.54–1.77 g cm⁻³, depending on the abundance of organic and inorganic aerosols during the observation period. Considering these previous studies, $\rho_{BC-free} = \rho_{BC-coat} = 1.5$ g cm⁻³ was used as a standard assumption in analyzing the ambient data obtained by the APM–hSP2 system. A value of $\rho_{BC-core} = 1.8$ g cm⁻³ was assumed for the BC core, based on Moteki et al. [2010] and references therein. The uncertainty in the assumed BC-core density was estimated to be ±5%.

The real part of the refractive index of AS at near-infrared wavelength is 1.50–1.53 [Toon et al., 1976]. According to Hess et al. [1998], the real part of the refractive index of water-soluble and water-insoluble aerosols (excluding BC and dust) at $\lambda = 1000$ nm is 1.52. On the basis of reported values of refractive indices at various wavelengths [e.g., Stelson, 1990; Ebert et al., 2002], the real part of the refractive index of BC-free particles is likely within the range 1.43–1.58. Taking these reported values into consideration, $n_{d_BC-free} = n_{d_BC-coat} = 1.52 + 0i$ was assumed in analyzing ambient APM–hSP2 data. Using an APM and SP2, Moteki et al. [2010] reported $n_{BC-core} = (2.26 \pm 0.13) + (1.26 \pm 0.13)i$ from measurements of ambient BC in Tokyo. This value was used for the analysis of ambient data.

Figure 2.16 shows time series of median GF at 85% RH and median hygroscopicity parameter κ for ambient BC-free particles measured by the APM–hSP2 method under the various assumptions. Data were collected on 8 August 2014 in Tokyo during a field campaign (details of this campaign are described in Chapter 3). The sensitivities of the assumed density and refractive index of the BC-free particles to the measured hygroscopic growth were tested by changing the assumed density by $\pm 20\%$ from the standard value or by setting a low refractive index of $1.45 + 0i$. The measured GF and κ can be shifted by about ± 0.1 ($\pm 25\%$) by changing the assumed $\rho_{BC-free}$. The effects of the assumed $n_{d_BC-free}$ on measurements were relatively small.

Figure 2.17 shows time series of median GF at 85% RH for ambient BC-containing particles with dry shell/core ratios of 1.95–2.25 and 1.26–1.46. In addition to the effects of changing the assumed density and refractive index of the BC coating on GF measurements, the effects of the newly assumed refractive index of the BC core ($n_{BC-core} = 2 + 1i$) were evaluated. For BC-containing particles with dry

shell/core ratios of 1.95–2.25, changing the assumed density by $\pm 20\%$ from the standard value caused a shift in the measured GF of ± 0.1 ($\pm 25\%$), which is greater than the shift

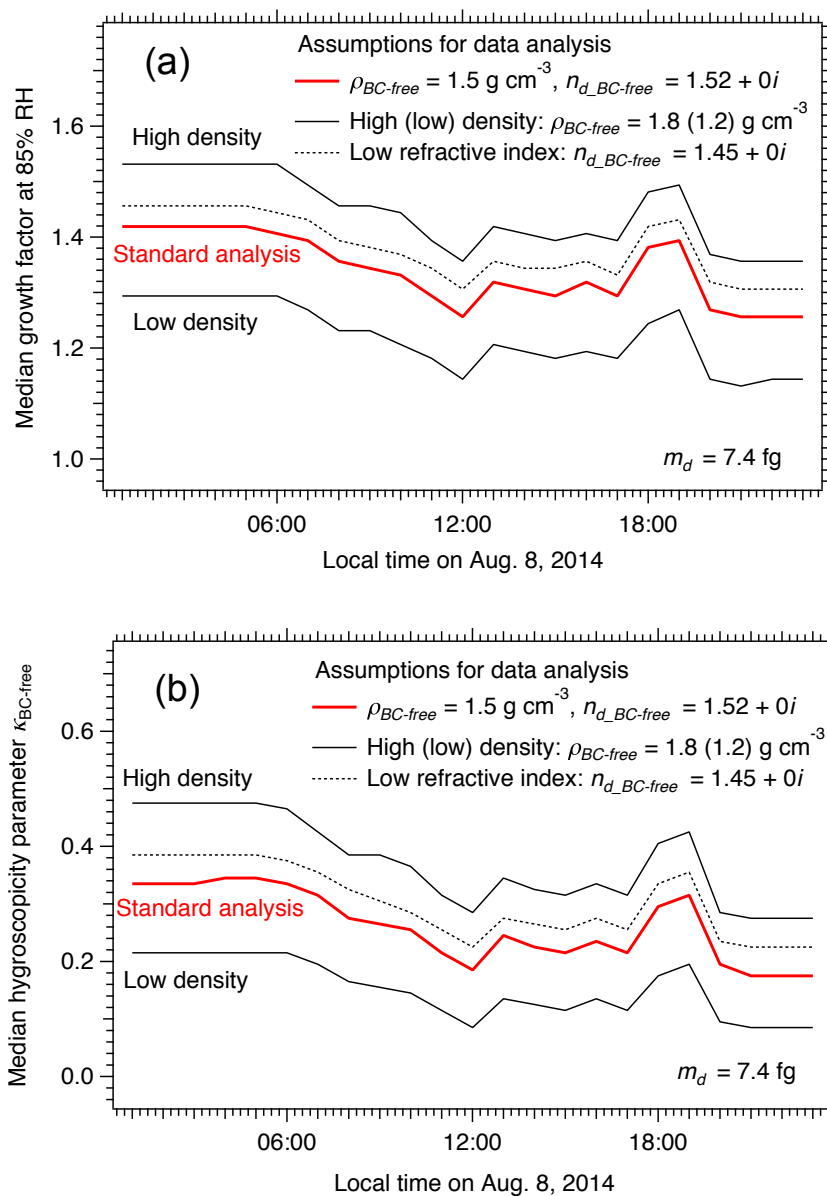


Figure 2.16. Time series of (a) median GF at 85% RH and (b) median hygroscopicity parameter κ for ambient BC-free particles measured by the APM–hSP2 method under various assumptions. Data were collected on 8 August 2014 in Tokyo. m_d was set at 7.4 ± 1.2 fg ($D_d \sim 200$ nm) by the APM.

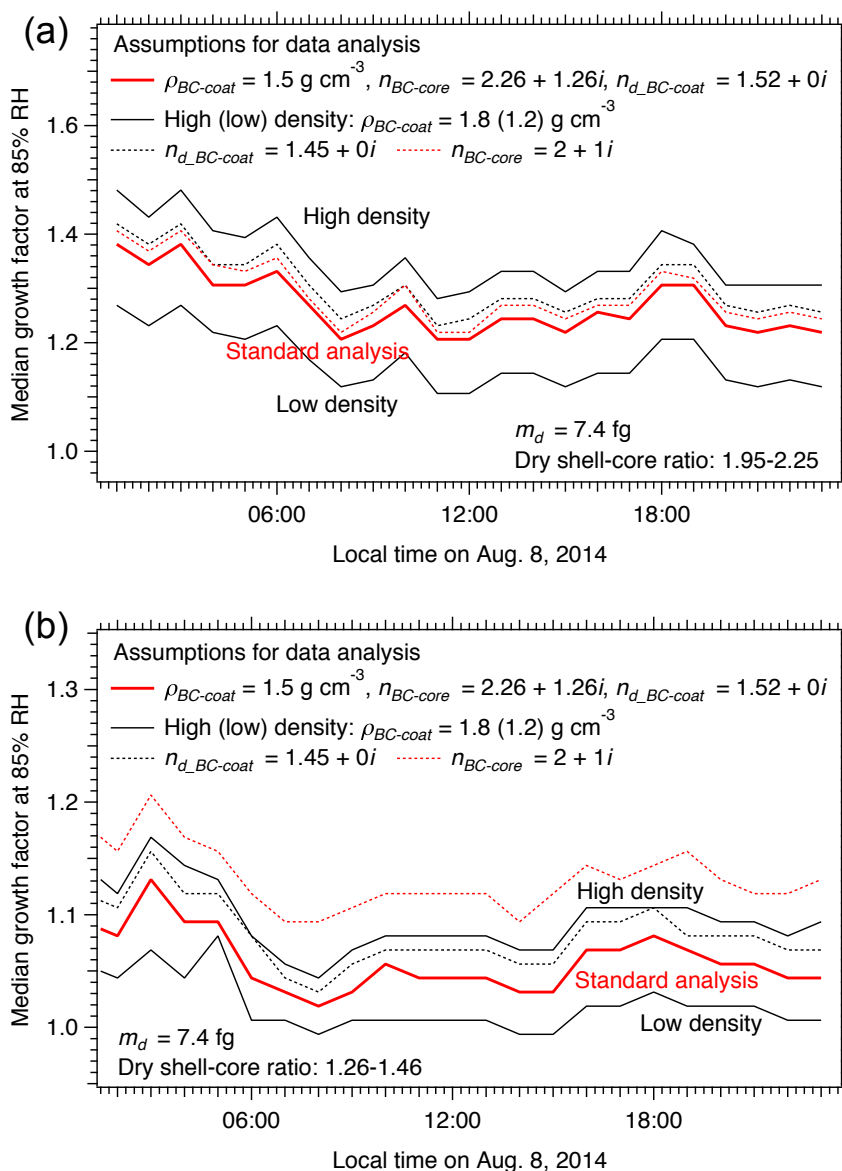


Figure 2.17. Time series of median GF at 85% RH for ambient BC-containing particles with dry shell/core ratios of (a) 1.95–2.25 and (b) 1.26–1.46 measured by the APM–hSP2 method under various assumptions. Data were collected on 8 August 2014 in Tokyo. m_d was set at 7.4 ± 1.2 fg ($D_d \sim 200$ nm) by the APM.

due to the change in the assumed refractive indices of the BC core and BC coating. For BC-containing particles with dry shell/core ratios of 1.26–1.46, the measured GF was

more sensitive to the assumed $n_{\text{BC-core}}$ than to the assumed $\rho_{\text{BC-coat}}$ and $n_{\text{d_BC-coat}}$.

In addition to measurement uncertainties due to the assumed densities and refractive indices, the assumption of the shape of the BC-coating particles (that is, the core-shell model) can also cause uncertainty, as discussed in section 2.4.3. For thinly coated BC particles with dry shell/core ratios of 1.07–1.23, the uncertainty in the measured GF was estimated to be $\pm 80\%$ from the difference between the laboratory experimental data and the theoretically predicted growth at 85% RH. For BC-containing particles with dry shell/core ratios greater than 1.4, the measurement uncertainty due to the core-shell model was estimated to be less than $\pm 25\%$.

The newly developed APM-hSP2 system enables simultaneous, independent measurement of the hygroscopic growth of BC-containing and BC-free particles. Although the output data from the APM-hSP2 system are similar to those from the HTDMA-SP2 system, there are several differences between the systems' data-processing procedures and the assumptions used to derive the particle hygroscopic growth. Whereas the GF measured by the HTDMA-SP2 is based on the mobility diameters of dry and humidified particles, the GF measured by the APM-hSP2 is based on the mass-equivalent and optical diameters of dry and humidified particles. To derive the GF of BC-containing particles as a function of the dry shell/core ratio, the HTDMA-SP2 assumes an effective density of the BC core, which depends on particle shape. If the particle shape becomes compact in the humidification system in the HTDMA, the measured GF can be underestimated. For the APM-hSP2 system, the uncertainty due to particle shape is related to the core-shell assumption. For both systems, the measured hygroscopic growth for thinly coated BC particles tends to be highly uncertain, in contrast to the case for thickly coated BC particles. Concerning the

time resolution of the measurements, the APM–hSP2 has an advantage over the HTDMA–SP2 because of rapid optical sizing of the humidified particles by the h-SP2. Although the time resolution depends on particle number concentration in the sample air, the APM–hSP2 generally provides 1-min data of the hygroscopicity distribution of the BC-free particles. The HTDMA–SP2 requires more than 10 min to obtain the data, depending on the setting of the time step for sizing the humidified particles by the second (scanning) DMA and the condensation particle counter/SP2.

To quantify the hygroscopic growth of BC-containing particles, the h-SP2 can be coupled with a standard SP2, instead of being coupled with the APM. Schwarz et al. [2014] has recently developed a new measurement system using two SP2s (one dry and the other humidified). In this system, the two SP2s measure sample air in parallel. For the BC-containing particles with a specific BC-core mass, water uptake of the particles is detected by comparing the scattering signals between the two SP2s. Although this system generally cannot measure the hygroscopic growth of BC-free particles, it enables high time-resolved measurement of the hygroscopicity of BC-containing particles, which is suitable especially for aircraft observation.

2.5. Summary

In this chapter, a humidified-SP2 (h-SP2) developed by modifying a standard SP2 was described. Under controlled RH, the h-SP2 quantified the BC mass and the amount of coating material within individual aerosol particles by detecting both the laser-induced incandescence emitted and the laser light scattered from each BC-containing particle. The RH of the sample air and sheath air in the h-SP2 was controlled by humidification units with Nafion tubes, and a control software program was developed. The sample air

RH and sheath air RH were automatically stabilized to within about $\pm 0.3\%$ RH.

Separate measurements of hygroscopic growth of BC-free and BC-containing particles could be achieved by combining an APM with the newly developed h-SP2.

The h-SP2 was tested in the laboratory using both homogeneous AS and internally mixed particles of BC (FS) and AS. These particles were dried and classified by the APM and subsequently measured by the h-SP2 between 60% and 90% RH. A core-shell geometry was assumed for the BC-containing particles, and the reduction in the refractive index of the BC-free particles and BC-coating materials due to their hygroscopic growth was taken into account. Although the measured growth factors of laboratory-generated, thinly coated BC particles tend to have large uncertainties partly because of the assumption of a core-shell structure, the measured growth factors of the pure AS and thickly coated BC particles agreed well with growth factors predicted by κ -Köhler theory to within measurement uncertainty, demonstrating the applicability of the h-SP2 for ambient measurements.

3. Field Observation of the Hygroscopicity and Wet Removal of Particles Containing Black Carbon in Tokyo Air

3.1. Introduction

Megacities are very large, concentrated anthropogenic sources of black carbon (BC) [e.g., Bond et al., 2013, and references therein]. Freshly emitted BC particles inside megacities not only affect local air quality but can influence regional and global climate. The microphysical properties (e.g., number size distribution, coating thickness, and hygroscopicity) of atmospheric BC-containing particles are important because their transport in, and efficiency of wet removal from, the atmosphere can be highly dependent on these properties. Once vertically transported from the atmospheric boundary layer to the free troposphere, BC-containing particles are unlikely to encounter a cloud precipitation process. Thus they can have a relatively long atmospheric lifetime and be transported to remote areas such as polar regions, where BC particles deposited in or on snow can reduce surface albedo.

BC-containing particles in the atmosphere of Tokyo, a Japanese megacity, have been investigated in previous studies. Diesel emissions have been identified as a major source of BC in Tokyo [Kondo et al., 2006], and thinly coated BC particles ($SCr \sim 1.1$; SCr is the dry shell/core ratio) were found to be dominant in August and September in 2009 [Kondo et al., 2011b]. Kuwata et al. [2009] measured the dependence of cloud condensation nuclei (CCN) activity of BC-containing particles on the mass of condensed compounds. Moteki et al. [2014] classified BC-containing particles into two

morphological types (i.e., attached type and coated type) and showed that the number fraction of attached-type particles was generally less than 0.1 in August 2012. However, the behavior of BC-containing particles in the urban atmosphere, including that of Tokyo, has not been fully characterized, especially in terms of their hygroscopicity and wet removal from the atmosphere.

The efficiency of wet removal of BC-containing particles depends on their hygroscopicity (CCN activity) and the atmospheric supersaturation (SS) that the particles experience during their upward transport. The hygroscopicity of BC-containing particles is controlled by their coating thickness and composition, which can be quantified by the newly developed APM–hSP2 system described in Chapter 2. On the other hand, direct information on BC-containing particles that have served as CCN and then been removed from the atmosphere via precipitation can be obtained by the number size distribution of BC particles suspended in rainwater samples. The number size distribution of BC particles in rainwater can be measured by the technique described and evaluated in Chapter 4. BC particles in rainwater can also be used as a particle tracer to investigate the properties of CCN-activated aerosols, including BC-free particles, because (1) BC particles (BC cores) are chemically inert, (2) BC particles are not produced in the cloud precipitation process, (3) coagulation of BC particles is believed to be negligible during a short-term precipitation process (experimentally supported in section 4.4.1 of Chapter 4), and (4) below-cloud scavenging of BC-containing particles with diameters of 0.05–1 μm by falling raindrops is not efficient [Slinn, 1983; Seinfeld and Pandis, 2006].

Measuring the hygroscopicity of BC-containing particles in the air surrounding a megacity and determining the efficiency of their wet removal are crucial to quantitative

understanding of the long-distance transport and lifetime of BC-containing particles in the atmosphere. The objectives of this chapter include characterizing the coating thickness and hygroscopicity of BC-containing particles in the atmosphere of Tokyo during the summer and quantifying the efficiency of wet removal of BC-containing particles as a function of BC-core diameter. These data will be useful for directly assessing previously proposed model schemes related to wet removal of aerosols.

In section 3.2, the observation site and experimental setup are described. Results for the measured hygroscopicity and wet removal of BC-containing particles are presented and discussed in section 3.3. The chapter is summarized in section 3.4.

3.2. Observation Site and Experimental Setup

Intensive measurements of BC-containing particles both in the surface air and in rainwater were made during the field campaign BC-CARE Tokyo (Black Carbon/Carbonaceous Aerosol Removal Experiment in Tokyo). The observation period was from 28 July through 15 August 2014 (20 days). Sample air was aspirated from the sixth floor and rooftop of Science Building 1 (about 20 and 40 m above ground level, respectively) at the Hongo campus of The University of Tokyo (35.71°N, 139.76°E). The observatory is located near the urban center of Tokyo and is about 10 km northwest of the Tokyo Bay coastline. This observatory is located in the highest carbon monoxide emission region in the Tokyo Metropolitan Area [Kondo et al., 2006; Figure 2].

The principal instruments employed during BC-CARE Tokyo were a standard single-particle soot photometer (SP2 or “dry-SP2” for clarity in this chapter), a humidified-SP2 (h-SP2), a wide-range SP2, and a quadrupole aerosol mass spectrometer (AMS). Measurement parameters for these instruments are summarized in

Table 3.1. The description of the dry-SP2 is given in section 2.2 of Chapter 2. The h-SP2 was coupled with an aerosol particle mass analyzer (APM) to quantify the hygroscopic growth of aerosols (dry diameter ~ 200 nm) at 85% relative humidity (RH). The experimental setup of the APM–hSP2 system was the same as that described in section 2.4 of Chapter 2. The wide-range SP2 is an SP2 with modified optical detectors to measure BC particles up to about 4000 nm in diameter. Coupling the wide-range SP2 with a nebulizer (Marin 5, Cetac Technologies Inc., Omaha, NE, USA) allowed measurements of the number and mass size distributions of BC particles suspended in

Table 3.1. Principal instruments employed for atmospheric and precipitation measurements during the BC-CARE Tokyo campaign.

	Instrument	Measurement parameters
Atmospheric measurement	Dry-SP2 (standard SP2)	Number and mass size distributions of BC cores ($70 < D_{\text{BC-core}} < 850$ nm), dry shell/core ratio ($D_{\text{BC-core}} > \sim 200$ nm)
	Humidified-SP2 (APM–hSP2)	Growth factor at 85% RH and hygroscopicity parameter κ of BC-free and BC-containing particles ($D_d \sim 200$ nm)
	AMS	Chemical composition (excluding BC) of PM1 aerosols
Precipitation measurement ^a	Precipitation sampling system	Precipitation rate, automatic nebulization of rainwater samples for extracting BC particles from rainwater to the air
	Wide-range SP2	Number and mass size distributions of BC cores in rainwater ($70 < D_{\text{BC-core}} < 4000$ nm)

^aSee Chapter 4, Appendix 4A.

rainwater. Details of the measurement system are described in Appendix 4A of Chapter 4. The AMS measures the chemical composition of nonrefractory (vaporized at 600 °C under high vacuum) submicron aerosols [Jayne et al., 2000]. AMS data were used to interpret the mixing state and hygroscopicity of BC-containing particles measured by the dry-SP2 and h-SP2.

3.3. Results and Discussion

3.3.1. Microphysical Properties of BC-Containing Particles

3.3.1.1. Hygroscopicity

Figure 3.1 shows time series of the median growth factors (GFs) of BC-free and BC-containing particles during the observation period. The GFs of the BC-containing particles in Figure 3.1 were segregated by dry shell/core ratio (SCr), which was derived from the APM-selected total dry mass of the individual BC-containing particles (m_d) and the SP2-incandescence-derived masses of the BC cores ($m_{\text{BC-core}}$). Thinly coated BC particles with $\text{SCr} = 1.08\text{--}1.26$ showed no detectable hygroscopic growth, whereas thickly coated BC particles with $\text{SCr} = 1.69\text{--}1.95$ showed hygroscopic growth with GFs of ~ 1.2 . The measured GFs of the thickly coated BC particles generally fell between those of thinly coated BC particles and those of BC-free particles. This is the first simultaneous, independent measurement of the detailed temporal variations of the hygroscopic growth of BC-free and BC-containing particles in Tokyo air.

The 1-h histograms of the measured GFs of the BC-free and BC-containing particles were bimodal, and the fractions in the second mode ($\sim 10\%$ to total) were multiply charged particles that had passed through the APM; therefore, the number fractions of particles with the top 10% GFs were removed to determine the median GFs

for the BC-free and BC-containing particles.

Figure 3.2 shows histograms of the median GFs of BC-free and BC-containing particles during the observation period. More thickly coated BC particles tended to have greater hygroscopicity, and BC-free particles were the most hygroscopic. The number fraction of BC-containing particles with low hygroscopic growth ($GF < 1.2$) was related to the number fraction of thinly coated BC particles ($SCr < 1.2$) measured by the dry-SP2 (section 3.3.1.2). Figure 3.3 shows the average GF distributions of BC-free and BC-containing particles during the observation period. The number fraction of BC-containing particles was about 10% of the total (BC-free + BC-containing) particles of $D_d \sim 200$ nm. Particles with low hygroscopic growth ($GF < 1.2$) and with $GF = 1.2$ – 1.5 were dominant for BC-containing particles and BC-free particles, respectively.

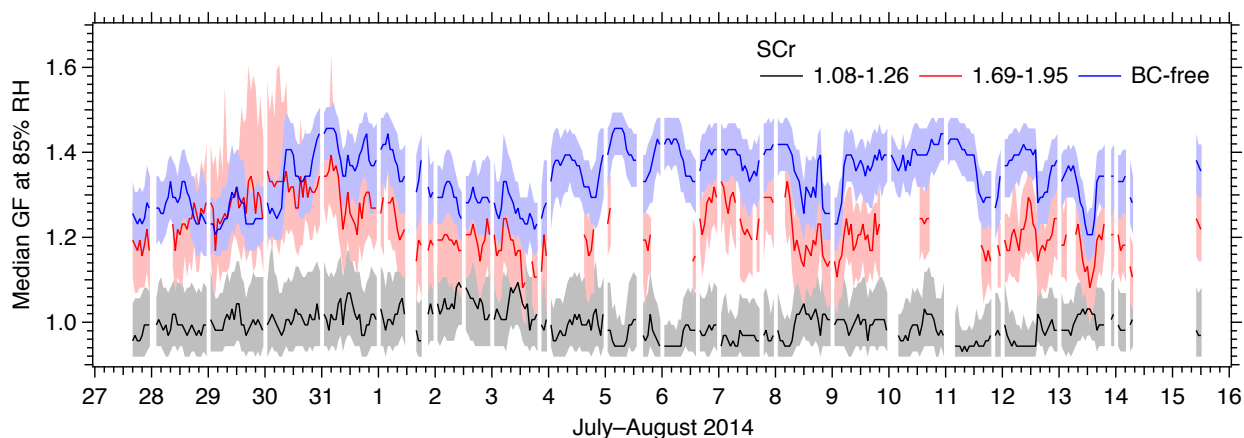


Figure 3.1. Time series (1-h data) of GFs at 85% RH for BC-free and BC-containing ($SCr = 1.08$ – 1.26 and 1.69 – 1.95) particles. m_d was set at 7.4 fg ($D_d \sim 200$ nm) by the APM. Solid lines show median GFs. Shading shows the range of the 25th–75th percentile. Data were not obtained during instrument maintenance. For statistical reasons, data were not available when the number of particles detected in an hour was less than 50.

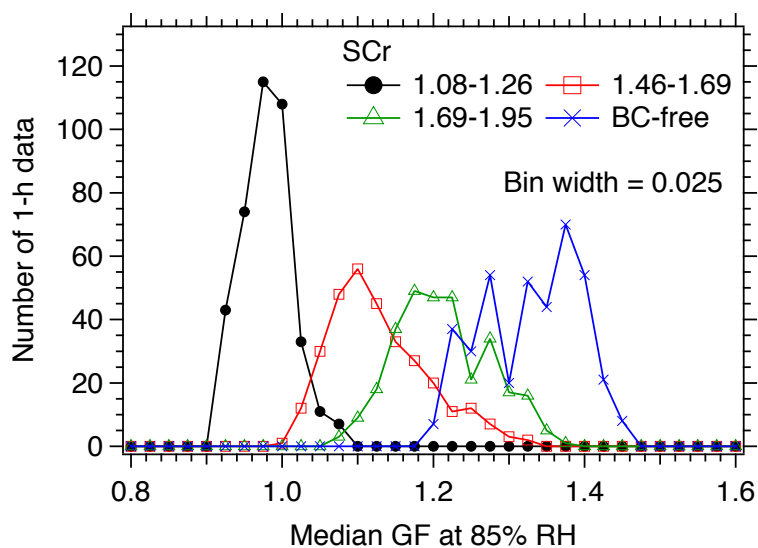


Figure 3.2. Histograms of 1-h data of the median GFs at 85% RH for BC-free and SCr-segregated BC-containing particles during the observation period.

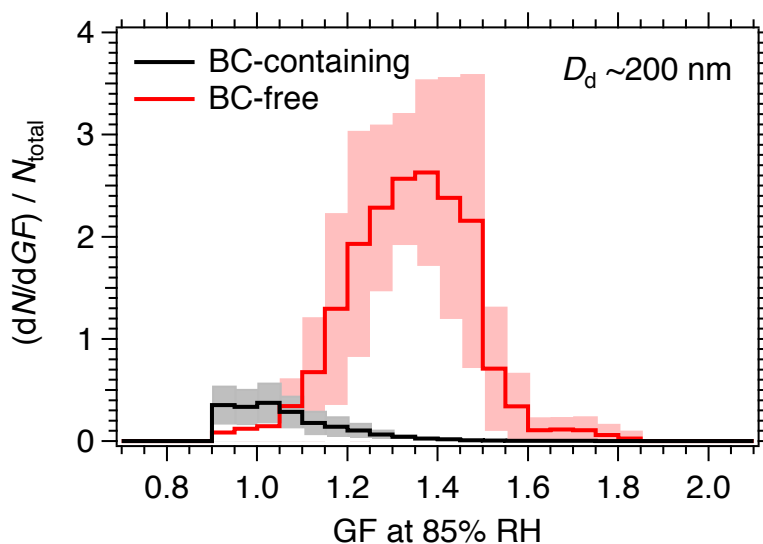


Figure 3.3. Normalized GF distributions (1-h data) of BC-free and BC-containing particles averaged over the observation period. N_{total} is the total (BC-free + BC-containing) number concentration of the particles with $D_d \sim 200$ nm. Shading shows the range of $\pm 1\sigma$.

Figure 3.4a shows the time variation of the distribution of the measured hygroscopicity parameter of BC-free particles ($\kappa_{\text{BC-free}}$). The median $\kappa_{\text{BC-free}}$ values (0.2–0.4) fell between the κ value for pure ammonium sulfate (0.53) and the κ values for some typical secondary organic aerosols (0.05–0.2) [e.g., Huff Hartz et al., 2005; VanReken et al., 2005; Petters and Kreidenweis, 2007; King et al., 2009]. This result indicates that the BC-free particles tended to be internally mixed with inorganic and organic aerosols. The APM–hSP2 system measures $\kappa_{\text{BC-free}}$ on a single-particle basis and thus provides information on the mixing states of the BC-free particles. This

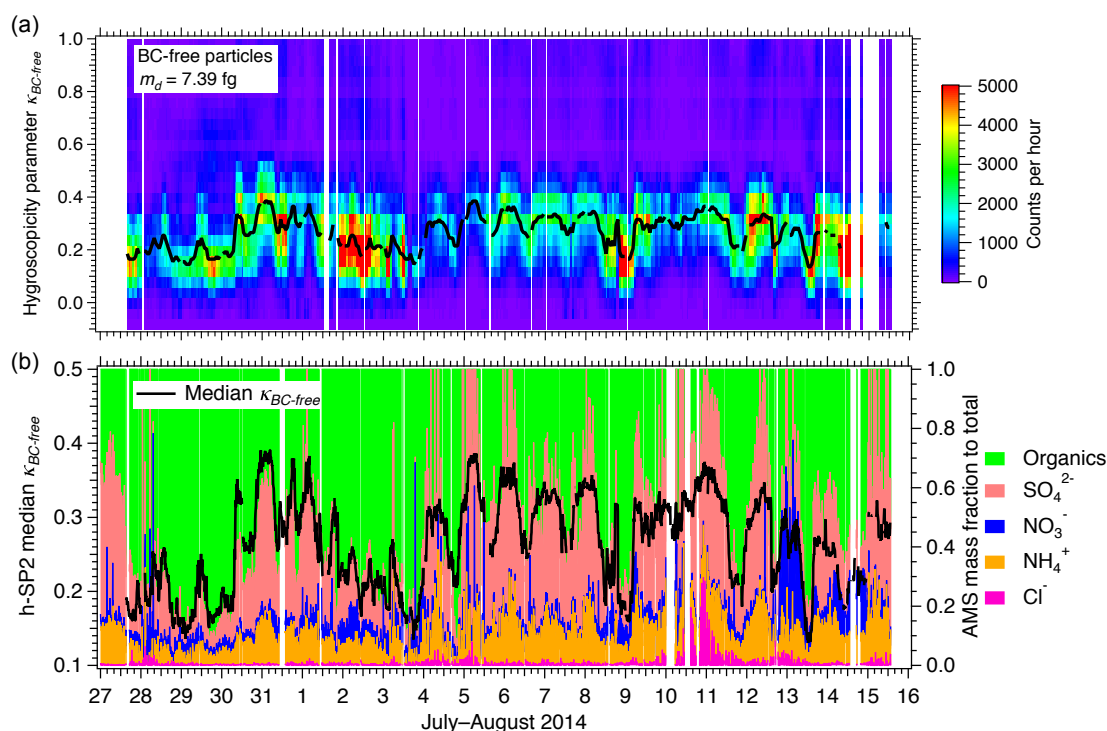


Figure 3.4. (a) Temporal variation (1-h data) of the distribution of the hygroscopicity parameter $\kappa_{\text{BC-free}}$. The black line shows the median value. (b) Temporal variation (10-min data) of median $\kappa_{\text{BC-free}}$ and mass fractions of organics, SO_4^{2-} , NO_3^- , NH_4^+ , and Cl^- in the total mass of PM1 aerosols.

information is not obtained by bulk measurement of the aerosol chemical composition by the standard AMS method used in this study. In Figure 3.4b, the time series of the median $\kappa_{\text{BC-free}}$ measured by the h-SP2 is compared with that of the mass fraction of each composition (organics and inorganics) measured by the AMS. The median $\kappa_{\text{BC-free}}$ corresponded well with the mass fraction of organic aerosols in the total mass of PM1 aerosols, confirming that the newly developed APM–hSP2 system has an excellent sensitivity to changes in chemical composition of the sampled aerosols. Figure 3.5 shows a scatter plot of the AMS-derived organic mass fraction and the h-SP2-derived 25th-percentile, median, and 75th-percentile $\kappa_{\text{BC-free}}$ values. When the mass fraction of organics was dominant, the value of $\kappa_{\text{BC-free}}$ ranged from about 0.1 to 0.25. In contrast,

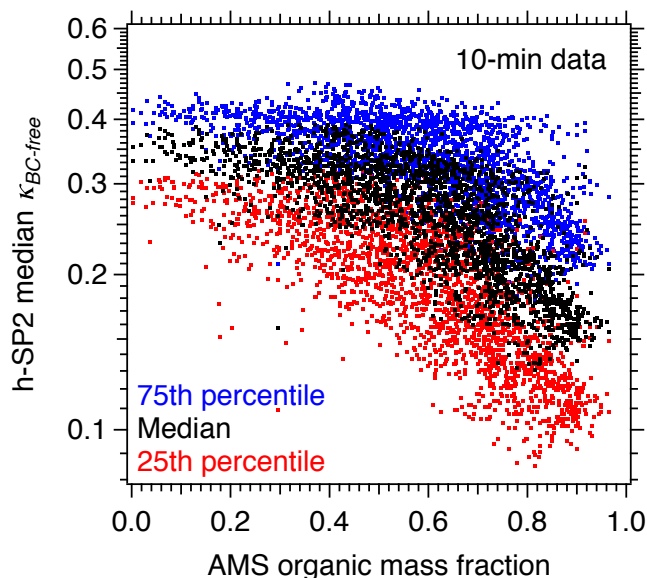


Figure 3.5. Scatter plot of the AMS-derived organic mass fraction and the h-SP2-derived 25th-percentile, median, and 75th-percentile $\kappa_{\text{BC-free}}$ (10-min data) during the observation period.

when the mass fraction of inorganics was dominant, the value of $\kappa_{\text{BC-free}}$ ranged from about 0.3 to 0.45. BC-free particles with a large organic fraction tended to have a low hygroscopicity, as expected from the above-mentioned values of $\kappa_{\text{BC-free}}$ for pure organic and inorganic aerosols.

Given the densities (ρ_{org} , ρ_{inorg}) and hygroscopicity parameters (κ_{org} , κ_{inorg}) of organics and inorganics, the values of $\kappa_{\text{BC-free}}$ can be estimated from the bulk chemical composition measured by the AMS, because BC-free particles tended to be internally mixed with organic and inorganic aerosols (Figure 3.4). Under the simple assumptions that inorganic materials are composed of ammonium sulfate ($\rho_{\text{inorg}} = 1.77 \text{ g cm}^{-3}$, $\kappa_{\text{inorg}} = 0.53$), and that $\rho_{\text{org}} = 1.2 \text{ g cm}^{-3}$ and $\kappa_{\text{org}} = 0.12$, the AMS-estimated $\kappa_{\text{BC-free}}$ agreed

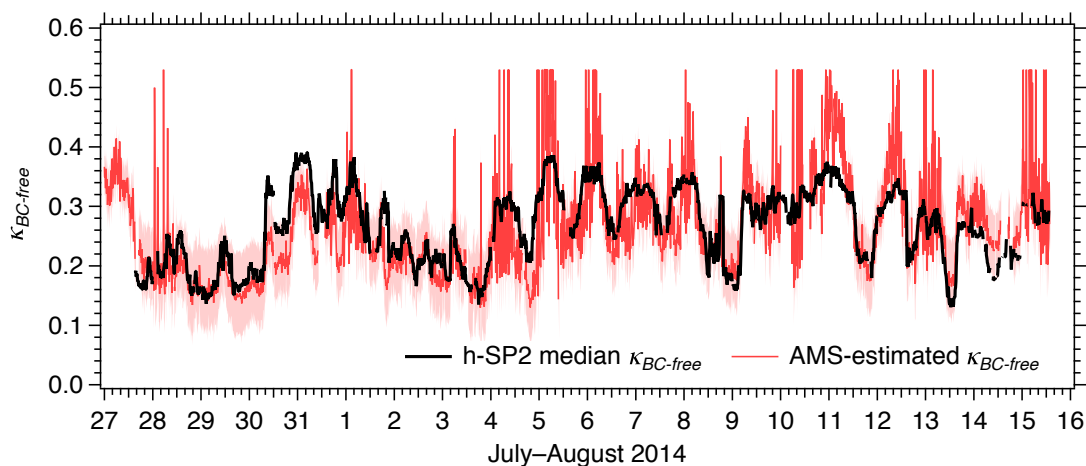


Figure 3.6. Temporal variation (10-min data) of the measured and estimated hygroscopicity parameter $\kappa_{\text{BC-free}}$. The black line shows the median $\kappa_{\text{BC-free}}$ values measured by the h-SP2. The red line shows the $\kappa_{\text{BC-free}}$ values estimated from chemical composition measured by the AMS, assuming that $\rho_{\text{inorg}} = 1.77 \text{ g cm}^{-3}$, $\kappa_{\text{inorg}} = 0.53$, $\rho_{\text{org}} = 1.2 \text{ g cm}^{-3}$ and $\kappa_{\text{org}} = 0.12$. Shading shows the range of estimated $\kappa_{\text{BC-free}}$ values under the assumption of $\kappa_{\text{org}} = 0.05\text{--}0.2$.

well with the median $\kappa_{\text{BC-free}}$ measured by the h-SP2, as shown in Figure 3.6. If the values ρ_{inorg} , κ_{inorg} , and ρ_{org} are fixed, the assumed κ_{org} value of 0.05–0.2 explained the h-SP2 median $\kappa_{\text{BC-free}}$ to within $\pm 20\%$.

The measured $\kappa_{\text{BC-free}}$ values were then compared with measured κ values of BC-coated materials ($\kappa_{\text{BC-coat}}$) to investigate differences between their chemical compositions. Values of $\kappa_{\text{BC-coat}}$ were derived from BC-containing particles with $\text{SCr} = 1.95\text{--}2.25$, because the uncertainty in the measured hygroscopic growth of thickly coated BC particles is relatively low (Chapter 2, section 2.4). Figure 3.7 shows the histogram of the ratio of the median $\kappa_{\text{BC-coat}}$ to the median $\kappa_{\text{BC-free}}$ obtained during the observation period. Values of the $\kappa_{\text{BC-coat}}/\kappa_{\text{BC-free}}$ ratio predominantly ranged from 0.7 to 1.1. Because the median $\kappa_{\text{BC-coat}}/\kappa_{\text{BC-free}}$ ratio for laboratory-generated, internally-mixed particles of fullerene soot and ammonium sulfate was measured as 0.83 (that is, $\kappa_{\text{BC-coat}}$ tended to be underestimated by 17%), the ratio obtained during the field observation indicates that the BC-coated materials and BC-free particles generally had similar chemical compositions. However, the median $\kappa_{\text{BC-coat}}/\kappa_{\text{BC-free}}$ ratio occasionally reached ~ 1.7 , when the lowest correlation between the measured mass concentration of BC and that of organic aerosols was observed. It was assumed that the emission sources of BC and organic aerosols were quite different during this poor-correlation period and furthermore that the BC and organic aerosols tended to be externally mixed. The APM–hSP2 system thus provided information on the composition of BC-coated materials in terms of their hygroscopicity. Another approach for quantifying the composition of BC-coated materials has involved the use of SP–AMS [Onasch et al., 2012] and LI–MS [Miyakawa et al., 2014] systems.

Measurement data of $\kappa_{\text{BC-coat}}$ as a function of SCr are not presented in this study

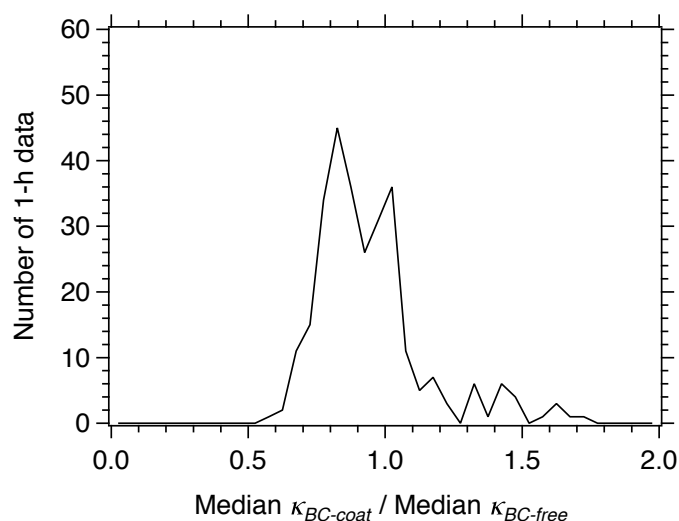


Figure 3.7. Histogram of the ratio of median $\kappa_{BC-coat}$ to median $\kappa_{BC-free}$ during the observation period.

because of the relatively large uncertainty in the measurement of the hygroscopic growth for thinly coated BC particles. Potentially, thin coatings might tend to be primary organic aerosols emitted together with BC particles, but so far, estimating chemical compositions of the thin coatings with the current APM–hSP2 system has been difficult.

3.3.1.2. Dry Shell/Core Ratio

The distribution of the dry shell/core ratio of BC-containing particles was measured for several ranges of BC-core size: 186–214, 214–245, 245–282, 282–324, and 324–372 nm. Figure 3.8 shows time variations of the median SCr for two different ranges of BC-core size. Additionally, Figure 3.9 shows histograms for the median SCr and the number fraction of thickly coated BC particles ($SCr > 1.2$). The temporal variation of

the median SCr was not significantly different among the BC-core sizes. Throughout the observation period, the median SCr predominantly ranged from 1.0 to 1.1, except for the aged air observed during 29–31 July. The number fraction of BC-containing particles with $SCr > 1.2$ was generally 0.1–0.4. Because BC particles become internally mixed with other aerosols on a time scale of about a half a day to a few days in urban plumes [Moteki et al., 2007; Riemer et al., 2010], the results in Figures 3.8 and 3.9 indicate that most of the BC-containing particles observed in Tokyo air in the summer of 2014 were freshly emitted BC particles and thus were generally bare or thinly coated ($SCr < 1.2$).

The ratio of the mass concentration of organic or inorganic aerosols to the BC-core mass concentration can be an indicator of the secondary formation of organic or inorganic aerosols. Figure 3.10 shows time series of AMS-measured ratios for organics, SO_4^{2-} , and NO_3^- . Figure 3.10 also shows time series of the dry-SP2-measured

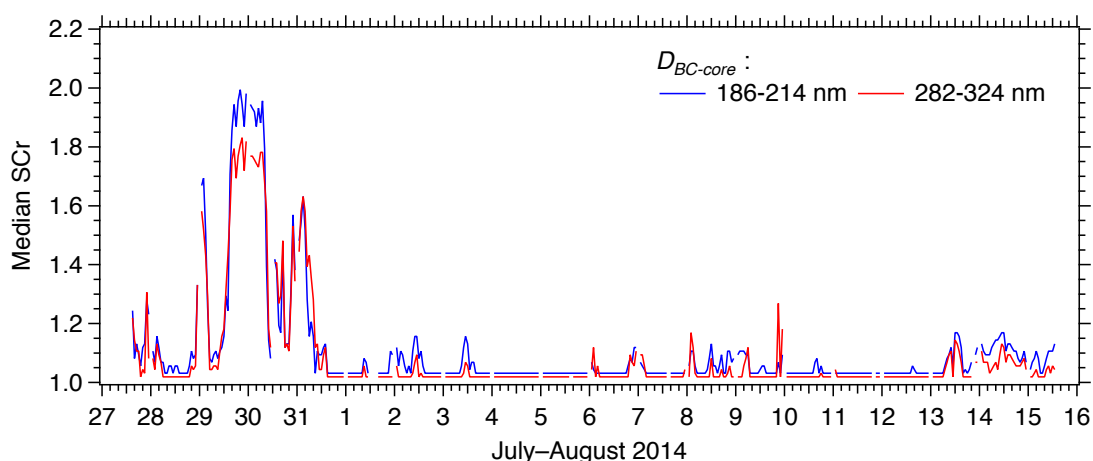


Figure 3.8. Time series (1-h data) of the median SCr for BC-containing particles with $D_{BC-core}$ of 186–214 and 282–324 nm.

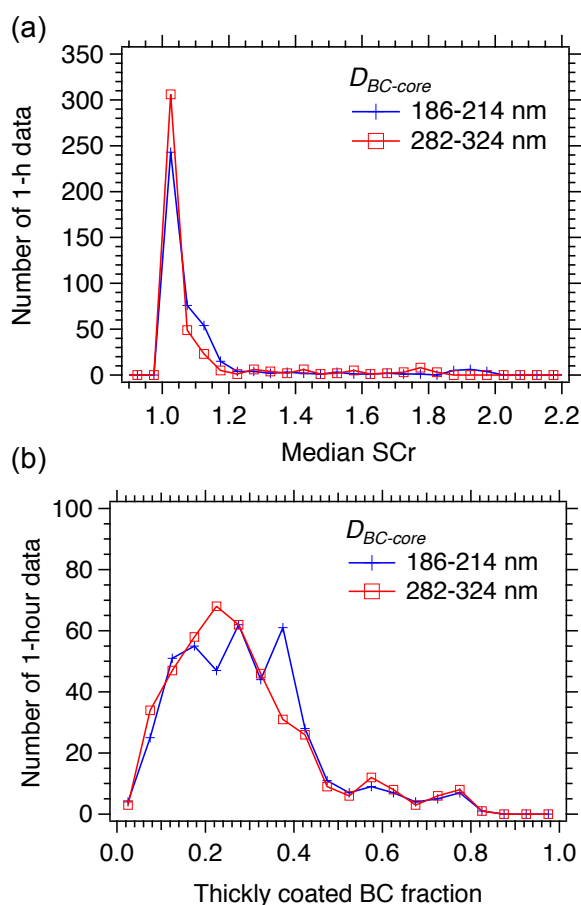


Figure 3.9. Histograms of the median SCr (a) and (b) number fraction of thickly coated BC particles ($SCr > 1.2$) for the $D_{BC-core}$ ranges 186–214 and 282–324 nm.

number fraction of thickly coated BC particles ($SCr > 1.2$) for the $D_{BC-core}$ range 186–214 nm. The temporal variation of the thickly coated BC fraction generally corresponded with that of the organics/BC ratio, SO_4^{2-} /BC ratio, or both. This result qualitatively shows that the number fraction of coated BC particles increased due to secondary formation of other aerosols. Although further analysis of the relationship between the shell/core ratio and the mass concentration ratio is not presented in this study, Shiraiwa et al. [2007] applied positive matrix factorization to data obtained by

the SP2 and AMS at a suburban site 50 km north of Tokyo during July–August 2004. In that study, the organics/BC and $\text{SO}_4^{2-}/\text{BC}$ ratios were reported to predominantly account for the coating thickness of BC particles during the daytime, whereas the NO_3^-/BC ratio was found to contribute substantially to the coating thickness during the nighttime under high-RH conditions.

Figure 3.11 shows both the temporal variation of the dry-SP2-measured number fraction of thinly coated BC particles ($\text{SCr} < 1.2$) for the $D_{\text{BC-core}}$ range 186–214 nm and the temporal variation of the h-SP2-measured number fraction of the less-hygroscopic BC-containing particles ($\text{GF} < 1.2$; corresponding to critical supersaturation (S_c) $> \sim 0.2\%$) with $m_d = 7.4$ fg. The temporal variations generally corresponded with each other, confirming that SCr strongly controls the hygroscopicity of BC-containing particles. Throughout the observation period, the number fraction of the less-hygroscopic BC-containing particles was greater than 0.7. This dominance of thinly

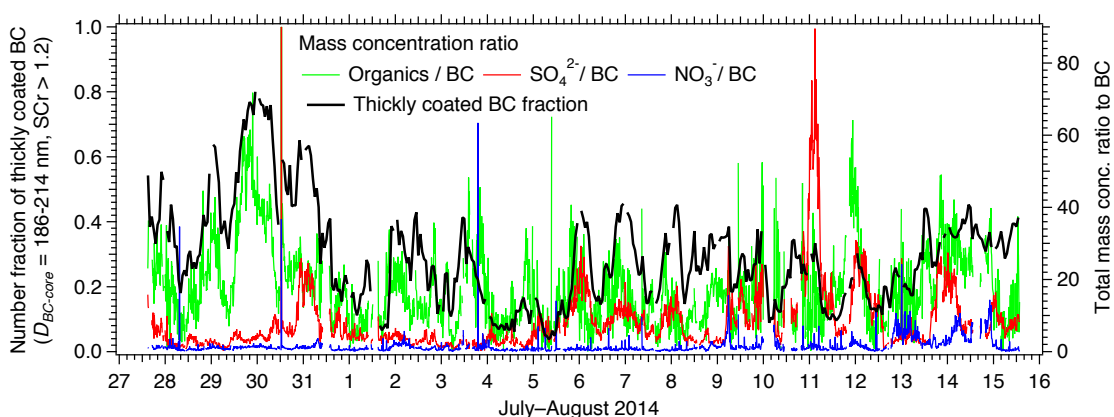


Figure 3.10. Time series of the number fraction of thickly coated BC particles ($\text{SCr} > 1.2$) for the $D_{\text{BC-core}}$ range 186–214 nm and of the organics/BC, $\text{SO}_4^{2-}/\text{BC}$, and NO_3^-/BC mass concentration ratios.

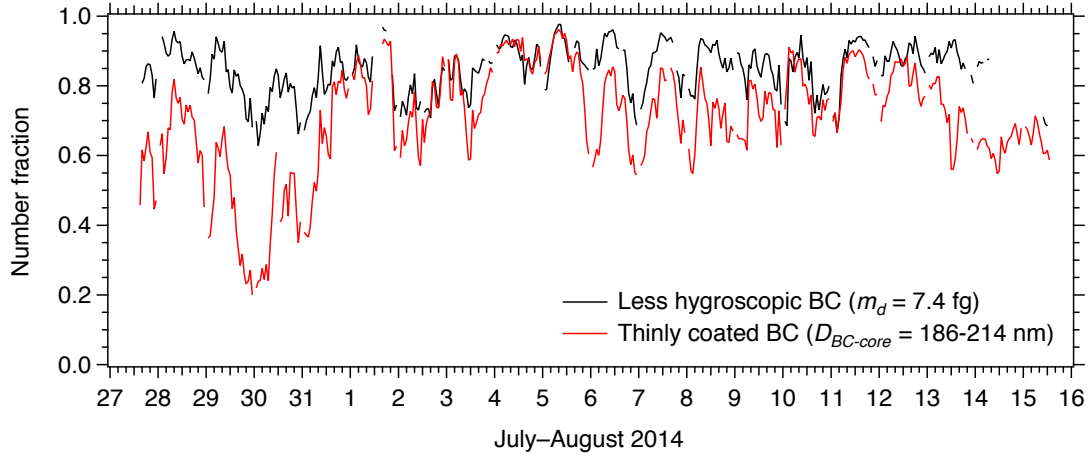


Figure 3.11. Time series of the number fraction of thinly coated BC particles ($SCr < 1.2$) for the $D_{BC-core}$ range 186–214 nm and of the number fraction of less-hygroscopic BC-containing particles ($GF < 1.2$) with $m_d = 7.4$ fg ($D_d \sim 200$ nm).

coated, less-hygroscopic BC particles in Tokyo air is characteristic of BC-containing particles in a megacity.

3.3.1.3. Average Single BC-Core Mass

To represent the average BC-core size measured by the dry-SP2 simply, the average single BC-core mass (m_{BC_ave}) was defined as the ratio of the total BC-core mass concentration to the total BC-core number concentration:

$$m_{BC_ave} = \frac{\int_{70\text{ nm}}^{850\text{ nm}} \frac{dM}{d\log D} d\log D}{\int_{70\text{ nm}}^{850\text{ nm}} \frac{dN}{d\log D} d\log D}, \quad [3.1]$$

where $dN/d\log D$ and $dM/d\log D$ are the number and mass size distributions of BC core,

respectively. The integration interval is the detection range of BC-core size for the dry-SP2. Figure 3.12 shows the temporal variation of $m_{\text{BC_ave}}$. The measured $m_{\text{BC_ave}}$ generally showed a diurnal variation: a small BC core in the daytime and a large BC core at night. An $m_{\text{BC_ave}}$ minimum was frequently observed before noon, probably due to the increase in the emission of fresh (small) BC particles from diesel vehicles in the morning. In the nighttime, the effects of coagulation of BC particles on the size distribution of the BC core may be large compared to the emission effects, and thus the average BC-core size might be larger in the nighttime than in the daytime. The difference between daytime $m_{\text{BC_ave}}$ and nighttime $m_{\text{BC_ave}}$ was about 1 fg, corresponding to a shift in mass-equivalent diameter of about 20 nm. The measured size distribution of the BC core, however, could also be affected by meteorological conditions such as precipitation or wind direction. In fact, $m_{\text{BC_ave}}$ tended to decrease during rain events on August 10 and 14, possibly due to larger BC cores' being

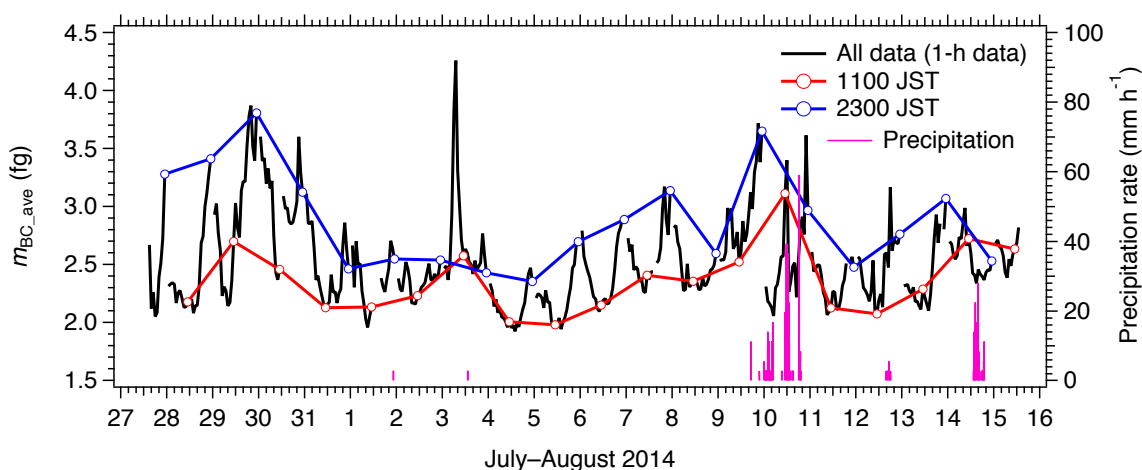


Figure 3.12. Time series (1-h data) of measured $m_{\text{BC_ave}}$ at 11:00 a.m. (red) and 11:00 p.m. (blue). Precipitation rates (10-s data) are also shown.

selectively removed through cloud precipitation processes. The size-dependent wet removal of BC-containing particles is discussed in section 3.3.2.

3.3.2. Wet Removal of BC-Containing Particles

3.3.2.1. Estimates of Critical Supersaturation

To investigate the dependence of the wet removal of BC-containing particles on their BC-core sizes, the temporal variation of the median critical supersaturation (S_c) was estimated from the BC-core-size-segregated median SCr measured by the dry-SP2 and the median $\kappa_{BC-coat}$ measured by the h-SP2. This estimate is based on κ -Köhler theory (Equation [1.10] of Chapter 1; S_c is the maximum value of the Köhler curve). It was assumed that median $\kappa_{BC-coat} = \text{median } \kappa_{BC-free}$, based on the discussion in section 3.3.1.1, and values of the measured median $\kappa_{BC-free}$ were used because the uncertainty in the measurement of $\kappa_{BC-free}$ is less than that of $\kappa_{BC-coat}$. Figure 3.13 shows time series of the median S_c of BC-containing particles with $D_{BC-core}$ of about 200 and 300 nm. Because the temporal variation of the median SCr was not significantly different among the BC-core sizes (Figure 3.8), BC-containing particles with small BC cores had a higher median S_c than did BC-containing particles with large BC cores. Figure 3.14 shows a histogram of the median S_c for different BC-core sizes during the observation period. BC-containing particles with $D_{BC-core}$ of about 350 nm generally serve as CCN at an atmospheric supersaturation (SS) of about 0.14%, whereas BC-containing particles with $D_{BC-core}$ of about 200 nm require an SS of about 0.24% to be CCN-activated. This indicates that the wet removal of BC-containing particles from Tokyo air can be highly dependent on the BC-core size.

During the observation period, seven rain events occurred on 9, 10, and 12

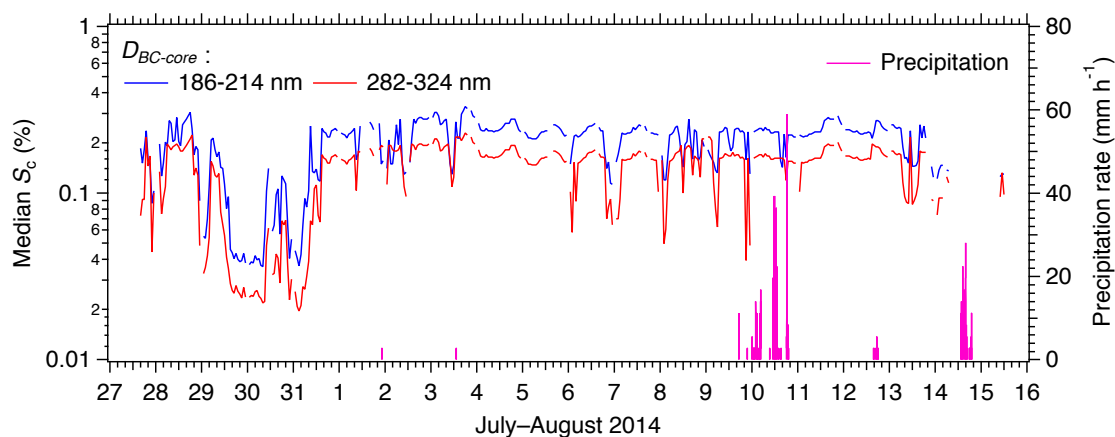


Figure 3.13. Time series (1-h data) of the median S_c of BC-containing particles estimated from the measured SCr and $\kappa_{BC-coat}$. The diameters of the BC cores are 186–214 and 282–324 nm. Precipitation rates (10-s data) are also shown.

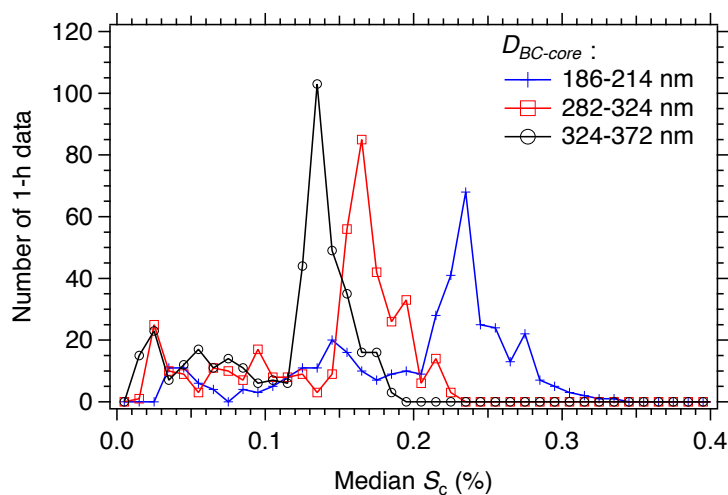


Figure 3.14. Histogram of the median S_c of BC-containing particles with $D_{BC-core}$ ranges of 186–214, 282–324, and 324–372 nm during the observation period.

August. Because the precipitation was convective rain or cyclonic rain associated with a depression or a front, BC-containing particles in the surface air (at the bottom of the atmospheric boundary layer) measured 1 h before precipitation began can be regarded as the particles that would be removed or vertically transported through subsequent cloud precipitation processes. In other words, it was assumed that the microphysical properties of BC-containing particles in the surface air just before precipitation began represented the initial status of BC-containing particles during the removal processes. On the basis of this assumption, the focus here is on the S_c of BC-containing particles just before precipitation began.

For BC-containing particles with a specific range of $D_{BC-core}$, the distribution of S_c was estimated from the measured distribution of the SCr and the measured median $\kappa_{BC-coat}$ (here $\kappa_{BC-free}$) based on κ -Köhler theory. Figure 3.15a and b show examples of the measured distribution of SCr and the estimated distribution of S_c for BC-containing particles with $D_{BC-core} = 245\text{--}282$ nm, during the 1-h period before precipitation began (a rain event on 9 August). The measured median $\kappa_{BC-free}$ value before precipitation began was 0.285 and used to estimate the distribution of S_c . The median S_c is determined from the distribution of S_c . In addition, given the maximum SS that the particles would experience in the ascending air parcel, the number fraction of BC-containing particles that should serve as CCN (F_{CCN}) can be estimated from the distribution of S_c :

$$F_{CCN}(SS, D_{BC-core}) = \frac{\int_{S_c=0}^{S_c=SS} \frac{dN_{BC}}{d\log S_c}(D_{BC-core}) d\log S_c}{N_{BC}(D_{BC-core})}, \quad [3.2]$$

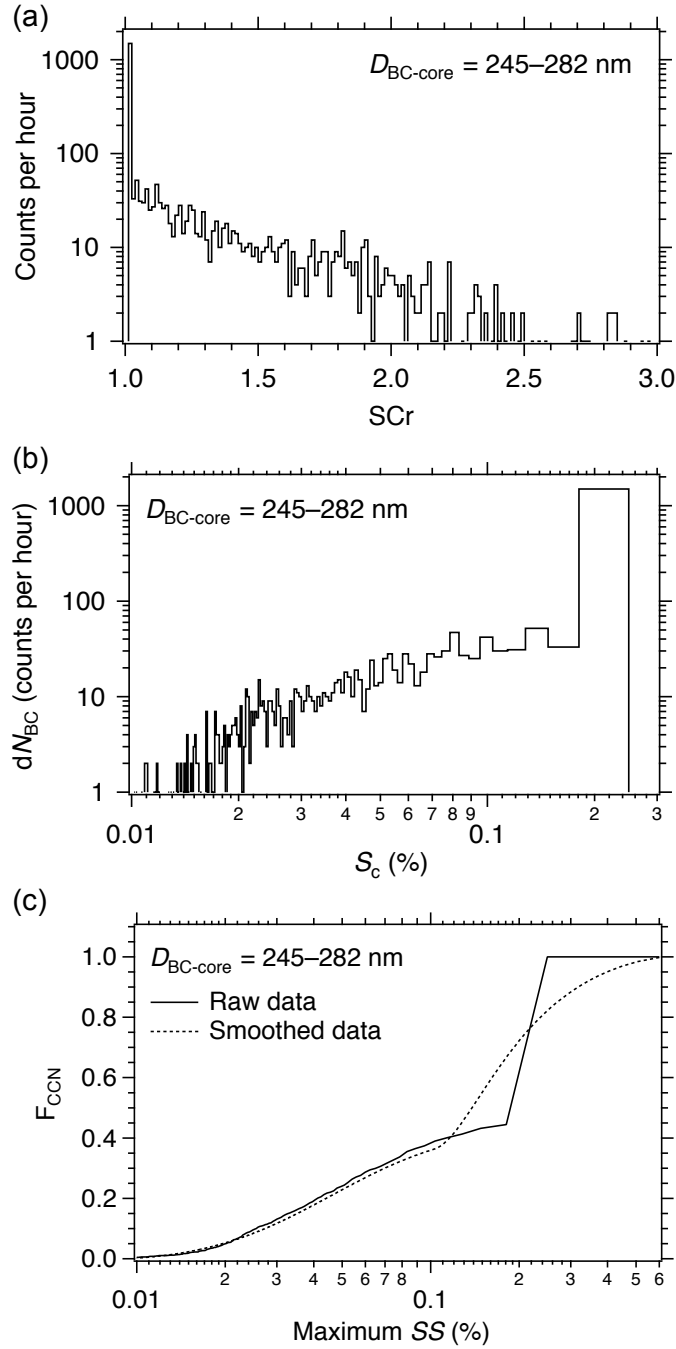


Figure 3.15. For BC-containing particles with $D_{\text{BC-core}} = 245\text{--}282 \text{ nm}$ during 1 h before precipitation began on 9 August 2014, (a) measured distribution of SCr, (b) dN_{BC} (distribution of S_c) estimated from the measured distribution of the SCr and the measured median $\kappa_{\text{BC-free}} (= 0.285)$ based on κ -Köhler theory, and (c) estimated F_{CCN} as a function of the assumed maximum SS that the particles would experience. The solid and dashed lines show the F_{CCN} derived from the raw and smoothed distribution of SCr, respectively.

where $N_{BC}(D_{BC-core})$ is the total number of BC-containing particles with a specific range of $D_{BC-core}$ and $dN_{BC}/d\log S_c(D_{BC-core})$ is the number distribution of S_c for the BC-containing particles. The distribution of S_c shown in Figure 3.15b corresponds to $dN_{BC}(S_c, D_{BC-core})$, which is the number of the BC-containing particles ($D_{BC-core} = 245\text{--}282$ nm) with a specific range of S_c . An example of the estimated F_{CCN} is also shown in Figure 3.15c, as a function of the assumed maximum SS that the particles would experience. Because the number of the measured BC particles with $SCr = 1.013\text{--}1.025$ was dominant (Figure 3.15a), it was estimated that the number of the BC particles with $S_c = 0.18\text{--}0.25\%$ was significant (Figure 3.15b), which resulted in the rapid increase in F_{CCN} at S_c of about 0.2% in Figure 3.15c (solid line). Taking the measurement uncertainty of SCr into account, F_{CCN} derived from a smoothed SCr distribution is also shown in Figure 3.15c (dashed line). To derive the smoothed F_{CCN} , it was assumed that the number distribution of the BC particles linearly decreased as their SCr value increased from 1 to 1.075. For the BC-containing particles with $D_{BC-core} = 245\text{--}282$ nm, this smoothing did not significantly affect the F_{CCN} for the maximum SS of less than 0.1% and greater than 0.3%. In contrast, the F_{CCN} for the maximum SS of about 0.2% was sensitive to the smoothing, indicating that the uncertainty of the F_{CCN} for the maximum SS of about 0.2% was potentially high (less than ± 0.2). Hereafter, smoothing of the distributions of the measured SCr is not made to derive F_{CCN} .

Figure 3.16 shows the average dependence of the CCN activity of BC-containing particles on BC-core size for the seven rain events. BC-containing particles with large BC cores tended to have low values of median S_c . Moreover, the F_{CCN} and its core-size dependence are highly dependent on the assumed maximum SS. If the value of the maximum SS that the particles experienced was greater than 0.3%, almost all

BC-containing particles in the $D_{\text{BC-core}}$ range of 200–350 nm should serve as CCN; thus wet removal of the BC-containing particles would not depend on BC-core size. In contrast, if the value of the maximum SS was less than 0.3%, the F_{CCN} was dependent

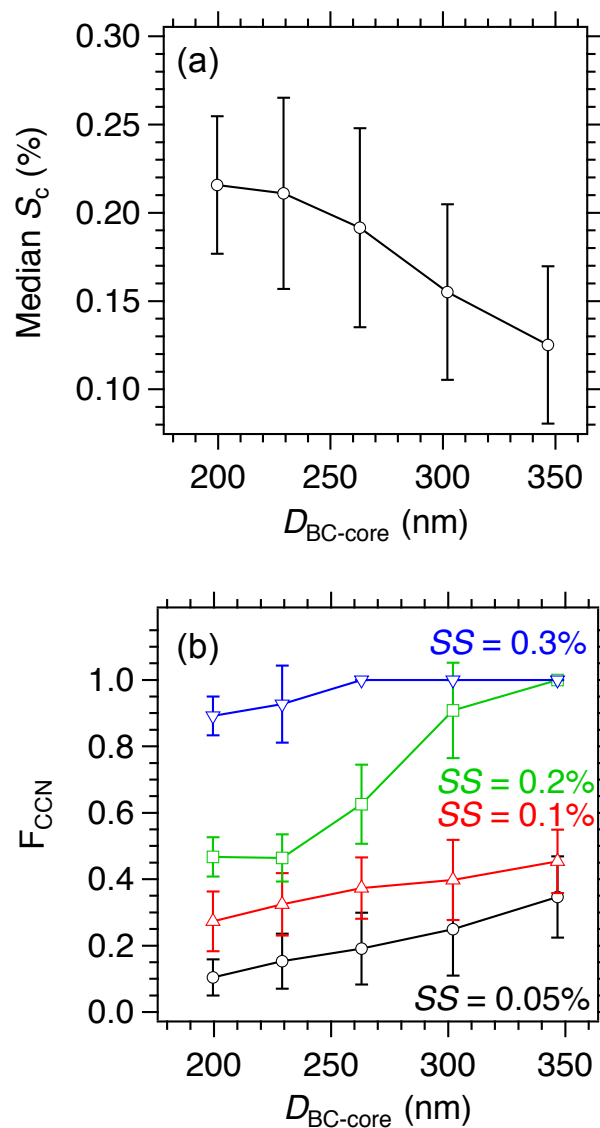


Figure 3.16. For BC-containing particles in the surface air 1 h before precipitation began: (a) median S_c ; (b) F_{CCN} under the assumed maximum SS that the BC-containing particles experienced. The data are averages for seven rain events. Bars indicate 1σ .

on BC-core size: that is, F_{CCN} decreased with decreasing BC-core size.

3.3.2.2. BC in Rainwater

The properties of BC-containing particles that were activated as CCN and then removed through precipitation can be investigated by measuring the BC-core sizes of BC particles suspended in rainwater. Because the water-soluble coatings of BC particles dissolve in rainwater, the coating thicknesses of individual BC particles (before CCN activation) cannot be quantified from rainwater measurements. However, the number size distribution of BC cores is measurable and useful for estimating the removal efficiency of BC-containing particles as a function of BC-core size.

The temporal variation of the number size distribution of BC cores in rainwater during the seven rain events was determined. The measured size distribution was normalized to represent the existence probability of BC cores as a function of BC-core size. Because the temporal variation of the normalized number size distribution of BC cores in rainwater was not significant during the rain events, the normalized number size distributions for the seven rain events were averaged (Figure 3.17) (the temporal variation of the normalized *mass* size distribution during the rain events was sometimes significant, but this topic is beyond the scope of this study). Figure 3.17 also shows the normalized number size distribution of BC cores in the surface air averaged during the 1-h period before precipitation began. For both the normalized size distribution in air and that in rainwater, the differences among the seven rain events were relatively small, in spite of the variability of the meteorological conditions. Therefore, Figure 3.17 shows the typical shape for the number size distribution of BC cores in Tokyo air and rainwater in summer. For all rain events, the size distribution of BC cores in rainwater

was larger than that in air before precipitation began, indicating that BC-containing particles with large BC cores were selectively removed through the cloud precipitation process.

To quantitatively represent the removal efficiency of BC-containing particles as a function of BC-core size, the relative removal efficiency (rRE) was defined as the ratio of the number size distribution of BC cores in rainwater to that in air:

$$rRE(D_{BC-core}) = \frac{dN_{rain}(D_{BC-core})}{dN_{air}(D_{BC-core})}, \quad [3.3]$$

where $dN_{rain}(D_{BC-core})$ and $dN_{air}(D_{BC-core})$ are number concentrations of BC-containing particles with a specific range of BC-core diameters in rainwater and in air,

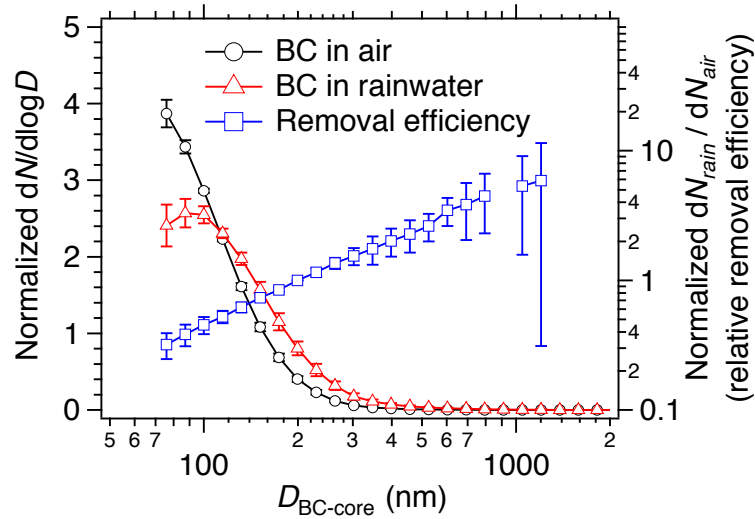


Figure 3.17. Normalized number size distributions of BC cores in the surface air before precipitation began and in rainwater. Data for seven rain events were averaged. The ratio of the normalized number size distributions in rain and air (relative removal efficiency) is also shown. Bars indicate 1σ .

respectively. The rRE was normalized to 1 for a $D_{\text{BC-core}}$ value of 200 nm. Figure 3.17 shows the average rRE measured during the seven rain events. On average, the value of rRE for CCN activity of BC-containing particles in the surface air before precipitation is BC-containing particles with $D_{\text{BC-core}} = 400$ nm was about 2, whereas the value for particles with $D_{\text{BC-core}} = 100$ nm was about 0.5. On a number-concentration basis, BC-containing particles with $D_{\text{BC-core}} = 400$ nm served as CCN twice as efficiently as particles with $D_{\text{BC-core}} = 200$ nm, whereas particles with $D_{\text{BC-core}} = 100$ nm served with half the efficiency of particles with $D_{\text{BC-core}} = 200$ nm.

The maximum SS that BC-containing particles experienced during the rain events affected the dependency of the F_{CCN} on BC-core size (Figure 3.16b). Because it was assumed that the removal process of BC-containing particles is limited to nucleation scavenging (i.e., CCN activation followed by precipitation), the rRE can be estimated from the F_{CCN} if the value of the maximum SS is assumed. The rRE estimated from the compared with the measured rRE in Figure 3.18. If the median value of the maximum SS that BC-containing particles experienced during the seven rain events was 0.1% (0.05–0.2%), the CCN activity, or S_c , of BC-containing particles in the air before precipitation explained the observed rRE.

On average, the F_{CCN} under the maximum SS value of 0.1% was estimated to be 0.27 and 0.45 for particles with $D_{\text{BC-core}}$ values of 200 and 350 nm, respectively (Table 3.2). These results indicate that BC-containing particles in Tokyo air, especially particles with small BC cores, were efficiently transported upward without being removed by precipitation. This is consistent with the aircraft observation by Moteki et al. [2012], who found that the size distribution of BC uplifted to the free troposphere with low transport efficiency tended to be smaller than that with high transport efficiency.

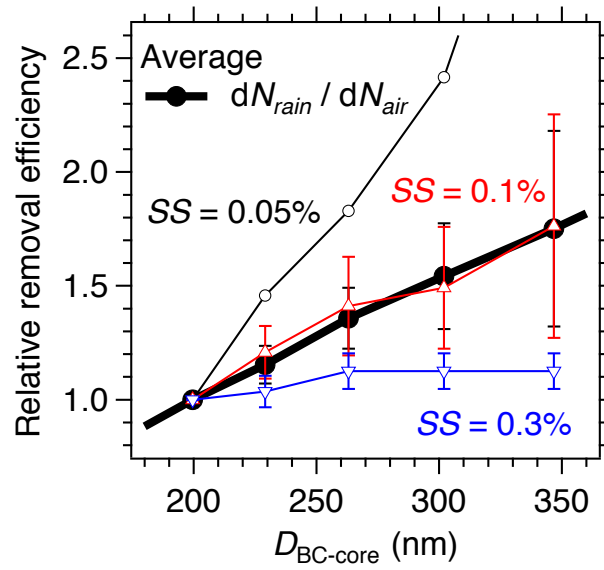


Figure 3.18. rRE determined from the number size distributions of BC cores in air and in rainwater (thick line), and rREs estimated from the F_{CCN} under several assumed maximum values of SS (thin lines). Data for seven rain events were averaged. Bars indicate 1σ . For clarity, some bars are not shown in the figure.

Table 3.2. Average number fraction of CCN-activated BC-containing particles under the assumed maximum SS that the particles would experience during the seven rain events

		$D_{BC-core}$ (nm)				
		186–214	214–245	245–282	282–324	324–372
Assumed maximum SS (%)	0.05	0.10	0.15	0.19	0.25	0.35
	0.1	0.27	0.32	0.37	0.40	0.45
	0.2	0.47	0.46	0.63	0.92	1
	0.3	0.89	0.93	1	1	1

The efficient vertical transport of BC-containing particles predicted from the observations in Tokyo is expected to be common in other megacities, highlighting the importance of vertical air motion near BC emission sources for long-distance transport and lifetime of BC-containing particles. The data obtained by simultaneous observation of the microphysical properties of BC-containing particles in air and in rainwater using the newly developed measurement system will be useful for directly assessing various model schemes related to wet removal of aerosols.

3.4. Summary

An intensive observation of the number size distribution, coating thickness, and hygroscopicity of BC-containing particles in the urban atmosphere of Tokyo was conducted during the summer of 2014. Simultaneously, BC particles suspended in rainwater were measured during seven rain events to quantify the efficiency of wet removal of BC-containing particles.

Using the newly developed h-SP2, detailed temporal variations of BC-free and BC-containing particles were independently measured in Tokyo air for the first time. Throughout the observation period, thinly coated BC particles tended to be less hygroscopic than thickly coated BC particles, and the number fraction of less hygroscopic ($GF < 1.2$ at 85% RH, or $S_c > \sim 0.2\%$) BC-containing particles was greater than 70% of the total BC-containing particles with a dry diameter of about 200 nm. The chemical compositions of BC-coating materials were generally similar to those of BC-free particles. The measured hygroscopicity of the BC-free particles was mostly between the hygroscopicities of typical inorganic and organic aerosols, indicating that individual BC-free particles were internally mixed with inorganic and organic

compounds.

The critical supersaturation (S_c) of BC-containing particles was estimated by κ -Köhler theory using the hygroscopicity of BC-coating materials and the coating thickness measured by the h-SP2 and dry-SP2. Throughout the observation period, the estimated S_c was higher for BC-containing particles with small BC cores because the measured BC particles were generally bare or thinly coated, regardless of the BC-core size. This result indicates that wet removal of BC-containing particles in Tokyo air can be highly dependent on the BC-core size. This size-dependent wet removal of BC-containing particles was confirmed by the large number size distribution of BC cores in rainwater compared to the number size distribution of BC cores in the surface air before precipitation.

The size-dependent wet removal of particles was explained by the estimated S_c of BC-containing particles and an assumed maximum supersaturation (SS) of 0.1% (0.05–0.2%) that the particles would have experienced during seven rain events. On average, the number fraction of CCN-activated BC-containing particles under a maximum SS of 0.1% was estimated to be 0.27 for particles with $D_{\text{BC-core}} = 200$ nm and 0.45 for particles with $D_{\text{BC-core}} = 350$ nm, indicating that BC-containing particles in Tokyo, especially particles with small BC cores (or with high S_c), were efficiently transported upward without being removed by precipitation. Thus the simultaneous observation of BC in air and BC in rainwater near BC emission sources provides useful data for directly assessing various model schemes related to wet removal of aerosols.

4. Evaluation of a Method to Measure BC Particles Suspended in Rain and Snow Samples

4.1. Introduction

Three principal methods are currently used for quantifying the mass concentration of BC particles in liquid water samples. The first method utilizes the thermo-optical technique [Ogren et al. 1983; Hadley et al. 2008; Wang et al. 2011]. In this method, the liquid water sample is filtered, and the BC particles retained on the filter are thermally converted into CO₂. The total mass of BC is derived by quantifying the CO₂ concentration while monitoring the transmittance or reflectance of the heated filter. This method can also provide the mass concentration of organic carbon (OC) suspended in water samples. The major uncertainty of the method derives from the collection efficiency of the filter and separation of the BC/OC contributions in the analysis. Different protocols of the analytical procedures may introduce additional uncertainties. Wang et al. [2011] also reported the effect of dust on the quantification of BC. The second method, which also uses a filter to collect particulate matter suspended in liquid samples, utilizes the Integrating Sphere/Integrating Sandwich Spectrometer (ISSW) [Doherty et al. 2010; Granfell et al. 2011]. The ISSW uses a multiple-wave-length light emitting diode and measures the attenuation of the light passing through the filter as a function of wavelength. Absorption by BC and non-BC material is differentiated by assuming the absorption angstrom exponent of the non-BC material. The mass concentration of BC is quantified from the BC absorption, via assumption of a mass

absorption coefficient of BC. The major uncertainties in this method derive from the collection efficiency of the filter used and the assumed optical properties. The third method, which was evaluated in this chapter, consists of an ultrasonic nebulizer (USN) and a Single Particle Soot Photometer (SP2) [McConnell et al. 2007; Kaspari et al. 2011; Schwarz et al. 2012]. The USN disperses a liquid sample into micron-size droplets and then dries them to release BC particles into the air. The extracted particles are transferred to the SP2, which measures the masses of the individual BC particles. Therefore, this method can generally be used to measure the number and mass size distributions of BC in liquid water. Another advantage of this method is that it typically requires less than 5 mL of sample water for analysis, substantially less than that required for the filter-based techniques. In addition, the SP2 is little affected by dust. The main uncertainty of this method derives from determining the efficiency of the USN in releasing BC particles in liquid water to air. In most of the aforementioned studies, the efficiency is considered to be a constant independent of the properties of the particles in the liquid samples. However, Schwarz et al. [2012] showed that the efficiency depends strongly on particle size, and the size dependence was different for the USN and the Collison-type nebulizer (CTN) used in the study.

Despite the increasing use of the USN–SP2 method for measuring BC particles in rainwater, snow, and ice samples, in-depth evaluation of the method has not been completed. The purpose of this study is to make a systematic evaluation of this method. This includes determination of the size-dependent extraction efficiency of the USN, assessments of the accuracy and reproducibility of the measured mass concentration of BC in sample water, and comparison of the data obtained with the USN and the CTN.

In section 4.2, the experimental setup and laboratory water samples used in this

study including suspensions of commercially available BC samples and polystyrene latex (PSL) spheres are described. In section 4.3, the size-dependent efficiency of the USN is evaluated using PSL spheres and the accuracy of the measured mass concentration of BC in water is assessed using three kinds of laboratory BC samples. Then, the reproducibility of the measured mass concentration and size distribution of BC in rainwater collected in Tokyo is discussed in section 4.4. The effect of agitation of BC samples by an ultrasonic bath prior to analysis on the measurement is also examined. In section 4.5, the method is tested by analyzing rainwater and snow samples collected at different locations in Japan and report their average BC size distributions. In section 4.6, the size distributions of BC in water measured by the present method are assessed by using the CTN. In section 4.7, results of a long-term measurement of BC concentration in rainwater at a remote site in the East China Sea are introduced as an example of the application of this method to field observation. A summary in this chapter is presented in section 4.8.

Note that recently a new concentric pneumatic nebulizer has been also used to measure BC particles suspended in water samples, instead of the USN or CTN. This new nebulizer is briefly described in Appendix 4A.

4.2. Method

4.2.1. Experimental Setup

The experimental setup is shown in Figure 4.1. Water samples containing BC particles are transferred to an ultrasonic nebulizer (U-5000AT, Cetac Technologies Inc., Omaha, NE, USA) by a peristaltic pump (REGRO Analog, ISMATEC SA., Feldeggstrasse, Glattbrugg, Switzerland) at a calibrated flow rate. Figure 4.2 shows an

expanded diagram of the U-5000AT nebulizer. Sample water is fed to a piezoelectric transducer by a peristaltic pump. Some fraction of the introduced water is converted to micron-size ($\sim 10 \mu\text{m}$) droplets on the surface of the piezoelectric transducer, which oscillates at a frequency of 1.4 MHz. The portion of the water sample not aerosolized by this process is removed through the first drain. Dry, clean air at a flow rate of $16 \text{ cm}^3 \text{ s}^{-1}$ at standard temperature and pressure (STP) is introduced near the transducer to produce an air flow. Downstream of the transducer, the water droplets are dried while passing through a tube heated at $140 \text{ }^\circ\text{C}$, generating a mixture of BC particles and water vapor molecules. Water vapor is removed through condensation onto a tube cooled at $3 \text{ }^\circ\text{C}$. The condensed water is taken out of the nebulizer through the second and third drains. By evaporation of droplets, BC particles or other types of residue particles are released into the air. The masses of individual BC particles are measured by the SP2, as described in section 2.2 of Chapter 2.

In addition to the SP2, an ultra high sensitivity aerosol spectrometer (UHSAS)

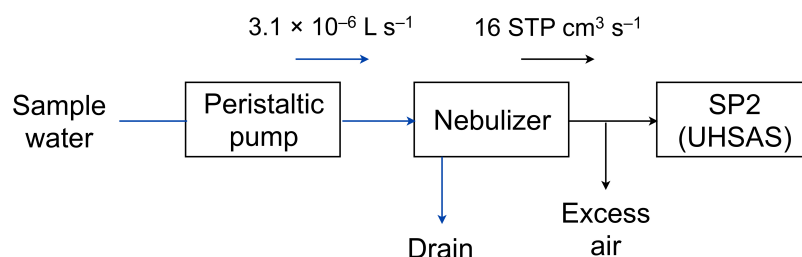


Figure 4.1. Schematic diagram of the experimental setup for measuring BC particles or PSL spheres in water samples. For measurement of BC, only the SP2 was used; for measurement of the PSL spheres, either the SP2 or the UHSAS was used.

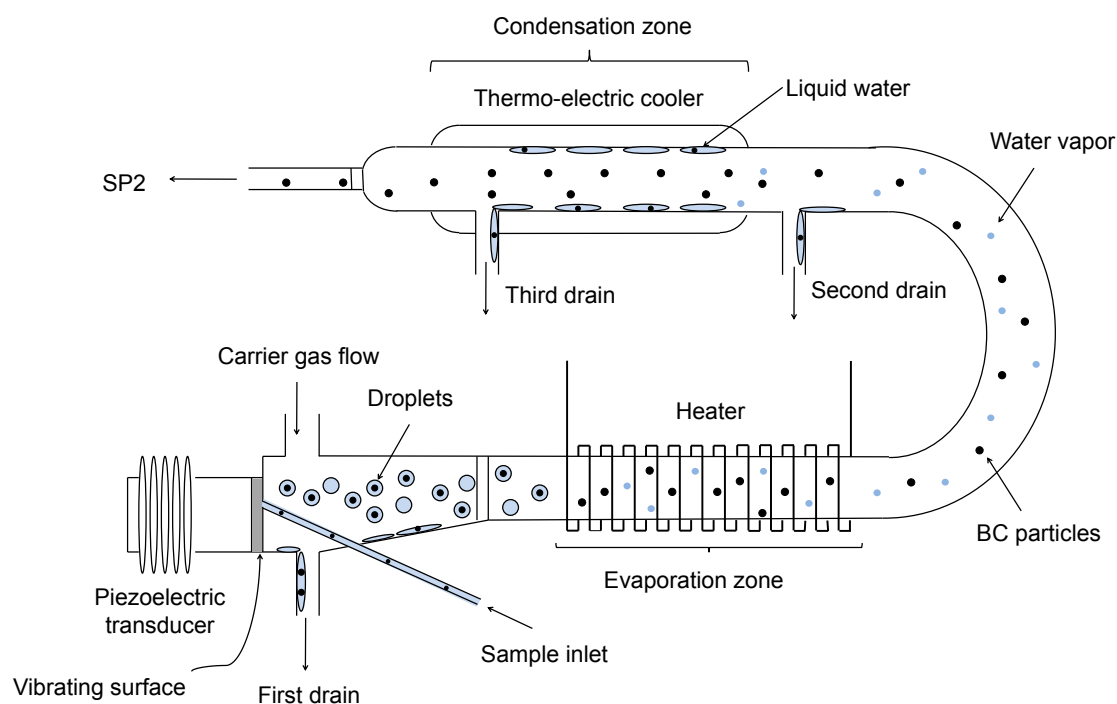


Figure 4.2. Expanded diagram of the ultrasonic nebulizer (U-5000AT).

was also used for measurement of the PSL spheres (Figure 4.1). The UHSAS is an optical particle counter covering a wide range of scattering particles with sizes between about 60 and 1500 nm. Characterization of the UHSAS can be seen in Cai et al. (2008). The UHSAS utilizes an intra-cavity Nd^{3+} :YLF laser with a wavelength of 1054 nm and detects scattering signals by two pairs of Mangin mirrors and avalanche photodiode detectors. In this chapter, the SP2 and the UHSAS were used to measure PSL spheres with sizes of 202–771 nm and 107–1025 nm, respectively, to determine the size-dependent extraction efficiency of the USN. PSL spheres with diameters of 202, 309, and 402 nm were used to check instrumental performance; and PSL concentrations in air measured by the SP2 and UHSAS were in agreement within 10%.

The extraction efficiency (ε) of the USN was determined as a function of the PSL diameter (D_{PSL}) by the following equation:

$$\varepsilon(D_{\text{PSL}}) = \frac{N_{\text{SP2/UHSAS}} \cdot F_{\text{neb}}}{n_{\text{samp}}(D_{\text{PSL}}) \cdot V_{\text{pump}}}. \quad [4.1]$$

Here $N_{\text{SP2/UHSAS}}$ is the number concentration of PSL spheres in air measured by the SP2 or UHSAS (cm^{-3}), F_{neb} is the nebulizer gas flow rate ($\text{cm}^3 \text{s}^{-1}$), $n_{\text{samp}}(D_{\text{PSL}})$ is the size-resolved number concentration of PSLs in water (L^{-1}), and V_{pump} is the liquid flow rate of the pump (L s^{-1}). n_{samp} was determined by an extinction measurement, as detailed in section 4.2.2. The values of the constants F_{neb} and V_{pump} are $16 \text{ STP cm}^3 \text{ s}^{-1}$ and $3.1 \times 10^{-6} \text{ L s}^{-1}$, respectively. The following equation was assumed:

$$\varepsilon(D_{\text{PSL}}) = \varepsilon(D_{\text{BC}}), \quad [4.2]$$

where D_{BC} is the mass-equivalent diameter of the BC particles (BC-core). As discussed in section 4.3, we assume that the size dependence of the loss of the particles in the USN is due to the effects of inertial impaction and thermophoresis; therefore the efficiency is also likely affected by density, shape, and thermal conductivity of the particles. A detailed evaluation of these effects was not made in this study. The applicability of Equation [4.2] to BC measurement is assessed using laboratory BC samples in section 4.3. Here note that Equation [4.2] is effectively consistent with that by Schwarz et al. [2012], who found a similar relationship based on analysis of the particle stopping distance. Then the BC mass concentration in sample water, m_{samp} (μg

L⁻¹), was determined by

$$m_{\text{samp}} = \int_{70 \text{ nm}}^{850 \text{ nm}} \frac{dm_{\text{samp}}}{d\log D_{\text{BC}}} d\log D_{\text{BC}} = \int_{70 \text{ nm}}^{850 \text{ nm}} \frac{F_{\text{neb}} \cdot \frac{dM_{\text{SP2}}}{d\log D_{\text{BC}}}}{V_{\text{pump}} \cdot \varepsilon(D_{\text{BC}})} d\log D_{\text{BC}}. \quad [4.3]$$

Here $dm_{\text{samp}}/d\log D_{\text{BC}}$ is the mass size distribution of BC in the sample water ($\mu\text{g L}^{-1}$), and $dM_{\text{SP2}}/d\log D_{\text{BC}}$ is the mass size distribution of BC in air measured by the SP2 ($\mu\text{g cm}^{-3}$). Only the mass concentration in the size range of detection of the SP2 (70–850 nm) was calculated. Note that recently an SP2 has been modified to measure BC particles up to about 4000 nm. This modified SP2 (wide-range SP2) is briefly described in Appendix 4A.

4.2.2. PSL Number Concentration in Water

The diameters of the PSL spheres used in this study were 107, 152, 202, 254, 309, 402, and 814 nm (JSR Inc., Ibaraki, Japan) and 220, 356, 505, 771, and 1025 nm (Polysciences Inc., Warrington, PA, USA). $n_{\text{samp}}(D_{\text{PSL}})$ was determined for each PSL suspension by placing the PSL suspension in a rectangular acrylic cell and measuring the attenuation of a 532-nm laser beam (GSHG-3020F, KTG Co. Ltd., Kochi, Japan). $n_{\text{samp}}(D_{\text{PSL}})$ was determined by using the Lambert-Beer law [e.g. Hinds 1999]:

$$n_{\text{samp}}(D_{\text{PSL}}) = \frac{4}{\pi \cdot D_{\text{PSL}}^2 \cdot Q_{\text{PSL}} \cdot L} \ln\left(\frac{I}{I_{\text{ref}}}\right). \quad [4.4]$$

Here Q_{PSL} is the extinction efficiency of the PSL calculated by Mie theory [Bohren and

Huffman 1983]. We assumed an ideal monodisperse size distribution of the PSL with a refractive index of $1.59 + 0i$. L is the length of the acrylic cell (30.0 cm). I and I_{ref} (W cm^{-2}) are the intensities of the laser passing through the PSL suspensions and pure water, respectively. A photodiode head (PD-300-3W, Ophir Japan Ltd., Saitama, Japan) was used to detect the laser intensity. The uncertainty of the detected intensity is about $\pm 3\%$, according to the manufacturer.

The attenuation of the laser beam passing through the cell was maintained at >0.2 by using deionized water to control the concentrations of the PSL suspensions (the concentration of the original PSL suspension was $\sim 10^{12} \text{ L}^{-1}$). Multiple scattering has little effect on the attenuation under this condition [e.g., Hinds 1999]. The measured $n_{\text{samp}}(D_{\text{PSL}})$ was in the range of 10^9 – 10^{11} L^{-1} , which was generated by diluting the original PSL suspensions with concentrations of $\sim 10^{12} \text{ L}^{-1}$.

The measured $n_{\text{samp}}(D_{\text{PSL}})$ for the Polysciences PSL spheres with diameters of 220, 356, 505, 771, and 1025 nm agreed to within $\pm 8\%$ of the $n_{\text{samp}}(D_{\text{PSL}})$ calculated from the solid fraction weight of the PSL samples provided by the manufacturer. The number concentrations of the JSR PSL suspensions were generally not provided by the manufacturer, so we determined the number concentration of the 202-nm JSR PSL suspensions by drying it and weighing the residual solid PSL. The value obtained agreed with the laser-determined n_{samp} to within $\pm 8\%$.

4.2.3. Laboratory BC Samples

Three kinds of laboratory BC samples were tested: two fullerene soot samples (Stock No. 40971, Lots F12S011 and G25N20) and Aqua-Black162. The incandescence–BC mass relationships for the SP2 were shown in Figure 2.4 in section

2.2.2 (Chapter 2). The procedure for generating known concentrations of fullerene soot in water is described in Schwarz et al. [2012]. The mixtures of fullerene soot and pure water were stored in a glass beaker for several days to allow large BC particles to settle out of solution. For the fullerene soot samples, a few weight percent of methanol was added to fully disperse the BC particles in water. The upper portions of the mixtures were then slowly transferred to five glass bottles by using a peristaltic pump. The mass concentrations of BC in water in three of the bottles were determined by the gravimetric method, in which water is evaporated and the mass of the residual solid BC is measured with an electronic balance. The standard deviation of the measured mass concentrations of BC in the three bottles was less than 10%. The remaining bottles were used as master bottles, for which suitable mass concentrations of BC in water were generated by diluting the samples with a known amount of deionized water.

The BC particles in Aqua-Black162 were stably dispersed in water without sedimentation or coagulation, due to the manufacture's treatment of the surface of individual BC particles by carboxyl groups. The mass fraction of solid BC particles was 19.2% of the total (liquid and solid) mass of Aqua-Black162, according to the manufacturer, which agreed to within 5% with our measurement made by drying and weighing the sample. We controlled the mass concentration of BC in Aqua-Black162 samples by diluting them with deionized water.

Figure 4.3 shows the measured mass size distributions of BC in the laboratory-generated BC samples. The size distributions were determined by taking the size-dependent extraction efficiency of the USN into consideration (discussed in section 4.3). The detection range of the SP2 (70–850 nm) covers the whole mass size distribution of BC in the gravimetrically settled fullerene soot samples, and the mass of

BC particles with diameters smaller than 70 nm and larger than 850 nm is negligible.

For Aqua-Black162, the mass fraction of BC particles smaller than 70 nm was estimated to be $(7 \pm 3)\%$, by fitting a lognormal function to the BC mass size distribution.

4.3. Size-dependent Nebulizer Efficiency

A large fraction of the BC particles in the water samples is lost during nebulization and transport in the USN tubing. One reason for the loss is that some of the sample water is

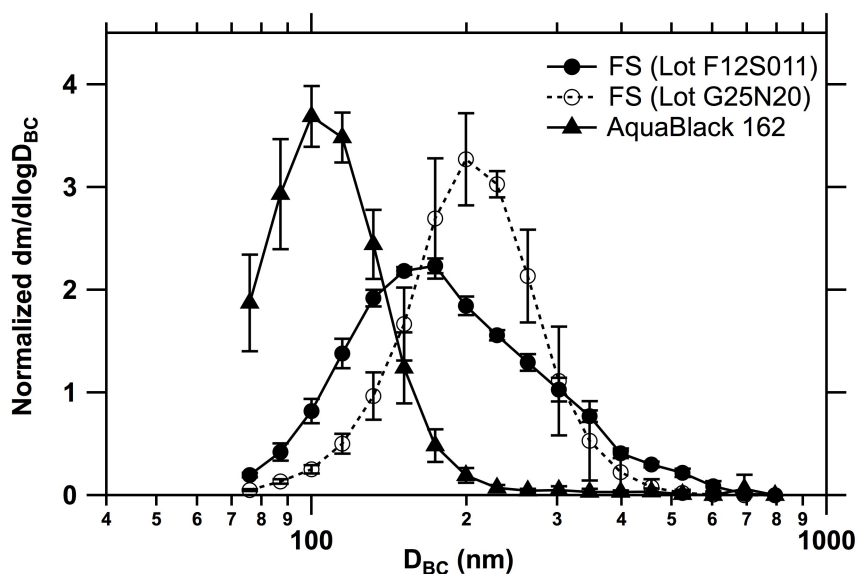


Figure 4.3. Normalized mass size distributions of laboratory BC samples: fullerene soot (FS, Lots F12S011 and G25N20) and Aqua-Black162. Bars indicate 1σ values derived from repeated measurements. The vertical axis is normalized by the integrated area of each size distribution between 70 and 850 nm to be 1. The diameter is equivalent assuming a void-free density of 2.0 g cm^{-3} . Note that in the other chapters, the density of BC is assumed to be 1.8 g cm^{-3} . This 10% difference in assumed density causes 3% difference in mass equivalent diameter.

not converted into droplets on the vibrating surface of the USN and is removed through the drain together with the BC particles. The collision of some of the generated droplets with the inner walls of the tubing before evaporation also results in the loss of BC particles. These loss mechanisms immediately remove about 20%–30% of the BC mass. Another possible reason for the loss is that some aerosolized BC particles attach to the wall due to inertial impaction or thermophoresis effects. After repeated use of the nebulizer for a few years, many black spots were observed on the glass wall just downstream of the 140 °C heater zone. This suggests that the thermal gradient between the heated airflow and the walls is relatively large in the area neighboring the heater zone, and therefore some BC particles deposit onto the relatively cold walls by thermophoresis. The size dependence of the extraction efficiency of the USN is possibly due to these loss mechanisms.

Using Equation [4.1] and the size-resolved PSL suspensions detailed in section 4.2.2, the size-dependent extraction efficiency of the USN was determined (Figure 4.4). The number concentration of PSL spheres in air detected by the SP2 during each measurement was stable to within 10%. For these measurements, each PSL sphere only within the appropriate size range was counted. The fraction of doublets, which consist of two coagulated PSL spheres, was <9% from the SP2 and UHSAS data and was excluded from our analysis. The efficiency showed a broad maximum of about 10% in the diameter range 200–500 nm and decreased substantially at larger sizes. The size-dependent efficiency, in percent, was fitted with a Gaussian function:

$$\varepsilon(D_{\text{PSL}}) = 11.87 \cdot \exp \left[- \left(\frac{D_{\text{PSL}} - 350.4}{323.9} \right)^2 \right]. \quad [4.5]$$

The lower efficiency (<2%) for particles with diameters larger than about 800 nm as compared to the efficiency (~10%) for particles with diameters of 200–500 nm is qualitatively consistent with that reported by Schwarz et al. [2012], as shown in Figure 4.4. Only a relative change versus diameters of the efficiencies of the two USNs is compared here, since their absolute values depend on various parameters, including V_{pump} . It is shown that the size dependence of the efficiency of the two USNs is very similar for the range of 200–1000 nm. The slight decrease in efficiency for smaller particles (<200 nm; Figure 4.4) may be caused by the thermophoretic effect because the thermophoretic velocity is larger for smaller particles [e.g., Hinds 1999].

The relative standard deviation of the discrepancies between the measured ϵ (D_{PSL}) and the fitted curve (Equation [4.5]) is 18% for PSL spheres with diameters between 107 and 505 nm. Typical errors for $dM_{\text{SP2}}/d\log D_{\text{BC}}$, F_{neb} , and V_{pump} , in Equation (3) were estimated to be 15%, 5%, and 5%, based on the repeated measurements. The overall uncertainty of the measured BC concentration in water (m_{sampl}) was calculated to be $\pm 25\%$ for this size range of BC and under the assumption that Equation (2) is valid. The uncertainties in the mass concentration of BC in the liquid samples, together with the uncertainties derived in the following sections, are summarized in Table 1.

To check the accuracy of the method, we measured the mass concentrations of the laboratory BC samples by using Equations [4.3] and [4.5] with the assumption of Equation [4.2] and compared the concentrations with those determined by the gravimetric method described in section 2.3 (Figure 4.5). The agreement and BC size distribution for each sample are summarized in Table 4.2. Figure 4.5 and Table 4.2

indicate that for samples containing BC particles with a mass median diameter of about 100-200 nm, the accuracy of the mass concentration of BC in water measured by the present method with the assumption of Equation [4.2] is $\pm 24\%$, which is within the uncertainty calculated above. This result supports the applicability of Equation [4.2] to the measurement of BC in liquid samples by the present method, although this does not fully address the applicability of Equation [4.2] to unknown samples containing BC. The mass size distributions of BC in water samples presented in this chapter were

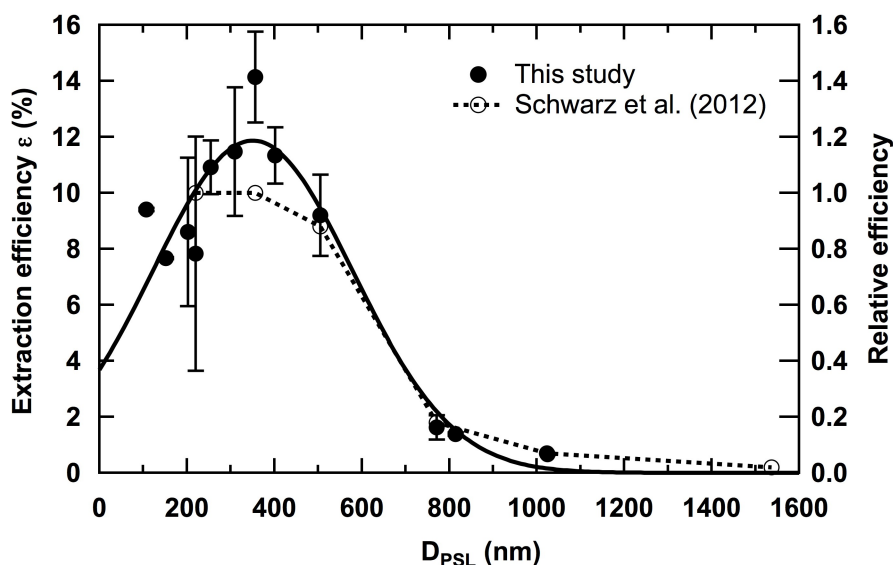


Figure 4.4. Size-dependent extraction efficiency of the USN. Bars show 1σ values derived from repeated measurements over 6 months. For PSL spheres with diameters of 107, 152, 814, and 1025 nm, two PSL suspensions of known concentration were measured for each diameter within 1 day, and therefore their 1σ values were much smaller than those of the other data. The solid curve indicates Gaussian fitting to the data. Relative extraction efficiency of the USN reported in Schwarz et al. [2012] is also shown. The efficiencies for PSL spheres with diameters of 220 and 350 nm were similar and therefore set to be 1, and the efficiencies for the other size are relative to them.

Table 4.1. Uncertainty and bias of the mass concentration of BC in liquid samples measured by the present method^a.

	Type of uncertainty and bias	Value	Explanation	Section
Measurement uncertainty	Accuracy	±25%	Propagation of the uncertainties of ϵ (D_{PSL}) (±18%), $dM_{\text{SP2}}/d\log D_{\text{BC}}$ (±15%), F_{neb} (±5%), and V_{pump} (±5%) in Equation (2) and (3). The accuracy was also checked by measuring laboratory BC samples (Figure 4.5).	4.3
	Reproducibility within the same experimental day	±10%	Repeated measurement of rainwater samples collected in Tokyo within one experimental day.	4.4.1
	Reproducibility after 12 months of storage	±35%	Repeated measurement of rainwater samples collected in Tokyo and at Cape Hedo after long-term storage. The uncertainty of the long-term stability of the overall measurement system, including the stability of the liquid samples, contributes to the value of 35%.	
Bias	Underestimate due to attachment of BC to the walls of the containers	-(18 ± 13)%	Without agitation by an UB just before measurement, the mass concentrations of BC in liquid samples stored in a refrigerator for several months were underestimated. The value was obtained using rainwater samples collected in Tokyo.	4.4.2

^aThe values reported are for samples containing a dominant fraction of BC mass in the diameter range 100–500 nm.

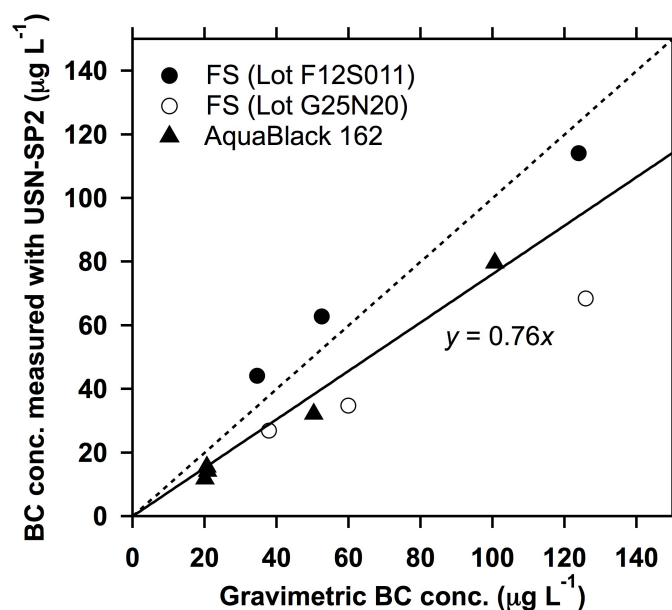


Figure 4.5. BC mass concentrations in laboratory BC samples measured by the gravimetric method versus those measured by the present method. The solid line is the line fitted to all data and the dashed line is 1:1.

similar to those of the Lot F12S011 fullerene soot samples (see section 4.5). Therefore, the accuracy for measurement of these samples is estimated to be $\pm 25\%$.

When the size distribution of BC in sample water is very different from that of laboratory-generated BC, the uncertainty of the measured BC mass concentration in water can be large, because the relative uncertainty of ϵ for particles larger than 500 nm or smaller than 100 nm is larger than that for particles between 100 and 500 nm (see Figure 4.4). Schwarz et al. [2012] found that the mass size distributions of BC in snow samples can be much larger than those in ambient air, and the measurement uncertainty under those conditions was estimated to be $\pm 60\%$ including the uncertainties of the extended SP2 calibration range and the efficiency of the CTN.

Extracted BC particles can be internally mixed with water-soluble species or coagulate with other insoluble species during the nebulization process. However, as shown in section 4.4.3, addition of ammonium sulfate ($0.1\text{-}100\text{ mg L}^{-1}$) to a rainwater sample has negligible effects on the nebulizer efficiency and measured size distributions of BC. This concentration range of ammonium sulfate covers the typical values in rainwater observed in Japan [e.g., Okuda et al., 2005] This experimental result indicates that the effects of shift in particle size due to internal mixing of BC with non-BC compounds during the nebulization process on the measurement of BC should be very small.

Table 4.2. BC mass concentrations in laboratory BC samples measured by the gravimetric method (m_{grav}) versus those measured by the present method ($m_{\text{USN-SP2}}$). Average number and mass size distributions of BC in the samples are also shown^a.

Sample name	Number of samples	Average $m_{\text{USN-SP2}} / m_{\text{grav}}$	Average number size distribution		Average mass size distribution	
			CMD (nm)	σ_{gc}	MMD (nm)	σ_{gm}
AquaBlack 162	5	0.69 ± 0.08 (0.59 – 0.79)	84	1.31	103	1.30
FS (Lot F12S011)	3	1.13 ± 0.19 (0.92 – 1.28)	115	1.41	174	1.54
FS (Lot G25N20)	4	0.62 ± 0.07 (0.54– 0.71)	153	1.343	204	1.32
Total	12	0.77 ± 0.24	NA	NA	NA	NA

^aCMD, MMD, σ_{gc} , and σ_{gm} are count median diameter, mass median diameter, and geometric standard deviations of the size distributions. NA, not applicable.

4.4. Reproducibility

4.4.1. Change of Size Distribution and Mass Concentration of BC in Water during Storage

Rainwater was collected in glass beakers on 11 November in 2011, in Tokyo to test the reproducibility of the measured BC size distributions and BC mass concentrations in samples after long-term storage. Immediately (<2 h) after sampling, the sample water was transferred to a glass bottle and analyzed. The mass concentration of BC in this sample was $48 \mu\text{g L}^{-1}$, which is typical for rainwater in mid-latitude urban sites [e.g., Ogren et al., 1984; Dasch and Cadle, 1989]. After analysis, the sample was kept in a refrigerator and reanalyzed about 1 month later and again 12 months later. The rainwater sample was agitated by an ultrasonic bath (UB) for 15 min just before analysis to disperse BC particles and detach them from the wall of the container. Figure 4.6 shows the measured mass size distribution of BC in this sample. The change in measured mass size distribution during storage was negligibly small, indicating that the effect of coagulation of BC particles in water during storage was not be significant for this sample. This supports the assumption made in section 3.1 of Chapter 3 that coagulation of BC particles in cloud droplets and raindrops is negligible during the cloud–precipitation process. The change in measured total mass concentration of BC during storage was within 35% (Table 4.1). Repeated measurements of a liquid sample within 1 day were reproducible to within $\pm 10\%$. However, for samples stored for a longer time, the uncertainty of the overall measurement system, including both the stability of the liquid sample and the nebulizer efficiency, can cause a relatively low reproducibility ($\pm 35\%$ after 12 month of storage).

Reproducibility of the measured size distribution and mass concentration after

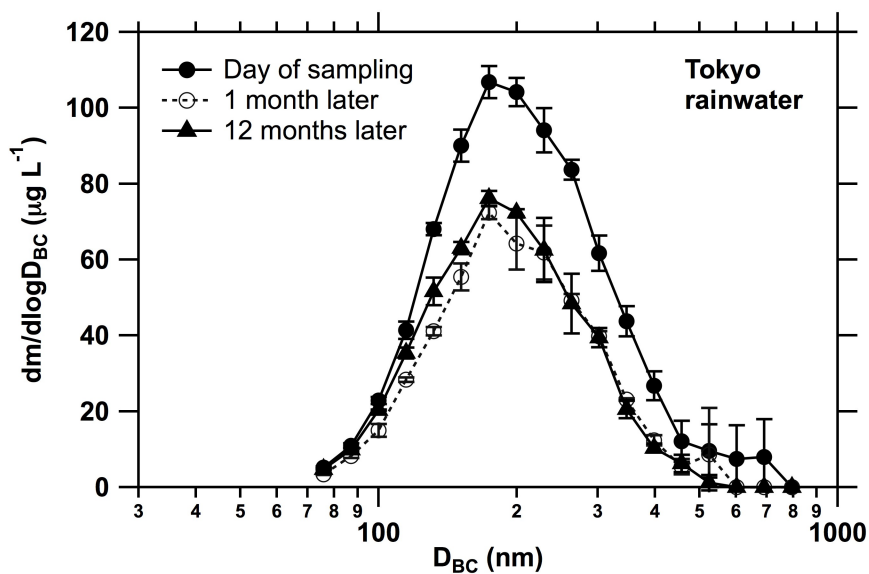


Figure 4.6. Mass size distributions of BC in rainwater repeatedly measured after long-term storage. Bars indicate 1σ values.

long-term storage was also determined for another rainwater sample collected on 16 April in 2011, at Cape Hedo (26.9°N, 128.3°E) in Okinawa over the East China Sea (remote site). Although this sample was not analyzed on the day of sampling, the shape of the BC size distribution measured after 2 and 9 months showed no significant difference, and the BC mass concentrations measured after 2 and 9 months were higher by 33% and lower by 10% than that of the first measurement, respectively. Therefore, reproducibility of the measured mass concentration for this sample was also within 35%.

4.4.2. Attachment of BC Particles to the Walls of Glass Container during Storage

To assess the loss of BC particles due to their attachment to the walls of the glass

container during storage, five rainwater samples collected in Tokyo were analyzed after storage for 9 months in the refrigerator, with and without agitation by an UB for 15 min just before analysis. We found that when the samples were simply shaken by hand (i.e., no UB agitation), the mass concentrations of BC in all five samples were lower by (18 ± 13) % on average, than the concentrations measured after UB agitation. This experiment was performed within 1 day, and therefore the underestimation is statistically significant, considering the good reproducibility that is obtained when samples are analyzed within a day.

The systematic underestimation described above indicates that the UB agitation just before analysis and transfer of sample water to other bottles is required for an improved analytical accuracy. The degree of underestimation reported here may depend on other factors, such as the period of sample storage and the ratio of water volume to area exposed to the glass surface. The size distribution of BC was little changed by UB agitation, indicating that UB agitation did not significantly break BC particles with diameters between 100 and 500 nm into smaller particles.

4.4.3. Effect of Water-Soluble Species

In rainwater, various chemical species, including inorganic (typically sulfate, nitrate, and ammonium) and water-soluble organic species, are dissolved, coexisting within dispersed BC particles [e.g., Willey et al. 2000; Okuda et al., 2005]. These water-soluble species may affect the surface tension of the rainwater. The number and size of droplets generated at the piezoelectric transducer and resulting nebulizer efficiency may change, possibly by changes in the surface tension of rainwater caused by coexisting water-soluble species.

Humic-like substances (HULIS) are known to be surface-active, and the effect of Suwannee River Fulvic Acid (SRFA) (one of the HULIS compounds) on surface tension was quantified by laboratory experiments [Kiss et al., 2005; Svenningsson et al., 2006]. Facchini et al. [2000] observed about a 15-20% decrease in surface tension of wet aerosol and fog samples at concentrations of water-soluble organic carbon (WSOC) of about 100 mg L^{-1} , compared to the surface tension of pure water. The concentrations of dissolved organic carbon (DOC) in rainwater collected in Tokyo in the winter and summer seasons of 1992 were reported to be in the range of $1\text{-}23 \text{ mg L}^{-1}$ [Sempere and Kawamura, 1994].

In order to assess the effect of water-soluble species on the nebulizer efficiency, BC concentrations in rainwater were changed by dilution with pure water by a factor of 10, and then measured by the USN–SP2 method. Rainwater was collected in Tokyo on 21 December in 2010. The BC concentration in this sample was measured to be as high as $208 \text{ } \mu\text{g L}^{-1}$. High BC concentrations were often observed at the initial phase of precipitation in Tokyo. The measured BC concentration was nearly proportional to the dilution ratio. This demonstrates no detectable effects of water-soluble species on the nebulizer efficiency for this rainwater sample. It should be noted that the BC concentration was one of the highest values measured in Tokyo and likely represents the highest concentrations of DOC there as well.

In addition to the dilution method, the dependence of the nebulizer efficiency on water-soluble species was estimated by adding ammonium sulfate ($(\text{NH}_4)_2\text{SO}_4$) and SRFA to sample rainwater collected on 10 June in 2010, in Okinawa, which should have already contained an unknown amount of water-soluble species. Concentrations of ammonium sulfate and SRFA were adjusted to be in the range of $0.1\text{-}100 \text{ mg L}^{-1}$ and

0.1-25 mg L⁻¹, respectively. This range of (NH₄)₂SO₄ concentration covers the typical values in rainwater observed in Japan. For example, Okuda et al. [2005] showed that the mean concentrations of NH₄⁺ and SO₄²⁻ at the nine sampling sites in the Tokyo metropolitan area between June 1990 and May 2002 were about 0.7 mg L⁻¹ and 2.4 mg L⁻¹, respectively. The SRFA concentration of 0.1-25 mg L⁻¹ covers the range of DOC concentrations measured in Tokyo (1-23 mg L⁻¹), discussed above.

Figure 4.7 shows the airborne BC concentrations extracted by the nebulizer versus the concentrations of SRFA added to the rainwater sample. The effect of dilution of the sample due to the addition of SRFA was taken into account in deriving the BC concentrations. At SRFA concentrations below 1 mg L⁻¹, the measured BC concentration was stable at about 2.2×10^{-7} μg cm⁻³. The BC concentration increased by 14% and 32% at SRFA concentrations of 10 mg L⁻¹ and 25 mg L⁻¹, respectively. These results suggest that the efficiency increases only at very high concentrations of HULIS, possibly due to the decrease in the surface tension of the sample water. The stability of the efficiency at lower SRFA concentrations is consistent with the results obtained by dilution with pure water. For the ammonium sulfate concentrations between 0.1 and 100 mg L⁻¹, the extracted BC concentrations were stable to within ±6.3%. This indicates no detectable interference by ammonium sulfate.

Not all the DOC should be composed of HULIS. In addition, the inclusion of soluble species into cloud droplets will be quite different from the simple addition of specified compounds in the laboratory. Dilution of rainwater samples with pure water provides the most robust estimate of the overall effect considering the complexity of the chemical and physical processes involved. Therefore, it is concluded that errors due to possible changes in surface tension are negligible (less than about 5%) for the analysis

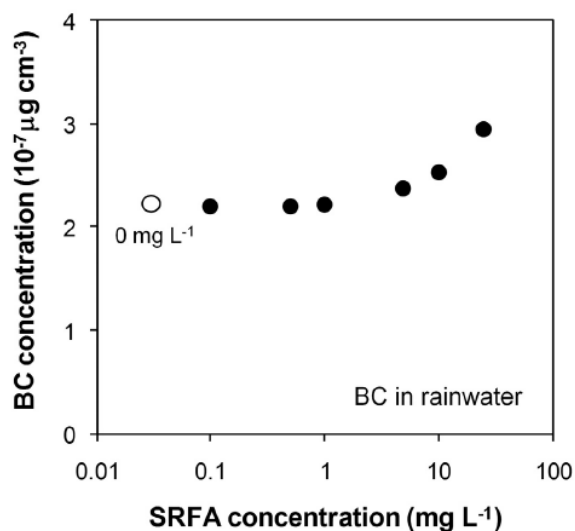


Figure 4.7. BC concentrations in airflow measured by the SP2 versus SRFA concentration added to the rainwater sample.

of rainwater samples used in this chapter. However, under the conditions of much higher HULIS concentrations, this effect can be significant. Even in such cases, the effect can best be estimated by diluting samples, without requiring chemical analysis of water-soluble species.

4.4.4. Change in BC Size in the Nebulizer

Possible changes in the sizes of BC particles in the nebulizer were assessed. Figure 4.8 shows a schematic diagram of the mechanism of changes in BC particle diameters through coagulation upon evaporation of water droplets in the nebulizer. The evaporation occurs in the heated evaporation zone, shown in Figure 4.2. Each droplet contains either a single BC particle (case (a)) or multiple BC particles (case (b)). For case (a), the size distribution of generated airborne BC particles is the same as that in

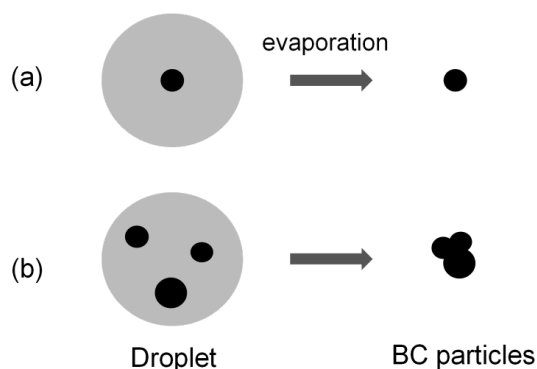


Figure 4.8. Expanded view of the process of evaporation of droplets containing (a) single BC particle and (b) multiple particles.

the water sample. In contrast, for case (b), the size distribution of BC particles shifted to larger sizes as compared to that in the water sample. The magnitude of this effect is anticipated to increase with the increase in BC concentration in water.

The effect of coagulation was assessed using a rainwater sample collected in Tokyo on December 21, 2010. This is the same sample used for assessment of the effect of water-soluble species on the efficiency, discussed in section 4.4.3. The BC concentration in this sample was measured to be $208 \mu\text{g L}^{-1}$. This sample was diluted with pure water in order to generate different BC concentrations in water. It should be noted that the concentrations of the other water-soluble species were diluted as well. Figure 4.9 shows the count median diameter (CMD) and mass median diameter (MMD) of airborne BC particles extracted from the rainwater sample, as a function of BC mass concentration in rainwater. The CMD and MMD decreased with the decrease in BC concentration, indicating less probability of coagulation of BC particles in the nebulizer. For the rainwater sample with BC mass concentration lower than $200 \mu\text{g L}^{-1}$, the

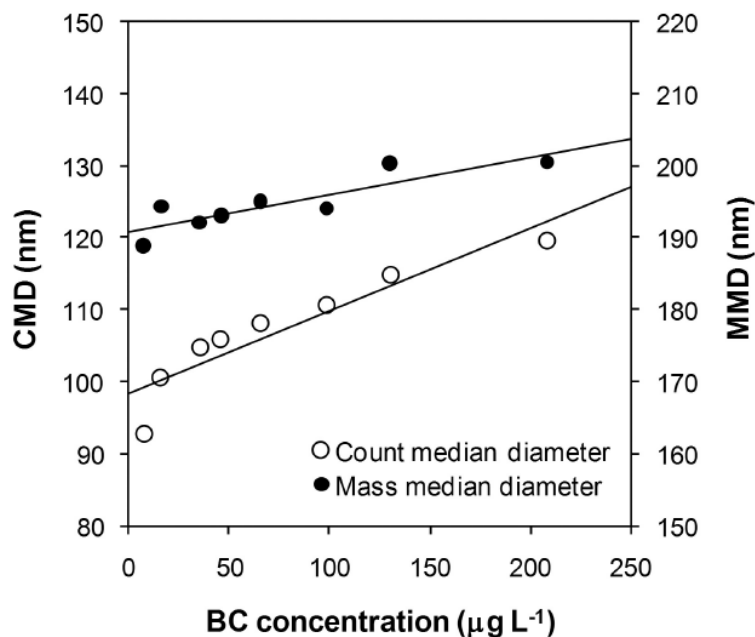


Figure 4.9. CMD and MMD of airborne BC particles extracted from diluted rainwater samples, as a function of BC mass concentration in rainwater. Solid lines indicate linear fitting.

coagulation effects on measured CMD and MMD were limited to less than 15 nm and 10 nm, respectively.

4.5. BC Size Distributions in Rainwater and Snow Samples

Rainwater samples collected in Tokyo and at Cape Hedo were analyzed. In Tokyo, rainwater was collected in glass beakers and stored in glass bottles in a refrigerator. These samples were used to determine the reproducibility of the measurements (section 4.4). At Cape Hedo, rainwater was collected daily in polyethylene bottles between April 2010 and March 2013. After storage for a few weeks in a refrigerator, the samples in the polyethylene bottles were transferred to glass bottles and stored in a refrigerator until

analysis. Seasonal variation of measured BC concentration in rainwater at Cape Hedo is briefly described in section 4.7 as a successful application of the USN-SP2 method to the long-term field observation. In this section, the average size distribution of BC in rainwater samples collected between April and July 2010 was determined to evaluate the method.

The USN-SP2 method was also applied to snow samples collected in Sapporo, a semi-urban area in northern Japan. Samples of the snow layer between the surface and 10-cm depth were collected in polyethylene bags twice per week from December 2011 to February 2012, and the samples were stored in a freezer for several months. Just before analysis, a fraction of each sample was put in a glass bottle and melted in an UB for 15 min.

Figure 4.10 shows the average mass and number size distributions of BC in Cape Hedo rainwater (25 samples) and in Sapporo snow (10 samples). The average mass concentrations of BC in Cape Hedo rainwater and in Sapporo snow were 38 ± 52 and $142 \pm 89 \mu\text{g L}^{-1}$, respectively. The average mass size distributions in Figure 4.10 for both Cape Hedo rainwater and Sapporo snow show that the contributions of BC particles smaller than 70 nm and larger than 850 nm to the total mass of BC is estimated to be less than 5%, by fitting lognormal functions. The slight increase in the mass size distribution for size ranges larger than 700 nm (Figure 4.10b) is due to a small number of large BC particles detected in some samples. For these rainwater and snow samples, which contain a dominant fraction of BC mass in the diameter range 100–500 nm, the USN-SP2 method enables measurement of the total BC mass concentration with an uncertainty of about $\pm 25\%$ (section 4.3). Contributions of BC particles larger than 300 nm to the total number of BC particles were negligible for both the Cape Hedo and

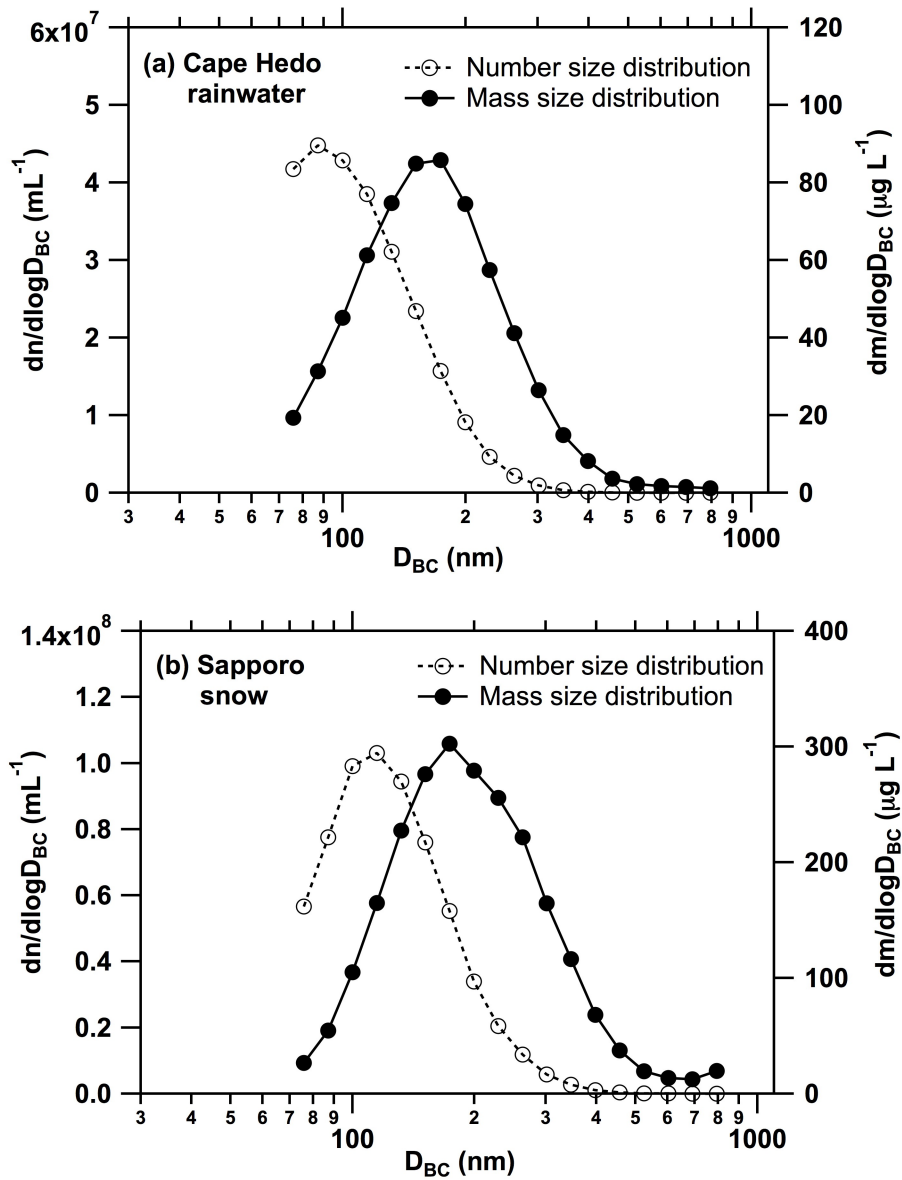


Figure 4.10. Average number and mass size distributions of BC in (a) Cape Hedo rainwater (25 samples) and (b) in Sapporo snow (10 samples).

Sapporo samples.

If a constant nebulizer efficiency of 10%, for example, is assumed, the measured

mass concentrations of BC particles between 70 and 850 nm in the rainwater and snow samples are $(15 \pm 7)\%$ lower than those determined using the size-dependent nebulizer efficiency, on average. Therefore, for liquid samples which are known to contain a dominant fraction of BC in the diameter range 100–500 nm, it is possible to use a constant value for the nebulizer efficiency in deriving BC mass concentrations with a reasonable ($\sim 30\%$) accuracy.

4.6. Ultrasonic Nebulizer Compared to Collision-Type Nebulizer

To assess the contributions of BC particles with diameters larger than 500 nm to the total BC mass concentrations, BC size distributions measured with a CTN were compared with those measured with the USN. The CTN utilizes compressed air to extract BC particles from liquid water to air. A detailed description of a CTN of the same design as used in this chapter is given in Schwarz et al. [2012]. Because the CTN was used only to assess the effect of large BC particles, a detailed evaluation of the accuracy and reproducibility of data obtained with the CTN was not made in this study. The extraction efficiency of the CTN was determined using PSL suspensions (section 4.2.2). The efficiency depended little on PSL sizes (similar results were obtained for the 220-, 356-, 505-, and 771-nm particles), and the efficiency was $(0.10 \pm 0.010)\%$. Figure 4.11 shows normalized size distributions of BC for a Cape Hedo rainwater sample and those averaged for three Sapporo snow samples measured with the USN and CTN. This comparison confirms a negligible contribution of BC particles larger than 500 nm to the total BC amount in these samples.

To assess the effects of the ultrasonic vibrating surface of the USN on the measured BC size distribution, USN-generated droplets of sample water were collected

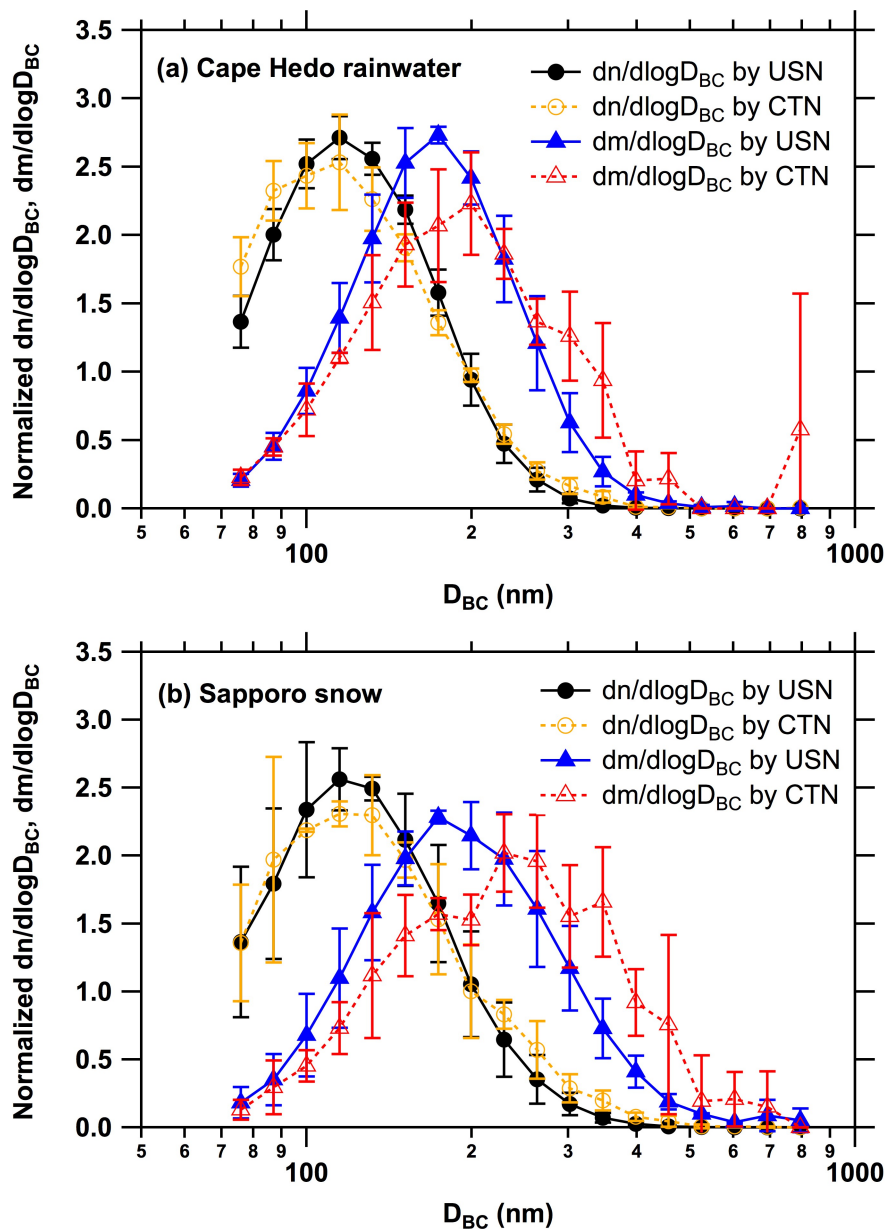


Figure 4.11. (a) Normalized number and mass size distributions of BC in a Cape Hedo rainwater sample measured with the USN and the CTN. Bars indicate 1σ values of repeated measurements. (b) Normalized number and mass size distributions of BC in three Sapporo snow samples measured with the USN and the CTN (averaged). Bars indicate 1σ values.

from the first drain of the USN and then the BC size distribution in the droplets was measured by renebulizing them with the CTN. To collect the droplets efficiently from the drain, the carrier gas was not injected into the USN during collection. The collected water included both the droplets and the fraction of water not converted into droplets. For the Cape Hedo rainwater sample, the measured BC size distributions in the USN-generated droplets were similar to those in the original rainwater sample measured with the CTN.

The USN has an advantage over the CTN in the much higher efficiency of extracting particles in water with particle size of about 100-500 nm. Due to the high extraction efficiency, the volume of rainwater and snow samples required for BC measurement with the USN was typically less than 5 mL, and sampling time to determine BC mass concentration is shorter. It is much less practical to apply the CTN to the quantification of BC concentration in the clean water samples (e.g., snow or ice samples in the polar region) because of insufficient counting statistics of BC particles under these conditions. For higher BC concentrations, application of the CTN is more easily achieved. For determination of size distribution of unknown samples, the CTN nebulization efficiency is less dependent on particle size, and thus can provide a less uncertain measurement of BC size distribution.

BC size distributions in snow samples collected in semi-urban Sapporo area (Figure 4.11b) were smaller than those in fresh snow samples collected in rural and semirural Colorado [Schwarz et al., 2012; 2013]. The negligible mass fraction of BC particles with diameters of 500–850 nm to the total BC mass in three Sapporo snow samples measured with both the USN and the CTN (Figure 4.11b) indicates variability in actual BC size distribution in snow consistent with Schwarz et al. [2013], and

highlights the continued need for better constraints on the limits of BC size in snow.

4.7. Wet Deposition of BC at a Remote Site in the East China Sea

The USN-SP2 method was applied to a long-term observation of wet deposition of BC at Cape Hedo. The observation site is located in the northern coast of Okinawa Island, 600 km from the main island of Japan and 800 km from the coast of southern China. The site is often influenced by Asian outflows within a few days of transport from the Asian Continent [Verma et al., 2011; Kondo et al., 2011a]. At this site, rainwater samples were collected on a daily basis from April 2010 to March 2013, and the BC mass concentrations in these samples (m_{BC}) were measured. Detailed descriptions of the measurement data and their climatological implication are given in Mori et al. [2014]. Here their major findings are summarized briefly. The monthly averaged m_{BC} showed marked seasonal variations, being highest in spring ($92 \pm 76 \mu\text{g L}^{-1}$) and lowest in summer ($8.0 \pm 4.1 \mu\text{g L}^{-1}$). The Wet deposition flux of BC (F_{BC}), estimated as the product of m_{BC} and precipitation amount, also showed distinct seasonal variation. The monthly average F_{BC} during four spring seasons ($16.8 \pm 6.7 \text{ mg m}^{-2} \text{ month}^{-1}$) was about 3 times higher than the annual average F_{BC} ($5.5 \pm 9.9 \text{ mg m}^{-2} \text{ month}^{-1}$) owing to the high m_{BC} and precipitation amount in spring. The F_{BC} in spring is comparable to the average BC net flux in North China, indicating the importance of precipitation over the East China Sea as a sink of BC transported from North China. This long-term observational study by Mori et al. [2014] fully demonstrates the usefulness of the USN-SP2 method for quantitative understanding of wet removal of BC.

4.8. Summary

In this chapter, evaluation of a method for quantifying the mass of BC particles suspended in rainwater and snow samples was conducted. The accuracy, reproducibility, and bias of the mass concentration of BC in liquid samples are summarized in Table 4.1.

The method uses an ultrasonic nebulizer (USN) and an SP2. The USN extracts BC particles from liquid water to air with efficiency ε . Extracted particles are detected by the SP2. The extraction efficiency ε depends on particle size. The size-dependent efficiency $\varepsilon(D)$ was determined using PSL suspensions; PSL number concentrations in water were measured by the extinction of a laser beam, based on Mie theory. The efficiency ε showed a broad maximum of about 10% in the PSL diameter range 200–500 nm, and decreased significantly for diameters larger than 800 nm. The accuracy of the measured BC mass concentration in sample water was estimated to be $\pm 25\%$ for samples containing a dominant fraction of BC mass in the diameter range 100–500 nm. The accuracy was assessed with laboratory BC samples containing BC particles with mass median diameters of about 100–200 nm. Hence, the present method is appropriate for use with even extremely clean samples with size distributions that are consistent with typical atmospheric BC size distributions. The reproducibility of the measured mass concentration in rainwater after refrigerated storage in glass containers for 12 months was $\pm 35\%$. Agitation of the sample water by an ultrasonic bath (UB) reduced the effect of attachment of BC particles to the wall of the container.

This method was applied to rainwater samples collected at Cape Hedo in Okinawa over the East China Sea and surface snow samples collected in Sapporo. A dominant fraction of the BC number concentration in these samples was observed for

particle diameters smaller than 300 nm, and these samples did not likely contain a significant mass of BC particles with diameters larger than 500 nm. The lack of substantial BC mass in BC particles with diameters larger than 500 nm in a rainwater and three snow samples was confirmed by SP2 measurements using a Collison-type nebulizer (CTN), whose efficiency is less dependent on particle size than that of the USN.

Appendix 4A. Recent Improvements in Measurements of BC Particles in Rainwater

Recently, a concentric pneumatic nebulizer (Marin-5; Cetac Technologies, Omaha, NE, USA) was used to extract BC particles from rainwater to air. The efficiency of the Marin-5 nebulizer was tested with PSL sphere suspensions in the same way as that for the ultrasonic nebulizer evaluated in this chapter (sections 4.2.2 and 4.3). The efficiency of the Marin-5 was determined to be about 50% for PSL spheres of about 200–2000 nm, which is greater than and less particle-size-dependent than that of the ultrasonic nebulizer.

In addition, the detection range of BC-core size of the standard SP2 was extended from about 70–850 nm to 70–4000 nm in mass-equivalent diameter by replacing the original position-sensitive avalanche photodiode detector (Chapter 2, Figure 2.1) with a new photomultiplier tube. The gain of the newly installed photomultiplier tube was adjusted to detect strong incandescence signals from micron-size BC particles. To convert the detected incandescence intensity into BC mass, the experimental relationship between incandescence and BC mass (F12S011 fullerene soot; Chapter 2, Figure 2.4) was extrapolated to a BC-core size of about 4000 nm (60000 fg). The

number size distribution of BC particles suspended in rainwater was measured with the modified SP2 (wide-range SP2) with the Marin-5 nebulizer during the BC-CARE Tokyo field campaign (Chapter 3).

5. General Conclusions

Laboratory studies and field observations focusing on the hygroscopicity and wet removal of black carbon (BC) aerosols were conducted. They include development of a new method to measure the hygroscopicity of ambient BC particles, evaluation of a method to measure the mass concentration and size distribution of BC particles suspended in rain and snow samples, and application of the methods to intensive field observation in the urban atmosphere of Tokyo.

A new method for the simultaneous, independent measurement of the hygroscopic growth of BC-free and BC-containing particles was presented. A humidified single-particle soot photometer (h-SP2), developed by modifying a standard SP2, was used to quantify the BC mass and the amount of coating material within individual aerosol particles under a controlled relative humidity (RH) by detecting both the laser-induced incandescence emitted and the laser light scattered from each BC-containing particle. The growth factor (GF) and hygroscopicity parameter κ for both BC-free and BC-containing particles were measured by combining an aerosol particle mass analyzer (APM) with the newly developed h-SP2 (APM-hSP2 method).

The h-SP2 was tested in the laboratory using both homogeneous ammonium sulfate (AS) and internally mixed particles of BC and AS. These particles were measured by the APM-hSP2 method between 60% and 90% RH. A core-shell structure was assumed for the BC-containing particles, and the reduction in the refractive index of the BC-free particles and BC-coating materials due to their hygroscopic growth was taken into account. Although the measured growth factors of laboratory-generated,

thinly coated BC particles tended to have large uncertainties partly because of the assumption of the core–shell structure, the measured growth factors of the pure AS and thickly coated BC particles agreed well with the growth factors predicted by κ -Köhler theory to within measurement uncertainty, demonstrating the applicability of the h-SP2 for ambient measurements.

Evaluation of a method for measuring the number and mass size distribution of BC particles suspended in rainwater and snow samples was also made. The method uses an ultrasonic nebulizer (USN) and an SP2 (USN–SP2 method). The USN extracts BC particles from liquid water to air with efficiency ε . Extracted particles are detected by the SP2. The extraction efficiency ε depends on particle size. The size-dependent efficiency $\varepsilon(D)$ was determined using polystyrene latex (PSL) spheres suspensions; the PSL number concentrations in water were measured by the extinction of a laser beam, based on Mie theory. The efficiency ε showed a broad maximum of about 10% in the PSL diameter range 200–500 nm, and decreased significantly for diameters larger than 800 nm. The accuracy of the measured BC mass concentration in sample water was estimated to be $\pm 25\%$ for samples containing a dominant fraction of BC mass in the diameter range 100–500 nm. The accuracy was assessed with laboratory BC samples containing BC particles with mass median diameters of about 100–200 nm. The reproducibility of the measured mass concentration in rainwater after refrigerated storage in glass containers for 12 months was $\pm 35\%$. The change in measured mass size distribution during storage was negligibly small, indicating that the effect of coagulation of BC particles in water during storage was not significant. Agitation of the sample water by an ultrasonic bath reduced the effect of attachment of BC particles to the wall of the container. The USN–SP2 method was applied to long-term measurement of

rainwater samples collected at Cape Hedo in Okinawa over the East China Sea. The measurement results indicated the importance of precipitation over the East China Sea as a sink of BC transported from North China.

Based on these new methods, intensive observation of the hygroscopicity and wet removal of BC-containing particles in the urban atmosphere of Tokyo was conducted during summer 2014. The newly developed h-SP2 successfully measured the detailed temporal variation of BC-free and BC-containing particles in Tokyo air for the first time. Throughout the observation period, thinly coated BC particles tended to be less hygroscopic than thickly coated BC particles, and the number fraction of the less hygroscopic ($GF < 1.2$ at 85% RH) BC-containing particles was more than 70% of the total BC-containing particles with a dry diameter of about 200 nm. The chemical compositions of BC-coating materials were generally similar to those of BC-free particles. The measured hygroscopicity of the BC-free particles was mostly between the hygroscopicities of typical inorganic and organic aerosols, indicating that individual BC-free particles were internally mixed with inorganic and organic compounds.

The number size distributions of BC in air and BC in rainwater measured during rain events indicated that BC-containing particles with larger BC cores were efficiently removed by cloud precipitation processes. This size-dependent wet removal has been successfully explained by the estimated critical supersaturation (S_c) of BC-containing particles in air and the maximum supersaturation of 0.1% (0.05–0.2 %) that the particles would have experienced during rain events. On average, the number fraction of cloud condensation nuclei (CCN)-activated BC-containing particles under a maximum a supersaturation of 0.1% was estimated to be 0.27 for particles with $D_{\text{BC-core}} = 200$ nm and 0.45 for particles with $D_{\text{BC-core}} = 350$ nm, indicating that BC-containing particles in

Tokyo air, especially particles with small BC cores (or with high S_c), were efficiently transported upward without being removed by precipitation. Thus the simultaneous observation of BC in air and BC in rainwater near BC emission sources provides useful data for directly assessing previously proposed schemes related to wet removal of aerosols, which are used in various regional or global models.

References

- Baumgardner, D., Popovicheva, O., Allan, J., Bernardoni, V., Cao, J., Cavalli, F., Cozic, J., Diapouli, E., Eleftheriadis, K., Genberg, P. J., Gonzalez, C., Gysel, M., John, A., Kirchstetter, T. W., Kuhlbusch, T. A. J., Laborde, M., Lack, D., Müller, T., Niessner, R., Petzold, A., Piazzalunga, A., Putaud, J. P., Schwarz, J. P., Sheridan, P., Subramanian, R., Swietlicki, E., Valli, G., Vecchi, R., and Viana, M. (2012). Soot Reference Materials for Instrument Calibration and Intercomparisons: A Workshop Summary with Recommendations, *Atmos. Meas. Tech.* 5:1869-1887.
- Bohren, C. F., and Huffman, D. R. (1983). *Absorption and Scattering of Light by Small Particles*, John Wiley & Sons, New York.
- Bond, T. C., Doherty, S. J., Fahey, D. W., Forster, P. M., Berntsen, T., DeAngelo, B. J., Flanner, M. G., Ghan, S., Kärcher, B., Koch, D., Kinne, S., Kondo, Y., Quinn, P. K., Sarofim, M. C., Schultz, M. G., Schulz, M., Venkataraman, C., Zhang, H., Zhang, S., Bellouin, N., Guttikunda, S. K., Hopke, P. K., Jacobson, M. Z., Kaiser, J. W., Klimont, Z., Lohmann, U., Schwarz, J. P., Shindell, D., Storelvmo, T., Warren S. G., and Zender, C. S. (2013). Bounding the Role of Black Carbon in the Climate System: A Scientific Assessment, *J. Geophys. Res.* 118: 1-173, doi:10.1002/jgrd.50171.
- Cai, Y., Montague, D. C., Mooiweer-Bryan, W., and Deshler, T. (2008). Performance Characteristics of the Ultra High Sensitivity Aerosol Spectrometer for Particles Between 55 and 800 nm: Laboratory and Field Studies, *J. Aerosol Sci.* 39:759-769.
- Chuang. (2003). Measurement of timescale of hygroscopic growth for atmospheric aerosols, *J. Geophys. Res.* 108(D9): 4282, doi:10.1029/2002JD002757.
- Clarke, A. D., and Noone, K. J. (1985). Soot in the Arctic Snowpack: A Cause for

- Perturbations in Radiative Transfer, *Atmos. Environ.* 19: 2045-2053.
- Dasch, J. M., and Cadle, S. H. (1989). Atmospheric Carbon Particles in the Detroit Urban Area: Wintertime Sources and Sinks, *Aerosol Sci. Technol.* 10:2, 236–248.
- Doherty, S. J., Warren, S. J., Granfell, T. C., Clarke, A. D., and Brandt, R. E. (2010). Light-absorbing Impurities in Arctic Snow, *Atmos. Chem. Phys.* 10:11647-11680.
- Duplissy, J., Gysel, M., Sjogren, S., Meyer, N., Good, N., Kammermann, L., Michaud, V., Weigel, R., Martins dos Santos, S., Gruening, C., Villani, P., Laj, P., Sellegri, K., Metzger, A., McFiggans, G. B., Wehrle, G., Richter, R., Dommen, J., Ristovski, Z., Baltensperger, U., and Weingartner, E. (2009). Intercomparison study of six HTDMAs: results and recommendations, *Atmos. Meas. Tech.* 2:363-378, doi:10.5194/amt-2-363-2009.
- Ebert, M., Weinbruch, S., Rausch, A., Gorzawski, G., Hoffmann, P., Wex, H., and Helas, G. (2002). Complex refractive index of aerosols during LACE 98 as derived from the analysis of individual particles, *J. Geophys. Res.* 107(D21):8121, doi:10.1029/2000JD000195.
- Facchini, M. C., Decesari, S., Mircea, M., Fuzzi, S., and Loglio, G. (2000). Surface Tension of Atmospheric Wet Aerosol and Cloud/fog Droplets in Relation to Their Organic Carbon Content and Chemical Composition, *Atmos. Environ.* 34:4853-4857.
- Gao, R. S., Schwarz, J. P., Kelly, K. K., Fahey, D.W., Watts, L. A., Thompson, T. L. et al. (2007). A Novel Method for Estimating Light–Scattering Properties of Soot Aerosols using a Modified Single–Particle Soot Photometer, *Aerosol Sci. Technol.* 41:125-135.
- Granfell, T. C., Doherty, S. J., Clarke, A. D., and Warren, S. G. (2011). Light

- Absorption from Particulate Impurities in Snow and Ice Determined by Spectrophotometric Analysis of Filters, *Appl. Opt.* 50:2037-2048.
- Hadley, O.L., Corrigan, C.E., and Kirchstetter, T.W. (2008). Modified Thermal-Optical Analysis Using Spectral Absorption Selectivity To Distinguish Black Carbon from Pyrolyzed Organic Carbon, *Environ. Sci. Technol.* 42:8459-8464.
- Henning, S., Wex, H., Wennrich, C., Hennig, T., Kiselev, A., Snider, J. R., Rose, D., Dusek, U., Frank, G. P., Pöschl, U., Kristensson, A., Bilde, M., Tillmann, R., Kiendler-Scharr, A., Mentel, Th. F., Walter, S., Schneider, J., and Stratmann, F. (2010). Soluble mass, hygroscopic growth, and droplet activation of coated soot particles during LACIS Experiment in November (LEXNo), *J. Geophys. Res.* 115:D11206, doi:10.1029/2009JD012626.
- Henning, S., Ziese, M., Kiselev, A., Saathoff, H., Möhler, O., Mentel, T. F., Buchholz, A., Spindler, C., Michaud, V., Monier, M., Sellegri, K., and Stratmann, F. (2012). Hygroscopic Growth and Droplet Activation of Soot Particles: Uncoated, Succinic or Sulfuric Acid Coated. *Atmos. Chem. Phys.* 12:4525-4537.
- Hess, M., Koepke, P., and Schult, I. (1998). Optical Properties of Aerosols and Clouds: The Software Package OPAC, *Bull. Am. Met. Soc.* 79:831-844.
- Hinds, W. C. (1999). *Aerosol Technology*, John Wiley & Sons, New York.
- Huff Hartz, K. E., Rosenørn, T., Ferchak, S. R., Raymond, T. M., Bilde, M., Donahue, N. M., and Pandis, S. N. (2005). Cloud condensation nuclei activation of monoterpene and sesquiterpene secondary organic aerosol, *J. Geophys. Res.* 110:D14208, doi:10.1029/2004JD005754.
- Huff Hartz, K. E., Tischuk, J. E., Chan, M. N., Chan, C. K., Donahue, N. M., Pandis, S. N. (2006). Cloud Condensation Nuclei Activation of Limited Solubility Organic

Aerosol, *Atmos. Environ.* 40:605-617.

Intergovernmental Panel on Climate Change (IPCC) (2013). *Climate Change 2013: The Physical Science Basis. Contribution of Working Group I to the 5th Assessment Report of the IPCC*. Cambridge University Press, Cambridge, UK.

Jayne, J. T., Leard, D. C., Zhang, X., Davidovits, P., Smith, K. A., Kolb, C. E., and Worsnop, D. R. (2000). Development of an Aerosol Mass Spectrometer for Size and Composition Analysis of Submicron Particles, *Aerosol Sci. Technol.* 33:49-70.

Kaspari, S. D., Schwikowsk, M., Gysel, M., Flanner, M. G., Kang, S., Hou, S., and Mayewski, P. A. (2011). Recent increase in black carbon concentrations from a Mt. Everest ice core spanning 1860–2000 AD, *Geophys. Res. Lett.* 38: L04703, doi:10.1029/2010GL046096.

King, S. M., Rosenoern, T., Shilling, J. E., Chen, Q., and Martin, S. T. (2009). Increased cloud activation potential of secondary organic aerosol for atmospheric mass loadings, *Atmos. Chem. Phys.* 9:2959-2971.

Kiss, G., Tombacz, E., and Hansson, H. (2005) Surface Tension Effects of Humic-Like Substances in the Aqueous Extract of Tropospheric Fine Aerosol, *J. Atmos. Chem.* 50:279-294.

Kuwata, M., Kondo, Y., Mochida, M., Takegawa, N., and Kawamura, K. (2007). Dependence of CCN Activity of Less Volatile Particles on the Amount of Coating Observed in Tokyo, *J. Geophys. Res.* 112: D11207, doi:10.1029/2006JD007758.

Koehler, K. A., Kreidenweis, S. M., DeMott, P. J., Prenni, A. J., Carrico, C. M., Ervens, B., and Feingold, G. (2006). Water Activity and Activation Diameters from Hygroscopicity Data – Part II: Application to Organic Species, *Atmos. Chem. Phys.* 6:795-809.

- Köhler, H (1936). The nucleus in and the growth of hygroscopic droplets, *Trans. Faraday Soc.* 32:1152-1161.
- Kondo, Y., Komazaki, Y., Miyazaki, Y., Moteki, N., Takegawa, N., Kodama, D., Deguchi, S., Nogami, M., Fukuda, M., Miyakawa, T., Morino, Y., Koike, M., Sakurai, H., and Ehara, K. (2006). Temporal Variations of Elemental Carbon in Tokyo. *J. Geophys. Res.* 111:D12205, doi:10.1029/2005JD006257.
- Kondo, Y., Matsui, H., Moteki, N., Sahu, L., Takegawa, N., Kajino, M., Zhao, Y., Cubison, M. J., Jimenez, J. L., Vay, S., Diskin, G. S., Anderson, B., Wisthaler, A., Mikoviny, T., Fuelberg, H. E., Blake, D. R., Huey, G., Weinheimer, A. J., Knapp, J. D., and Brune, H. (2011a). Emissions of Black Carbon, Organic, and Inorganic Aerosols from Biomass Burning in North America and Asia in 2008, *J. Geophys. Res.* 116:D16201, doi:10.1029/2011JD015637.
- Kondo, Y., Sahu, L., Moteki, N., Khan, F., Takegawa, N., Liu, X., Koike, M., and Miyakawa, T. (2011b). Consistency and traceability of black carbon measurements made by laser-induced incandescence, thermal-optical transmittance, and filter-based photo-absorption techniques, *Aerosol Sci. Technol.* 45:295-312.
- Kuwata, M., Kondo, Y., and Takegawa, N. (2009). Critical Condensed Mass for Activation of Black Carbon as Cloud Condensation Nuclei, *J. Geophys. Res.* 114:D20202, doi:10.1029/2009JD012086.
- Laborde, M., Mertes, P., Zieger, P., Dommen, J., Baltensperger, U., and Gysel, M. (2012). Sensitivity of the Single Particle Soot Photometer to Different Black Carbon Types, *Atmos. Meas. Tech.* 5:1031-1043.
- Liu, D., Allan, J., Whitehead, J., Young, D., Flynn, M., Coe, H., McFiggans, G., Fleming, Z. L., and Bandy, B. (2013) Ambient black carbon particle hygroscopic

- properties controlled by mixing state and composition, *Atmos. Chem. Phys.* 13:2015-2029, doi:10.5194/acp-13-2015-2013.
- Martin, S.T. (2000). Phase Transitions of Aqueous Atmospheric Particles, *Chem. Rev.* 100:3403-3453.
- Matsui, H., Koike, M., Kondo, Y., Moteki, N., Fast, J. D., and Zaveri, R. A. (2013). Development and Validation of a Black Carbon Mixing State Resolved Three-Dimensional Model: Aging Processes and Radiative Impact, *J. Geophys. Res.* 118: 2304-2326, doi:10.1029/2012JD018446.
- McConnell, J. R., Edwards, R., Kok, G. L., Flanner, M. G., Zender, C. S., Saltzman, E. S., Banta, J. R., Pasteris, D. R., Carter, M. M., and Kahl, J. D. W. (2007). 20th-Century Industrial Black Carbon Emissions Altered Arctic Climate Forcing, *Science* 317: 1381–1384.
- McMeeking, G. R., Good, N., Petters, M. D., McFiggans, G., and Coe, H. (2011). Influences on the fraction of hydrophobic and hydrophilic black carbon in the atmosphere, *Atmos. Chem. Phys.* 11:5099-5112, doi:10.5194/acp-11-5099-2011.
- McMurry, P. H., Wang, X., Park, K., and Ehara, K. (2002). The Relationship between Mass and Mobility for Atmospheric Particles: A New Technique for Measuring Particle Density, *Aerosol Sci. Technol.* 36:227-238.
- Mikhailov, E., Vlasenko, S., Martin, S. T., Koop, T., and Pöschl, U. (2009). Amorphous and Crystalline Aerosol Particles Interacting with Water Vapor: Conceptual Framework and Experimental Evidence for Restructuring, Phase Transitions and Kinetic Limitations, *Atmos. Chem. Phys.* 9:9491-9522.
- Miyakawa, T., Takeda, N., Koizumi, K., Tabaru, M., Ozawa, Y., Hirayama, N., and Takegawa, N. (2014). A New Laser Induced Incandescence–Mass Spectrometric

- Analyzer (LII-MS) for Online Measurement of Aerosol Composition Classified by Black Carbon Mixing State, *Aerosol Sci. Technol.* 48:853-863.
- Mori, T., Kondo, Y., Ohata, S., Moteki, N., Matsui, H., Oshima, N., and Iwasaki, A. (2014). Wet deposition of black carbon at a remote site in the East China Sea, *J. Geophys. Res.* 119, doi:10.1002/2014JD022103.
- Moteki, N., Kondo, Y., Miyazaki, Y., Takegawa, N., Komazaki, Y., Kurata, G., Shirai, T., Blake, D. R., Miyakawa, T., and Koike, M. (2007). Evolution of Mixing State of Black Carbon Particles: Aircraft Measurements over the Western Pacific in March 2004, *Geophys. Res. Lett.* 34, L11803, doi:10.1029/2006GL028943.
- Moteki, N., and Kondo, Y. (2010). Dependence of Laser-induced Incandescence on Physical Properties of Black Carbon Aerosols: Measurements and Theoretical Interpretation, *Aerosol Sci. Technol.* 44:663-675.
- Moteki, N., Kondo, Y., and Nakamura, S. (2010). Method to Measure Refractive Indices of Small Nonspherical Particles: Application to Black Carbon Particles, *J. Aerosol Sci.* 41:513-521.
- Moteki, N., Kondo, Y., Oshima, N., Takegawa, N., Koike, M., Kita, K., et al. (2012). Size Dependence of Wet Removal of Black Carbon Aerosols during Transport from the Boundary Layer to the Free Troposphere. *Geophys. Res. Lett.* 39:L13802, doi:10.1029/2012GL052034.
- Moteki, N., Kondo, Y., and Adachi, K. (2014). Identification by single-particle soot photometer of black carbon particles attached to other particles: Laboratory experiments and ground observations in Tokyo, *J. Geophys. Res.* 119:1031–1043, doi:10.1002/2013JD020655.
- Ogren, J. A., and Charlson, R. J. (1983). Determination of Elemental Carbon in

- Rainwater, *Anal. Chem.* 55:1569-1572.
- Ogren, J. A., Groblicki, P. J., and Charlson, R. J. (1984). Measurement of the Removal Rate of Elemental Carbon from the Atmosphere, *Sci. Tot. Environ.* 36:329-338.
- Okuda, T., Iwase, T., Ueda, H., Suda, Y., Tanaka, S., Dokiya, Y., Fushimi, K., and Hosoe, M. (2005). Long-term Trend of Chemical Constituents in Precipitation in Tokyo Metropolitan Area, Japan, from 1990 to 2002, *Sci. Tot. Environ.* 339:127-141.
- Onasch, T. B., Trimborn, A., Fortner, E. C., Jayne, J. T., Kok, G. L., Williams, L. R., Davidovits, P., and Worsnop, D. R. (2012). Soot Particle Aerosol Mass Spectrometer: Development, Validation, and Initial Application, *Aerosol Sci. Technol.* 46:7, 804-817.
- Petters, M. D., and Kreidenweis, S. M. (2007). A Single Parameter Representation of Hygroscopic Growth and Cloud Condensation Nucleus Activity, *Atmos. Chem. Phys.* 7:1961-1971.
- Petzold, A., Ogren, J. A., Fiebig, M., Laj, P., Li, S. M., Baltensperger, U., Holzer-Popp, T., Kinne, S., Pappalardo, G., Sugimoto, N., Wehrli, C., Wiedensohler, A., and Zhang, X., Y. (2013). Recommendations for reporting “black carbon” measurements, *Atmos. Chem. Phys.* 13:8365-8379.
- Riemer, N., West, M., Zaveri, R. A., and Easter, R. C. (2010). Estimating black carbon aging time scales with a particle-resolved aerosol model, *J. Aerosol Sci.*, 41:143-158, doi:10.1016/j.jaerosci.2009.08.009.
- Schwarz, J. P., Doherty, S. J., Li, F., Ruggiero, S. T., Tanner, C. E., Perring, A. E., Gao, R. S., and Fahey, D. W. (2012). Assessing Single Particle Soot Photometer and Integrating Sphere/Integrating Sandwich Spectrophotometer Measurement

- Techniques for Quantifying Black Carbon Concentration in Snow, *Atmos. Meas. Tech.* 5:2581-2592.
- Schwarz, J. P., Gao, R. S., Perring, A. E., Spackman, J. R., and Fahey, D. W. (2013), Black carbon aerosol size in snow, *Nature Sci. Rep.* 3:1356, doi:10.1038/srep01356.
- Schwarz, J. P., Perring, A. E., Markovic, M. Z., Gao, R. S., Ohata, S., Langridge, J., Law, D., McLaughlin, R., and Fahey, D. W. (2015). Technique and theoretical approach for quantifying the hygroscopicity of black-carbon-containing aerosol using a single particle soot photometer, *J. Aerosol Sci.*, 81:110–126.
- Seinfeld, J. H., and Pandis, S.N. (2006). *Atmospheric Chemistry and Physics*. John Wiley & Sons, New York.
- Sempere, R., and Kawamura, K. (1994). Comparative Distributions of Dicarboxylic Acids and Related Polar Compounds in Snow, Rain and Aerosols from Urban Atmosphere, *Atmos. Environ.* 28:449-459.
- Shiraiwa, M., Kondo, Y., Moteki, N., Takegawa, N., Miyazaki, Y., and Blake, D. R. (2007). Evolution of Mixing State of Black Carbon in Polluted Air from Tokyo. *Geophys. Res. Lett.* 34:L16803, doi:10.1029/2007GL029819.
- Sjogren, S., Gysel, M., Weingartner, E., Baltensperger, U., Cubison, M. J., Coe, H., Zardini, A. A., Marcolli, C., Krieger, U. R., and Peter, T. (2007). Hygroscopic growth and water uptake kinetics of two-phase aerosol particles consisting of ammonium sulphate, adipic and humic acid mixtures, *J. Aerosol Sci.* 38:157-171.
- Slinn, W. G. N. (1983). *Precipitation Scavenging, in Atmospheric Sciences and Power Production – 1979. Division of Biomedical Environmental Research, U.S. Department of Energy, Washington, DC, Chapter 11.*
- Stelson, A. W. (1990). Urban aerosol refractive index prediction by molar refraction

- approach, *Environ. Sci. Technol.* 24:1676-1679.
- Toon, O. B., Pollack, J. B., and Khare, B. N. (1976). The optical constants of several atmospheric aerosol species: Ammonium sulfate, aluminum oxide, and sodium chloride, *J. Geophys. Res.* 81:5733-5748.
- Turpin, B. J., and Lim, H. (2001). Species Contributions to PM_{2.5} Mass Concentrations: Revisiting Common Assumptions for Estimating Organic Mass, *Aerosol Sci. Technol.* 35:602-610.
- VanReken, T. M., Ng, N. L., Flagan, R. C., and Seinfeld, J. H. (2005). Cloud condensation nucleus activation properties of biogenic secondary organic aerosol, *J. Geophys. Res.* 110: D07206, doi:10.1029/2004JD005465.
- Verma, R. L., Kondo, Y., Oshima, N., Matsui, H., Kita, K., Sahu, L. K., Kato, S., Kajii, Y., Takami, A., and Miyakawa, T. (2011). Seasonal variations of the transport of black carbon and carbon monoxide from the Asian continent to the western Pacific in the boundary layer, *J. Geophys. Res.* 116:D21307, doi:10.1029/2011JD015830.
- Wang, M., Xu, B., Zhao, H., Cao, J., Joswiak, D., Wu, G., and Lin, S. (2011). The Influence of Dust on Quantitative Measurements of Black Carbon in Ice and Snow when Using a Thermal Optical Method, *Aerosol Sci. Technol.* 46:60–69.
- Warren, S. G., and Wiscombe, W. J. (1980). A Model for the Spectral Albedo of Snow, II, Snow Containing Atmospheric Aerosols, *J. Atmos. Sci.* 37:2734-2745.
- Willey, J. D., Kieber, R. J., Eyman, M. S., and Avery, Jr., G. B. (2000). Rainwater Dissolved Organic Carbon: Concentrations and Global Flux, *Global Biogeochem. Cycles* 14:139-148.
- Zhang, R. Y., Khalizov, A. F., Pagels, J., Zhang, D., Xue, H., and McMurry, P. H. (2008). Variability in morphology, hygroscopicity, and optical properties of soot

aerosols during atmospheric processing, *P. Natl. Acad. Sci.* 105:10291–10296,
doi:10.1073/pnas.0804860105.

Acknowledgments

I am deeply grateful to Prof. Y. Kondo at The University of Tokyo, for his continued support and encouragement during the course of my study. I am also grateful to Dr. N. Moteki at The University of Tokyo, for his invaluable advice and encouragement throughout my study. I would like to express sincere thanks to Prof. M. Koike at The University of Tokyo, and Prof. N. Takegawa at Tokyo Metropolitan University, for their insightful comments and suggestions on my study. I would like to thank Dr. J. P. Schwarz and Dr. D. W. Fahey at National Oceanic and Atmospheric Administration, for their kind support and suggestions on my study. I would also like to thank Prof. T. Nakajima and Prof. M. Uematsu at The University of Tokyo, for their valuable comments and suggestions on this study. I received generous support from Dr. T. Miyakawa, Dr. H. Matsui at Japan Agency for Marine-Earth Science and Technology, Dr. N. Oshima, and M. Kajino at Meteorological Research Institute during the course of my study. I would like to thank Dr. M. Irwin for laboratory support and fruitful discussions on wide-ranging topics. I wish to acknowledge all of the laboratory members for their kind support. I would like to thank many researchers for rainwater sampling at Cape Hedo and snow sampling in Sapporo. I am indebted to all of the BC-CARE Tokyo campaign participants for their cooperation and support. I am thankful to A. Sasaki for her warm encouragement during the course of my study. Finally, I would also like to express my gratitude to my family for all the things that they have done for me.

I was supported by the Japan Society for the Promotion of Sciences (JSPS) KAKENHI Grant Number 246736.

Publication List

Ohata, S., Moteki, N., and Kondo, Y. (2011). Evaluation of a Method for Measurement of the Concentration and Size Distribution of Black Carbon Particles Suspended in Rainwater, *Aerosol Sci. Technol.* 45:1326–1336.

Ohata, S., Moteki, N., Schwarz, J. P., Fahey, D. W., and Kondo, Y. (2013). Evaluation of a Method to Measure Black Carbon Particles Suspended in Rainwater and Snow Samples, *Aerosol Sci. Technol.* 47:1073–1082.

Mori, T., Kondo, Y., **Ohata, S.**, Moteki, N., Matsui, H., Oshima, N., and Iwasaki, A. (2014). Wet deposition of black carbon at a remote site in the East China Sea, *J. Geophys. Res.* 119, doi:10.1002/2014JD022103.

Schwarz, J. P., Perring, A. E., Markovic, M. Z., Gao, R. S., **Ohata, S.**, Langridge, J., Law, D., McLaughlin, R., and Fahey, D. W. (2015). Technique and theoretical approach for quantifying the hygroscopicity of black-carbon-containing aerosol using a single particle soot photometer, *J. Aerosol Sci.*, 81:110–126.